AD-A174 662   VISCOUS INTERACTIONS AT HYPERSONIC SPEED(U) CALSPAN UB   1/
RESEARCH CENTER BUFFALO NY* M S HOLDEN ET AL.
12 SEP 86 CUBRC-86611 AFOSR-TR-86-2072 F49620-84-K-0009
UNCLASSIFIED   F/G 20/4   NL

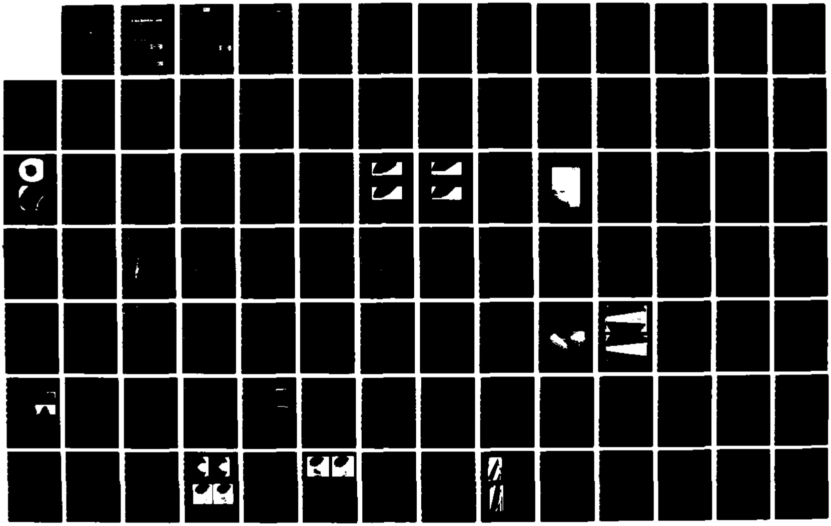

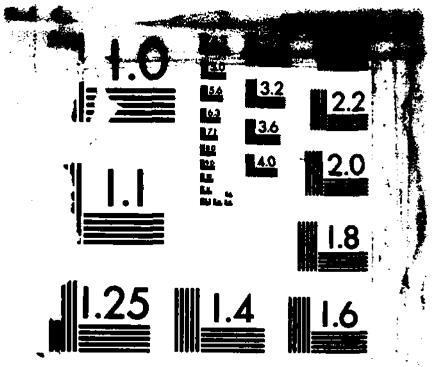
1.0
1.1
1.25
1.4
1.6
1.8
2.0
2.2
3.2
3.6
4.0

MICROCOPY RESOLUTION TEST CHART
NATIONAL BUREAU OF STANDARDS-1963-A

②

AD-A174 662

CALSPAN-UB
RESEARCH CENTER

VISCOUS INTERACTIONS AT HYPERSONIC SPEED

Final Report
October, 1986

AFOSR-TR- 86-2072

TECHNICAL REPORT

DTIC
ELECTE
S DEC 0 2 [illegible] D
D

DTIC FILE COPY

DISTRIBUTION STATEMENT A
Approved for public release;
Distribution Unlimited

CALSPAN
UB
RESEARCH CENTER

CALSPAN-UB RESEARCH CENTER P.O. BOX 400 BUFFALO, NEW YORK 14225

86 11 25 378

②

CALSPAN
UB
RESEARCH CENTER

AIR FORCE OFFICE OF SCIENTIFIC RESEARCH (AFSC)
NOTICE OF TRANSMITTAL TO DTIC
This technical report has been reviewed and is
approved for public release IAW AFR 190-12.
Distribution is unlimited.
MATTHEW J. KERPER
Chief, Technical Information Division

VISCOUS INTERACTIONS AT HYPERSONIC SPEED

Final Report
October, 1986

AFOSR-TR- 86-2072

Principal Investigators:

Michael S. Holden
Calspan Corporation
Telephone: (716) 631-6853

Jhin Ho Lee
Calspan-UB Research Center
Telephone: (716) 631-6900

DTIC
ELECTE
DEC 0 2 1986
S D
D

Prepared for:

Air Force Office of Scientific Research
Directorate of Aerospace Sciences
Bolling Air Force Base

DISTRIBUTION STATEMENT A
Approved for public release;
Distribution Unlimited

86 11 25 378

CALSPAN-UB RESEARCH CENTER P.O. BOX 400, BUFFALO, NEW YORK 14225 TEL. (716) 631-6900

UNCLASSIFIED
SECURITY CLASSIFICATION OF THIS PAGE

REPORT DOCUMENTATION PAGE

1a. REPORT SECURITY CLASSIFICATION: UNCLASSIFIED

1b. RESTRICTIVE MARKINGS

2a. SECURITY CLASSIFICATION AUTHORITY: -

2b. DECLASSIFICATION / DOWNGRADING SCHEDULE: -

3 DISTRIBUTION / AVAILABILITY: ~~Approval Required~~

DISTRIBUTION STATEMENT A
Approved for public release;
Distribution Unlimited

4. PERFORMING ORGANIZATION REPORT NUMBER(S): CUBRC Report No. 86611

5. MONITORING ORGANIZATION REPORT NUMBER(S): AFOSR-TR- 86-2072

6a. NAME OF PERFORMING ORGANIZATION: Calspan - UB Research Center

6b OFFICE SYMBOL (If applicable)

7a. NAME OF MONITORING ORGANIZATION: AFOSR/Directorate of Aerospace Sciences

6c. ADDRESS (City, State, and ZIP Code)
4455 Genesse Street
Buffalo, NY 14225

7b. ADDRESS (City, State, and ZIP Code)
Building 410
Bolling AFB, DC 20332-6448

8a. NAME OF FUNDING / SPONSORING ORGANIZATION: USAF/AFSC/AFOSR

8b. OFFICE SYMBOL (If applicable): NA

9. PROCUREMENT INSTRUMENT IDENTIFICATION NUMBER: F49620-84-K-0009

8c. ADDRESS (City, State, and ZIP Code)
Building 410
Bolling AFB, DC 20332

10. SOURCE OF FUNDING NUMBERS

PROGRAM ELEMENT NO.	PROJECT NO.	TASK NO.	WORK UNIT ACCESSION NO.
61102F	2307/A1		

11 TITLE (Include Security Classification): Viscous Interactions at Hypersonic Speed

12 PERSONAL AUTHOR(S): Dr. Michael S. Holden, Calspan Corporation; Jhin Ho Lee, Calspan-UB Research Center

13a. TYPE OF REPORT: Final

13b. TIME COVERED FROM 3/17/84 TO 10/86

14. DATE OF REPORT (Year, Month, Day): 1986, 09, 12

15. PAGE COUNT: 47

16. SUPPLEMENTARY NOTATION

17 COSATI CODES

FIELD	GROUP	SUB-GROUP

18. SUBJECT TERMS (Continue on reverse if necessary and identify by block number)

19. ABSTRACT (Continue on reverse if necessary and identify by block number)

This report summarizes the research conducted and documents published under this contract during 1985. This work has been directed toward investigations of fundamental aerothermal phenomena in hypersonic flow, with particular emphasis on viscous/inviscid interaction phenomena. The experimental studies were conducted to examine the changes in the structure at the base of a hypersonic turbulent boundary layer as it is subjected to a strong self-induced pressure gradient in regions of shock wave/boundary layer interaction. The initial phase of the theoretical program was directed toward summarizing existing techniques for obtaining Navier/Stokes solutions for laminar flow over flat plates in hypersonic flow. In the experimental program, surface and flow field measurements were made to examine the detailed flow mechanics associated with turbulent boundary layer separation over a large cone flare model at Mach 11, 13 and 16 for Reynold numbers up to 100 ~~$\times 10^6$~~ million. Three papers were written and presented at international meetings during the

to p 43

20 DISTRIBUTION / AVAILABILITY OF ABSTRACT: ☒ UNCLASSIFIED/UNLIMITED ☐ SAME AS RPT. ☐ DTIC USERS

21. ABSTRACT SECURITY CLASSIFICATION: UNCLASSIFIED

22a NAME OF RESPONSIBLE INDIVIDUAL: ~~Michael S. Holden~~ DR JAMES D WILSON

22b. TELEPHONE (Include Area Code): ~~(716) 632-6853~~ 202-767-4935

22c. OFFICE SYMBOL: AFOSR/NA

DD FORM 1473, 84 MAR
83 APR edition may be used until exhausted.
All other editions are obsolete.

SECURITY CLASSIFICATION OF THIS PAGE

19. ABSTRACT (Cont.)

past year, including an invited review paper on aerothermal problems associated with hypersonic flight, which were supported in part by contracts through CUBRC.

TABLE OF CONTENTS

Section	Subject	Page
	TABLE OF CONTENTS	iii
	LIST OF FIGURES	v
	LIST OF TABLES	vi
I	INTRODUCTION	1
II	A REVIEW OF RECENT PUBLICATIONS ASSOCIATED WITH THE PRESENT CONTRACT	3
III	SUMMARY OF EXISTING SOLUTION TECHNIQUE	5
	3.1 Introduction	5
	3.2 Numerical Schemes	8
	3.3 Explicit Scheme of MacCormack	9
	3.4 Implicit Method of Beam-Warming	10
	3.5 Implicit (Explicit) Method of MacCormack	12
	3.6 Conservative Supra-Characteristics Method (CSCM)	12
	3.7 Flux Splitting	13
	3.8 Time Splitting	14
	3.9 Computational Sub-Layer	15
IV	EXPERIMENTAL PROGRAM	17
	4.1 PROGRAM OBJECTIVE AND DESIGN OF THE EXPERIMENTAL STUDY	17
	4.2 MODELS AND INSTRUMENTATION	18
	4.2.1 Heat Transfer Instrumentation	18
	4.2.2 Pitot and Static Pressure Instrumentation	27
	4.2.3 Total Temperature Instrumentation	27
	4.2.4 Test Conditions and Model Configurations	27
	4.3 RESULTS AND DISCUSSION	31
V	CONCLUSIONS	43
VI	REFERENCES	45
Appendix		
A	"Experimental Studies of the Effects of Asymmetric Transition on the Aerothermal Characteristics of Hypersonic Blunted Slender Cones"	A-1
B	"Aerothermal Problems Associated with Viscous/Inviscid Interaction Over Hypersonic Flight Vehicles"	B-1
C	"Studies of Potential Fluid-Mechanical Mechanisms For Enhanced Stagnation-Region Heating"	C-1

This page intentionally blank.

LIST OF FIGURES

Number	Title	Page
1	Sharp 6° Cone/30° Flare Model Installed in Calspan's 96" Shock Tunnel	19
2	Installation Drawing of Cone/Flare Model	20
3	Distribution of Pressure and Heat Transfer in Attached Flow Over the Large 6° Cone/30° Flare Configuration	21
4	Distribution of Pressure and Heat Transfer in Separated Flow Over the Large 6° Cone/36° Flare Configuration	22
5	Distribution of Pressure and Heat Transfer in Attached Flow Over the Large 6° Cone/30° Flare Configuration	23
6	Distribution of Pressure and Heat Transfer in Separated Flow Over the Large 6° Cone/36° Flare Configuration	24
7a	Attached Flow Over Cone/Flare Configuration, $M=11$	25
7b	Separated Flow Over Cone/Flare Configuration, $M=11$	25
8a	Attached Flow, $M=13$	26
8b	Separated Flow, $M=13$	26
9	Rake Assembly	28
10	Schematic Diagram of Total Temperature Gage	29
11	Typical Response of Total Temperature Gage	29
12	Reynolds Analogy Factors for Turbulent Hypersonic Boundary Layers	33
13	Reynolds Analogy Factors for Turbulent Hypersonic Boundary Layers	33
14	Comparison Between the Measured Heat Transfer and the Theory of Van Driest on Sharp Cones $(\Theta_{V} = \Theta_{B} + \Theta_{BE/2})$	35
15	Distribution of Pitot Pressure Across Boundary Layer Upstream of Cone/Flare Interaction	36
16	Distribution of Total Temperature Across Boundary Layer	37
17	Distribution of Pitot Pressure Across Boundary Layer Upstream of Cone/Flare Interaction	38

☐
☐

Availability Codes

Dist	Avail and/or Special
A-1	

QUALITY INSPECTED 4

LIST OF FIGURES (Cont.)

Number	Title	Page
18	Distribution of Total Temperature Across Boundary Layer	39
19	Total Temperature and Velocity Measurements Presented in Crocco Framework	41

LIST OF TABLES

Number	Title	Page
1	Classification of Navier-Stokes Equations	6
2	Typical Test Conditions	30

Section I. INTRODUCTION

Regions of shock wave/turbulent boundary layer interaction, in which large pressure gradients, flow separation and turbulent non-equilibrium flows are generated, have traditionally been the testing ground of prediction techniques, particularly based on the solution of the full Navier-Stokes equations where the recirculating flow can be handled "more exactly." However, despite the significant advances in computational techniques during the past decade, there remain significant gaps in our understanding and ability to predict regions of shock wave/turbulent boundary interactions in hypersonic flows. At the heart of the problem lies the difficulty of describing the generation and development of turbulence in the extremely large pressure gradients developed across hypersonic interaction regions. However, many of the problems which have been blamed on poor turbulence modeling may in fact stem from the grid selection or nature of the numerical scheme. In the rush to demonstrate that the Navier-Stokes codes can be successfully applied to describe a variety of interaction problems, very little emphasis has been placed on the demonstration that the numerical schemes are indeed an accurate representation of the equations upon which they are based. At a minimum, the sensitivity to grid size should be examined, and, particularly for turbulent interacting flows, an analysis of the characteristic scale lengths, like that employed in triple deck theory, should be performed to aid in grid positioning.

The complexity of turbulent interaction regions makes it essential that detailed information from experiments be used to construct realistic models of the turbulent transport mechanisms. The harsh aerothermal environment in hypersonic turbulent interacting flows makes delicate probing of these flows difficult, and because the typical natural frequencies in these flows are of the order of 500 KHz, the instrumentation and recording requirements for capturing fluctuating features of the flow are far from simple. While skin friction and heat transfer measurements are useful in the evaluation of turbulence modeling techniques, employing comparisons with surface pressure data to support the models used in a Navier-Stokes code is a weak verification.

The complexity of the flow field in regions of shock wave/turbulent boundary layer interaction is such that it is unrealistic to expect to describe such regions in any detail within the framework of the boundary layer equations. Indeed, there are some who would question whether the time or mass averaged Navier-Stokes equations capture the basic fluid mechanics associated with the intrinsically unsteady nature of separated regions. In hypersonic flows, the effects of compressibility on the structure and development of turbulence must also be considered.

While there have been strenuous efforts to obtain predictions of two-dimensional and three-dimensional turbulent interaction regions, it is currently recognized that "successes" with "Navier-Stokes" code in describing some three-dimensional turbulent interaction regions is a result of the dominance of the pressure and inertial terms in these flows. In two recent studies (References 1 & 2) it was shown that turbulence modeling could be changed signficantly without significantly changing the numerical solution for a three-dimensional interaction region. For two-dimensional interactions it appears that turbulence modeling is more critical. To obtain good agreement for these latter flows, some very gross assumptions must be made in the turbulence model. Shang and Hankey[3], for example, chose to apply an empirical relationship (selected by matching the length of the separated region) to rapidly decrease the turbulent scale size through the interaction region. Horstmann[4], however, found the best agreement with Settles[5] measurements in wedge-induced separated regions using a two equation model for turbulence scale size and vorticity. Working with this same turbulence model, however, Horstmann was unable to predict the occurrence of separation on two incident *shock/turbulent boundary* layer configurations studied by Holden[6] at Mach 11.2. In the later studies for flow which were clearly separated, the numerical solution failed to predict the characteristic plateaus in either the heat transfer or pressure distributions. The modeling of turbulence in separated interaction regions at hypersonic Mach numbers should account for the effects of compressibility and the generation of turbulence by the unsteady movement of the incident and induced shocks as they traverse and interact with a major region of the turbulent boundary layer and the unsteady movement of the separated region. Clearly, further detailed experimental work on insightful theoretical modeling is required to develop numerical prediction techniques which are capable of describing separated turbulent interaction regions in hypersonic flow.

In this report, we first review the papers which have been prepared under the present contract and presented at international meetings. We then review the various techniques which are currently available for providing numerical solutions to the Navier-Stokes equations. Finally, the experimental program that has been carried out is described.

Section II. A Review of Recent Publications Produced Under the Present Contract

Measurements made in earlier AFOSR/BMO programs have been further analyzed during the past year to examine some fundamental fluid mechanical phenomena which are of significant importance in the design of hypersonic vehicles. From this work we have prepared and published two AIAA papers and one Ver Springer publication. Here we briefly summarize the results and conclusions from this work.

A knowledge of the occurrence and structure of boundary layer transition is one of the most important requirements for the accurate design of hypersonic re-entry vehicles. Apart from important increases in the levels of heating and skin friction which occur when transition takes place, boundary layer transition exerts a major influence on the size and structure of regions of viscous/inviscid interaction and the occurrence of flow separation. Thus, while meaningful studies of transition in hypersonic flow are difficult, through careful experiment and analysis insight can be gained on the key phenomena controlling transition and a body of information can be generated to model the transition phenomenon empirically.

In a number of earlier studies conducted for AFOSR and BMO we examined boundary layer transition on slender bodies with sharp and blunted leading nosetips and a number of different surface characteristics. One interesting feature of these studies (discussed in Appendix A) was that for the conditions at which they were conducted (Mach numbers above 11 in the large contoured nozzles), the laminar boundary became unstable in the 'classical' instability modes and the Reynolds numbers at which this occurred were very similar to those measured in ballistic range and flight tests. However, in the author's opinion, it is dangerous to trust in transition criteria developed from wind tunnel studies with the exception of those in which transition is tripped by internal mechanisms such as surface discontinuities or highly destabilizing phenomena such as shock/boundary layer interaction or surface blowing. It for this reason that most of the transition studies we have conducted have involved internally tripped flows. In a study to examine the influence of transition on the aerothermal characteristics of slender cones, we examined the effects of asymmetric transition regions on vehicle characteristics (see Appendix A). It was demonstrated that in flows where the boundary layer over the slender body has been stabilized with nosetip bluntness, wedge-shaped transition regions can readily be induced by small gouges in the nosetip or surface roughness near the nosetip. In contrast, gaps in the surface were not found to be effective trips. The destabilizing force levels generated by asymmetric transition regions were in agreement with calculations based on the asymmetric increased skin friction and pressure distributions induced by transition.

A body of measurements from flight tests, ballistic range and wind tunnel studies have suggested that stagnation point heating enhancement occurs as transition moves close to the stagnation region on a blunt body. While a number of mechanisms have been advanced to explain stagnation region heating enhancement, the phenomenon is not clearly understood. In a paper presented at the Thermophyics Conference in Williamsberg, and soon to be published in the AIAA "Advances Series," the results of a large number of studies performed over the past 10 years for AFOSR were examined to explore potential fluid mechanical mechanisms for enhanced stagnation region heating. In this paper (see Appendix B) mechanisms for enhanced heating associated with transition region proximity, surface roughness, surface blowing and shock layer/particle interaction were explored. It was concluded that the disturbance created by particle shock layer interaction can cause transient increases in the heat transfer rate to the stagnation region of a blunt body in high Reynolds number flows. High Reynolds number hypersonic facilities may be intrinsically susceptible to this problem and this aspect of their performance must be carefully monitored.

In a paper presented at the IUTAM Symposium on "Turbulent Shear Layer Shock/Wave Interaction" (Sept. 9-12, 1985), a review was presented on Aerothermal Problems Associated with Viscous/Inviscid Interaction over Hypersonic Flight Vehicles; this review is presented in Appendix C.

Section III. Summary of Existing Solution Technique

3.1 Introduction

While the Navier-Stokes equations were formulated nearly 140 years ago, only recently has computational speed increased enough to handle the entire set of instantaneous equations. Even with the advent of the new generation "super" computers (e.g., CRAY1, CRAYXMP, CDC7600, new generation array processors, etc.), economics remains a major consideration. However, D.R. Chapman[7] noted the cost of these types of calculations have been decreasing by a factor of ten every eight years. It may be just a matter of time before these types of large numerical simulations are of some consequential value to a practical engineering problem.

In most applications to turbulent flows, the Navier-Stokes equations are simplified by Reynolds time averaging. We are then faced with the difficult task of developing a model for turbulence. There have been many approaches to the turbulent closure problem, from simple algebraic closure to various two equation models (e.g., k-e, k-w, see Anderson and Tannehill[8], Tennekes and Lumley[9], Jones and Launder[10]), and the Reynolds stress equations. The lack of progress in this area stems from three basic reasons. One, we lack the physical understanding to model these complex turbulent flows. Two, we lack the computational resources to deal with so-called higher order turbulence models, which add nine more unknowns (in an incompressible flow) and two or three more equations. Three, we still lack the ability to solve the laminar portion of the Navier-Stokes equations in an efficient and accurate manner. Most existing differencing schemes (which will be discussed here) are second-order accurate with various restrictions applied by the numerical stability. The various techniques that have been used to solve these equations are reviewed in this section.

There are several levels of complexity of Navier-Stokes equations which fall between a full Navier-Stokes equation (see Table 1) and a boundary layer equation. Common names for these types of equations are "parabolized" Navier-Stokes equations and "thin-layer" Navier-Stokes equations. These sets of equations are characterized by their applicability in both viscous and inviscid flow regions; they all contain the normal pressure terms which are usually dropped in any boundary layer formulation.

Table 1
CLASSIFICATION OF NAVIER-STOKES EQUATIONS

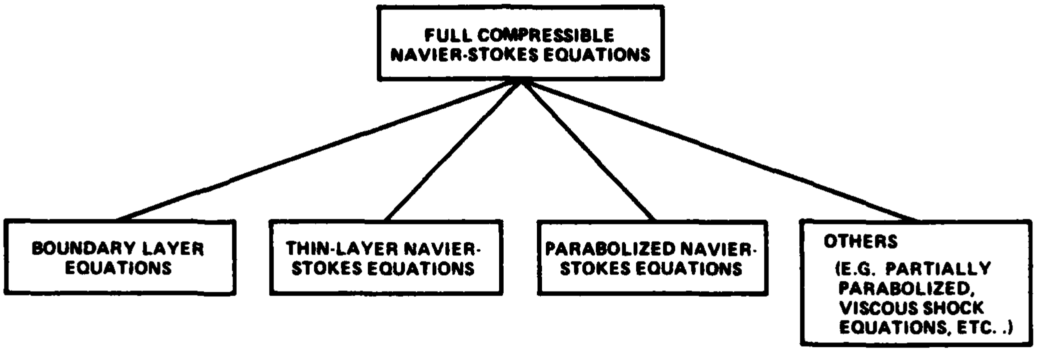
FULL COMPRESSIBLE NAVIER-STOKES EQUATIONS
BOUNDARY LAYER EQUATIONS
THIN-LAYER NAVIER-STOKES EQUATIONS
PARABOLIZED NAVIER-STOKES EQUATIONS
OTHERS (E.G. PARTIALLY PARABOLIZED, VISCOUS SHOCK EQUATIONS, ETC. .)

COMPRESSIBLE NAVIER-STOKES EQUATIONS*

$$\frac{\partial U}{\partial t} + \frac{\partial E}{\partial x} + \frac{\partial F}{\partial y} = 0$$

$$U = \begin{array}{l} \rho \\ \rho u \\ \rho v \\ E_t \end{array}$$

$$E = \begin{array}{l} \rho u \\ \rho u^2 + P - \tau_{xx} \\ \rho uv - \tau_{xy} \\ (E_t + P)\, u - u\tau_{xx} - v\tau_{xy} + q_x \end{array}$$

$$F = \begin{array}{l} \rho v \\ \rho uv - \tau_{yy} \\ \rho v^2 + P - \tau_{yy} \\ (E_t + P)\, v - u\tau_{xy} - v\tau_{yy} + q_y \end{array}$$

$$\tau_{xx} = \frac{2}{3}\mu(2\ \frac{\partial y}{x} - \frac{\partial v}{y})$$

$$\tau_{yy} = \frac{2}{3}\mu(2\ \frac{\partial v}{y} - \frac{\partial u}{x})$$

$$\tau_{xy} = \tau_{yx} = \mu(\frac{\partial v}{\partial y} + \frac{\partial y}{\partial x})$$

$$q_y = -K\ \frac{\partial T}{\partial y}$$

$$q_x = -K\ \frac{\partial T}{\partial x}$$

$$E_t = (P + \frac{U^2 + v^2}{2})$$

THIN-LAYER NAVIER-STOKES EQUATIONS*

$$\frac{\partial U}{\partial t} + \frac{\partial E}{\partial x} + \frac{\partial F}{\partial y} = 0$$

$$U = \begin{array}{l} \rho \\ \rho u \\ \rho v \\ E_t \end{array}$$

$$E = \begin{array}{l} \rho u \\ \rho u^2 + P \\ \rho uv \\ (E_t + P)u \end{array}$$

$$F = \begin{array}{l} \rho v \\ \rho uv - \mu\frac{\partial u}{\partial y} \\ \rho v^2 + P - \frac{4}{3}\mu\frac{\partial v}{\partial y} \\ (E_t + P)\, v - u(\mu\frac{\partial u}{\partial y}) \\ - v(\frac{4}{3}\mu\ \frac{\partial v}{\partial y}) - K\ \frac{\partial T}{\partial y} \end{array}$$

- ASSUMPTION MADE WAS THAT ALL VISCOUS TERMS CONTAINING DERIVATIVES PARALLEL TO THE WALL ARE DROPPED.

PARABOLIZED NAVIER-STOKES EQUATIONS*

$$\frac{\partial E}{\partial x} + \frac{\partial F}{\partial y} = 0$$

$$E = \begin{array}{l} \rho u \\ \rho u^2 + P \\ \rho uv \\ (E_t + P)u \end{array}$$

$$F = \begin{array}{l} \rho v \\ \rho uv - \mu\frac{\partial u}{\partial y} \\ \rho v^2 + P - \frac{4}{3}\mu\frac{\partial v}{\partial y} \\ (E_t + P)\, v - u(\mu\frac{\partial u}{\partial y}) \\ - v(\frac{4}{3}\mu\ \frac{\partial v}{\partial y}) - K\ \frac{\partial T}{\partial y} \end{array}$$

- PARABOLIC TYPE OF EQUATIONS WILL NORMALLY DROP ($\frac{\partial P}{\partial x}$) TO ACHIEVE PARABOLIC NATURE, BUT IT WAS LATER ADDED TO ACHIEVE MORE GENERAL FORMULATION.**
- NORMALLY WRITTEN IN A FORM WHERE THE VISCOUS AND INVISCID TERMS ARE SEPARATED.**

*ALL EQUATIONS ARE WRITTEN IN TWO-DIMENSIONAL FORM.

**SEE TANNEHILL (1984) FOR FURTHER DETAIL.

Table 1
CLASSIFICATION OF NAVIER-STOKES EQUATIONS (Cont.)

SCHEME PROPOSED TO DATE

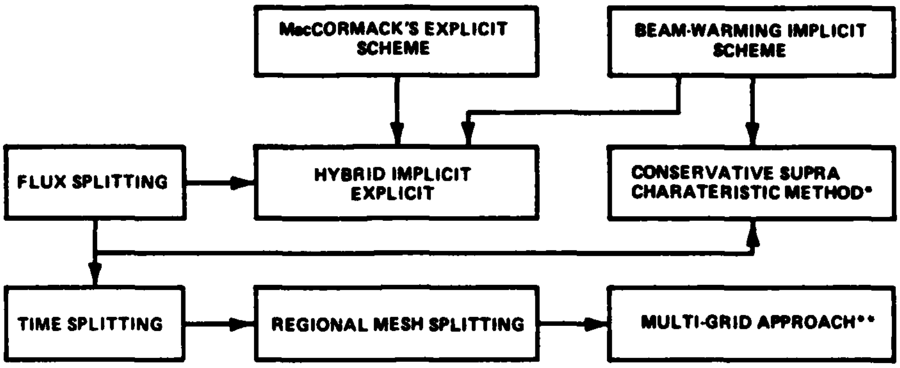
MacCORMACK'S EXPLICIT SCHEME
BEAM-WARMING IMPLICIT SCHEME
FLUX SPLITTING
HYBRID IMPLICIT EXPLICIT
CONSERVATIVE SUPRA CHARATERISTIC METHOD*
TIME SPLITTING
REGIONAL MESH SPLITTING
MULTI-GRID APPROACH**

*ONLY KNOWN APPLICATION TO DATE WAS FOR THE PNS.

**APPLIED AS EULER SOLVER BY JAMESON (1986); NOT DISCUSSED IN PRESENT REPORT

***ALL METHODS ARE APPLICABLE TO BOTH FULL COMPRESSIBLE N-S EQUATIONS AND ANY OTHER SIMPLER VERSIONS OF N-S.

To arrive at the thin layer approximation shown in Table 1, a scaling argument is used (see Anderson and Tannehill[8]), and terms on the order of 1/ReL and smaller are neglected. Here all viscous terms containing derivatives parallel to the wall are dropped because they are substantially smaller than the viscous terms normal to the wall. If this same argument were to be used for the normal (y) direction, the equation could be reduced to dp/dy=0. For this approximation to handle a possible flow reversal, it is necessary to retain all terms in the momentum equations except for the viscous terms parallel to the flow (the upstream diffusion terms). The final set of equations are as shown in Table 1, in Cartesian coordinate system. This mixed set of hyperbolic-parabolic partial differential equations are solved instead of the elliptic-hyperbolic partial differential equations, using a "time-dependent" approach. The overall complexity of the equations are reduced, but the difficulty of solving a hyperbolic system still remains.

The parabolized Navier-Stokes equations are derived using an argument similar to the employed to derive the thin-layer equations. An asymptotic expansion (see Karvorkin and Cole[11]) is performed (Rudman and Rubin[12]) with the Navier-Stokes equations, and all of the terms exhibiting characteristic order of magnitude of (1/δ*2) or higher are retained. The normal pressure gradient terms are deleted from the x-momentum equation, which restricts the solutions of the flows without upstream influences. The most commonly used form of the parabolized Navier-Stokes equations (formulated by Cheng[13]) contained the streamwise pressure gradient term. Thus, the most common form of this type of equation is obtained by assuming that only the streamwise viscous derivative terms and the heat flux terms are negligible compared to the normal transverse viscous derivative terms. The parabolized Navier-Stokes equations are derived by dropping all viscous and heat flux terms containing partial derivatives with respect to the streamwise direction, from a steady Navier-Stokes equation. A set of parabolized Navier-Stokes equations are shown in Table 1.

3.2 Numerical Schemes

The numerical scheme most widely used today is the explicit differencing scheme, first proposed by R. MacCormack[14], and the implicit method of Beam-Warming[15]. There has been no new scheme developed since these were introduced, but there has been considerable effort in the CFD (computational fluid dynamic) field to improve the efficiency and accuracy of these two schemes. The terms like "strongly-implicit," "time-sharing," "flux-splitting," "implicit-explicit," "computational-sublayer," "multi-grid" and "CSMS" are some of the terms used to describe these improvements. These terms will be explained further below with some examples. The present work will deal mainly with technology presently available for solving various forms of the Navier-Stokes equations.

3.3 Explicit Scheme of MacCormack

This scheme is the easiest to understand and use. The basic development is as follows:

One-dimensional wave equation $\frac{\partial^2 u}{\partial t^2} = c^2 \frac{\partial^2 u}{\partial x^2}$

Predictor $u_j^{\overline{n+1}} = u_j^n - c\frac{\Delta t}{\Delta x}\left(u_{j+1}^n - u_j^n\right)$

Corrector $u_j^{n+1} = \frac{1}{2}\left[u_j^n + u_j^{\overline{n+1}} - c\frac{\Delta t}{\Delta x}\left(u_j^{\overline{n+1}} - u_{j-1}^{\overline{n+1}}\right)\right]$

Notice that the forward differencing in space and time is done in the predictor step, and the corrector step is used to perform a backward differencing in space and time, which leads to an overall differencing scheme with second order accuracy.

Applied to three-dimensional Navier-Stokes equations $\frac{\partial U}{\partial t} + \frac{\partial E}{\partial x} + \frac{\partial F}{\partial y} + \frac{\partial G}{\partial z} = 0$

Predictor $u_{ijk}^{\overline{n+1}} = u_{ijk}^n - \frac{\Delta t}{\Delta x}\left(E_{i+1jk}^n - E_{ijk}^n\right) - \frac{\Delta t}{\Delta y}\left(F_{ij+1k}^n - F_{ijk}^n\right) - \frac{\Delta t}{\Delta z}\left(G_{ijk+1}^n - G_{ijk}^n\right)$

Corrector $u_{ijk}^{n+1} = \frac{1}{2}\left[u_{ijk}^n + u_{ijk}^{\overline{n+1}} - \frac{\Delta t}{\Delta x}\left(E_{ijk}^{\overline{n+1}} - E_{i-1jk}^{\overline{n+1}}\right) - \frac{\Delta t}{\Delta y}\left(F_{ijk}^{\overline{n+1}} - F_{ij-1k}^{\overline{n+1}}\right) - \frac{\Delta t}{\Delta z}\left(G_{ijk}^{\overline{n+1}} - G_{ijk-1}^{\overline{n+1}}\right)\right]$

(see MacCormack[16])

The numerical stability analysis is done by analyzing the linear/non-linear terms separately (MacCormack[14,17]) which leads to the following equation:

$$(\Delta t)_{CFL} \leq \left(\frac{|u|}{\Delta x} + \frac{|v|}{\Delta y} + \frac{|w|}{\Delta z} + C\sqrt{\frac{1}{(\Delta x)^2} + \frac{1}{(\Delta y)^2} + \frac{1}{(\Delta z)^2}} \right)^{-1}; \; C = \sqrt{\frac{\gamma P}{\rho}}$$

This statment indicates that largest time step (Δt) corresponds to smallest length scale of the problem.

The major disadvantage of this scheme is that the stability conditions are set so that the entire time dependent marching is done at the smallest time scale of the flow, which corresponds to the smallest length scale. This is a major limitation of the scheme, since the scale length that needs to be resolved in the viscous layer close to the wall (Stwertson[18]) are of an order of magnitude smaller than those required in the inviscid flow. This problem could be illustrated easily by stating the statistic of the flat plate solution *obtained* using the Shang-Hankey explicit code (described later). The converged solution required 40,000 time steps at a time step size of 10×10^{-1} seconds at a computational cost of $1,500 (40 min of CPU time) for a two-dimensional flat plate solution at Mach 11.6. Clearly, this limitation imposes severe time requirements when the higher order turbulence models are added and the algorithm is extended to three-dimensional flows.

3.4 Implicit method of Beam-Warming

The Beam-Warming implicit scheme is used with a conservative form of the Navier-Stokes equations:

$$\frac{\partial u}{\partial t} + \frac{\partial F(u)}{\partial x} + \frac{\partial G(u)}{\partial y} = \frac{\partial V(u, u_x, u_y)}{\partial x} + \frac{\partial W(v, u_x, u_y)}{\partial y}$$

The differencing scheme could be summarized by the following:

$$\left\{\text{Numeric}\right\} \delta u_{ij}^{n+1} = -\Delta t\left(\frac{DF}{\Delta x} + \frac{DG}{\Delta y}\right); \frac{D}{\Delta x} \text{ Difference operators}$$

A numerical procedure used to advance the Navier-Stokes Equations in time at each mesh point is

$$\Delta u_{ij}^{n} = -\Delta t\left(\frac{DF}{\Delta x} + \frac{DG}{\Delta y}\right)_{ij}^{n}$$

-explicit local approximation of the right-hand side of the difference equation. Differencing over space represents the physics of the flow.

$$\left\{I + \Delta t \frac{DA}{\Delta x} + \Delta t \frac{DB}{\Delta y}\right\} \delta u_{ij}^{n+1} = \Delta u_{ij}^{n}$$

-place the locally calculated solutions into an implicit form, numeric part (coefficient matrix operator) of the equation is then inverted to solve for a change in flow property.

$$u_{ij}^{n+1} = u_{ij}^{n} + \delta u_{ij}^{n+1}$$

-update solution in time.

In order to arrive at two tridiagonal matrices, the coefficient matrix operator is factored into:

$$\left\{I + \Delta t \frac{DA}{\Delta x} + \Delta t \frac{DB}{\Delta y}\right\} \text{ is then factored into } \left\{I + \Delta t \frac{DA}{\Delta x}\right\} \left\{I + \Delta t \frac{DB}{\Delta y}\right\}$$

which introduces an error term when multiplied together and compared with the original differencing scheme.

$$\Delta t^{2} \frac{DA}{\Delta x} \frac{DB}{\Delta y}$$

Thus this error term introduces a set of stability conditions which limits the size of the timesteps.

The Beam-Warming implicit method differs from MacCormack's explicit method in that all of the unknown quantities are formulated as functions of the known quantities and not as finite differenced values of the known quantities. Thus, the implicit method requires an inversion of a coefficient matrix in order to solve for the updated value (u_{ij}^{n+1}). This method has an advantage over the explicit method; it is no longer bounded by the numerical stability in time-marching of the solution. Thus, the major obstacle for an implicit method from having a one-step convergence is the lack of an efficient inversion technique for pentadiagonal matrix operators. In order to avoid this difficulty (of inverting large matrices) most implicit methods separate their coefficient matrix in to series of tridiagonal matrices for which there are inversion techniques readily available (e.g., Thomas' algorithm). This separation thus causes an unwanted numerical stability conditions similar to the explicit methods.

3.5 Implicit (Explicit) method of MacCormack

In order to overcome the restriction of his earlier explicit scheme, MacCormack[19] proposed a two-step approach to this problem. First, the local fluid properties are calculated based on his explicit scheme. Then, the time marching is done using an implicit scheme. The implicit formulation is very similar to that of Beam-Warming; thus, it is also faced with the problem of inverting a large, higher order matrix operator. The coefficient matrix operators are separated into several tridiagonal matrices, causing an unwanted restriction on the timestep sizes. MacCormack[19] made several attempts to further reduce the problem into bi-diagonal problems, but had very little success with the boundary conditions on the implicit part of the problem.

Example of the numerics are:

$$\left\{I+\Delta t\left(\frac{D_+A_-}{\Delta x}+\frac{D_-A_+}{\Delta x}-\frac{D_-M_x\frac{D_+N}{\Delta x}}{\Delta x}\right)+\Delta t\left(\frac{D_+B_-}{\Delta y}+\frac{D_-B_+}{\Delta y}-\frac{D_-M_y\frac{D_+N}{\Delta y}}{\Delta y}\right)\right\}\delta u_{ij}^{n}$$

$$=\Delta u_{ij}^{n}=\text{Explicit Scheme}$$

where the vectors are defined by MacCormack[19].

3.6 Conservative Supra-Characteristic Method (CSCM)

CSCM was first proposed by Lombard[20,21,22] to solve the Parabolized Navier-Stokes (PNS) equations, and has recently been utilized by Tannehill[23] to yield some excellent results for laminar shock/boundary layer interaction problems. The CSCM method separates the equations' coefficients into a series of eigenvectors according to their signs. This effectively separates the hyperbolic (conservative) terms of the matrix, which in turn are easier to difference (e.g., negative-backward difference only, positive-forward difference only). This separation also allows the differencing to take place using either the characteristic or the dynamic form of the gas dynamics equations. Lombard[22] was later able to propose a stable space marching technique. The major advantage of this process over other processes is its ability to sweep forward and backward, whereby the upstream influence is efficiently transmitted downstream. The core origin of this method extends from the Split Coefficient Method of Chakravarthy[24] (also see Anderson and Tannehill[8]).

3.7 Flux splitting

The flux splitting method was originally developed by Steger and Warming[25] and used to describe a procedure which takes into consideration the direction of information travel to compute the fluxes; therefore, the physics of the governing equations are more efficiently calculated. The basic splitting procedure is based on the fact that the coefficient matrix or numerical vector could be separated by the sign of its components. Thus, the numerics are written to accommodate the directionality of the numerical information travel, which eliminates the need for differencing unrelated variables. The ability of this technique to handle a sonic line has proven to be poor as compared to other schemes, because of a small numerical oscillation caused by the change in sign of the eigenvector when the first derivatives are discontinous. But Steger[26] later reported excellent success with redefined eigen value.

Based on the property of an eigenfunction which states that:

$$[A] = [T][\lambda][T]^{-1} = [A]^{+} + [A]^{-} = [T][\lambda^{+}][T]^{-1} + [T][\lambda^{-}][T]^{-1}$$

Thus, each of the vectors in the Navier-Stokes equations could be written as:

$$\frac{\partial u}{\partial t} + \frac{\partial E}{\partial x} = 0 \; ; \; \frac{\partial u}{\partial t} + \frac{\partial E^{+}}{\partial x} + \frac{\partial E^{-}}{\partial x} = 0$$

and when applied to the explicit scheme,

$$u_j^{\overline{n+1}} = u_j^{n} - \frac{\Delta t}{\Delta x}\left(\Delta E_j^{+} + \Delta E_j^{-}\right)$$

but most commonly applied to implicit formulations to separate the flux direction as shown.

$$\left\{ I + \frac{\Delta t}{\partial \Delta x}\left(\Delta [A_j]^{+} + \Delta [A_j]^{-}\right)\right\} \Delta U_i^{n} = -\frac{\Delta t}{\Delta x}\left[\Delta E^{+} + \Delta E^{-}\right]$$

3.8 Time splitting

The term "time splitting" originates from the original work of MacCormack[17], and MacCormack and Baldwin[16]. The main idea of the time split method is to split the original MacCormack explicit scheme into a series of one-dimensional operators, thereby achieving less restrictive stability conditions. In this approach, the original MacCormack explicit scheme is split into a series of one-dimensional operators, to achieve less restrictive stability conditions. The computation can progress in any local region with the maximum allowable timesteps in any direction. This scheme is extremely advantageous if the allowable local timestep is much different from the maximum allowable timestep, due to differences in mesh spacing. Other properties of this scheme are: (1) it is numerically stable, as long as the local timestep of each operator does not exceed the allowable total timestep size of the operator, ($\Delta t_1 \leq \Delta t_m$); (2) consistent, if the sum of the timestep for each operator is equal ($\Delta t = \Delta t_1 + \Delta t_{12} \ldots$); (3) second order accurate, if the sequence is symmetric ($L_y L_x L_y$, or $L_x L_y L_x$, and not $L_y L_y L_x$).

Application of this method is often written in the following form:

$$u^{m+1} = L_x L_y u^m$$

where L_x, L_y are defined to be one-dimensional operators defined below.

$$L_x : \; u_{ij}^{\overline{m+1}} = u_{ij}^{m+1/2} - \frac{\Delta t}{\Delta x}\left(F_{ij}^{m+1/2} - F_{i-1j}^{m+1/2}\right)$$

Forward

$$u_{ij}^{m+1} = \frac{1}{2}\left\{u_{ij}^{m+1/2} + u_{ij}^{\overline{m+1}} - \frac{\Delta t}{\Delta x}\left[F_{ij}^{\overline{m+1}} - F_{i-1j}^{\overline{m+1}}\right]\right\}$$

Backward

Ly is similar in formulation but differenced along the y direction. Note that the local timestep size may be different in either direction, but must add up to the same.

3.9 Computational sub-layer

This is a concept first introduced by D. Knight[27] to solve a supersonic inlet problem, this approach differs from previous efforts in that an improved algorithm is made by utilizing the physical understanding of the problem and not by trying to find ways of improving overall differencing schemes. Knight further improved the computational efficiency by applying the concept of computational sub-layer. The core differencing scheme utilized by Knight is a time-splitted MacCormack explicit scheme, however, he was able to overcome all of the critical faults of the stability conditions by incorporating a separate algorithm for dealing with the viscous sublayer and wall regions of the turbulent boundary layers. This is the region which he calls the computational sublayer.

The governing equations for the computational sublayer are derived using a set of arguments analogous to those of the boundary layer equations. The assumptions made are 1) negligible streamwise variation of mass, momentum, and total enthalpy, 2) boundary layer approximations, 3) the height of CSL is small compared to the curvature of the wall (if any), 4) constant pressure across the layer (dp/px=0), and 5) velocity in the cross stream direction is negligible $(v^{12}2c^2/(\gamma-1)$. Thus the set of governing equations are:

$$\dot{m}\frac{\partial u}{\partial y} = -\frac{\partial D}{\partial x} + \frac{\partial \tau_{xy}}{\partial y} \quad \text{Momentum Eqn.}$$

where m = normal mass flux at the surface

$$\frac{\partial}{\partial y}\left[\dot{m}\left(CPT + \frac{1}{2}u^2\right) + Q_y - u\tau_{xy}\right] = 0 \quad \text{En. Eqn.}$$

where

$$\tau_{xy} = (\mu + \varepsilon)\frac{\partial u}{\partial y}$$

$$Q_y = -C_p\left(\frac{\mu}{P_r} + \frac{\varepsilon}{P_{r t}}\right)\frac{\partial T}{\partial y}$$

The solutions to the computational sublayer are then used to update the information near the wall region in the overall explicit flow calculations, which eliminated the need for resolving the length scale in the viscous layer near the wall.

This type of formulation allowed Knight[28] to solve larger and more complex three-dimensional problems in his later efforts. There are very few known successful efforts made in three-dimensional problems due to the lack of both appropriate hardware and software. In fact, Knight[28], Horstmann[29], Shang[30] and Kumar[31] are the only known successful efforts made in solving a three-dimensional problem using a full set of Navier-Stokes equations. There also has been considerable effort made in solving three-dimensional PNS equations (e.g., Tannehill). Further efforts made by Knight[32] to add various turbulence models of Baldwin-Lomax[33], and Jones-Launder[10] yielded some excellent results in his latest effort.

Section IV. EXPERIMENTAL PROGRAM

4.1 Program Objective and Design of the Experimental Study

The major objective of the current study was to develop and use models and instrumentation to obtain detailed measurements of the profile characteristics of a turbulent boundary layer ahead and through regions of flow separation induced by shock wave/boundary layer interaction over a cone/flare configuration. Such measurements are of key importance in the evaluation of the theoretical modeling of the turbulent separation process in hypersonic flows. As discussed in the introduction, current turbulence models apparently are incapable of describing the development of turbulence in regions of strong pressure gradients and boundary layer separation in hypersonic flow, possibly because of compressibility, shock/turbulence interaction, or unsteady effects under hypersonic highly-cooled wall conditions. Because in hypersonic high Reynolds number flows over highly-cooled walls the "wall layer," in which our earlier studies have suggested separation first takes place, and which contain the principal information on the character of the boundary layer, is very thin. Boundary layer thicknesses of over 1 inch are required to enable this layer to be probed with the required resolution. While the turbulent boundary layer on the walls of hypersonic nozzles have been used as the source of thick turbulent boundary layers in experimental studies, it has been shown that significant turbulent non-equilibrium effects can exist in these nozzle flows[37]. The distortion of the structure and turbulent characteristics of the boundary layer generated through the strong expansion in the nozzle can persist well downstream of the nozzle exit plane and can significantly influence the characteristics of a separating turbulent boundary layer. For this reason we elected to perform studies to examine the characteristics of the turbulent boundary ahead and in regions of shock wave/boundary layer interaction on a large slender cone/flare configuration in the large contoured "D" nozzle in the 96-Inch Shock Tunnel. The technique employed in the design of the "D" nozzle, and indeed most contoured nozzles, is such that the test core is a cone-shaped region of uniform flow which originates well upstream of the exit plane. Thus, by designing a conical model so that it can be fit within this uniform conical region it is possible to develop a constant pressure boundary layer over a large conical model which extends well into the contoured nozzle. The ultimate objective of this study is to obtain both mean and fluctuation measurements on the surface and across the turbulent layer. However, during this phase of the study we concentrated on obtaining measurements of the mean properties across the viscous layer, more specifically to obtain measurements of the pitot pressure, total temperature, total heat transfer rate and, using holographic interferometry, the mean density distribution.

4.2 Models and Instrumentation

The experimental studies were conducted in the Calspan 96-Inch Shock Tunnel at Mach numbers of 11 and 13 in the large contoured "D" nozzle. As discussed in the previous section, the large conical region of uniform flow which extends well up into the contoured "D" nozzle allows us to generate a constant pressure boundary layer on a conical model which extends into the nozzle.

For these studies we selected the large 6 degree cone with flares of 30 and 36 degrees attached at its base. The cone/flare configuration is shown in Figure 1. The cone angle and length were selected on the basis of calculations to achieve the maximum length over which uniform constant pressure flow could be established within the furthe constraints of tunnel blockage and sting loading. A diagram of the cone/flare model and its positioning within the "D" nozzle is shown in Figure 2. In an initial study to demonstrate that this large model could be used to produce the required flow we obtained pressure and heat transfer for this model equipped with both sharp and blunt nosetips. The good agreement between the measured pressure and heat transfer distribution and theory for these configurations, shown in Figures 3-6, demonstrate that the design and positioning of the model have produced the required testing environment. Schlieren photographs of the flow field for these cases are shown in Figures 7 and 8.

4.2.1 Heat Transfer Instrumentation

Platinum thin-film instrumentation was used to obtain heat transfer measurements on the surface of the flat plate/cone model and as the sensing element of the .05-inch diameter stagnation heating probes. Because this gage has a megahertz frequency response, it can be used to examine the unsteady characteristics of the turbulent boundary layer and separated region. The large gradients which are generated along the walls and in the flow in the separation and reattachment region of shock wave/boundary layer interactions make it essential that distortion of the heat transfer distribution resulting from lateral heat conduction be minimized by employing models constructed with low conductivity materials. The pyrex-backed thin-film gages with their high resolution, sensitivity and frequency response are almost ideal for this type

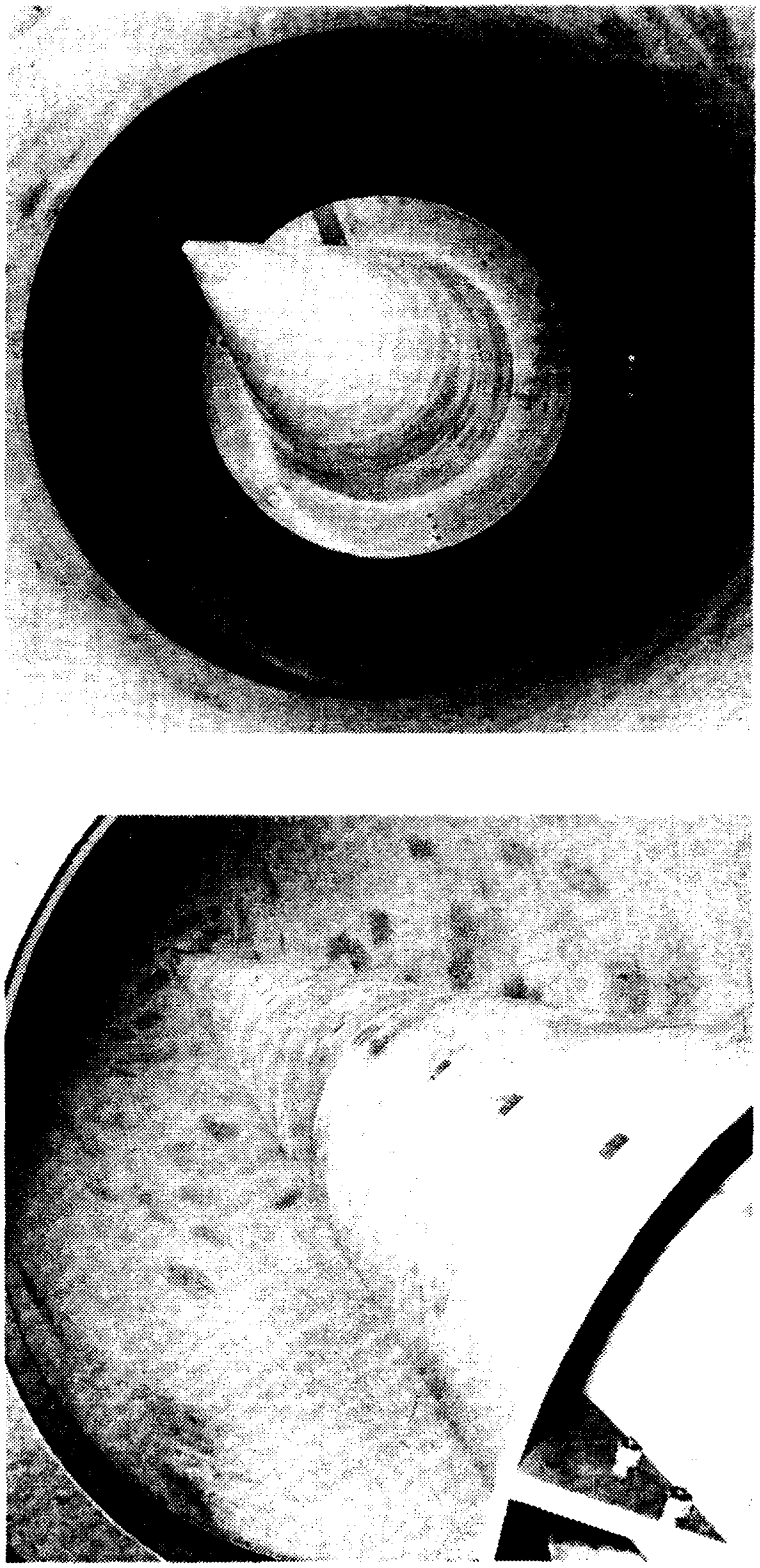

Figure 1 SHARP 6° CONE/30° FLARE MODEL INSTALLED IN CALSPAN'S 96" SHOCK TUNNEL

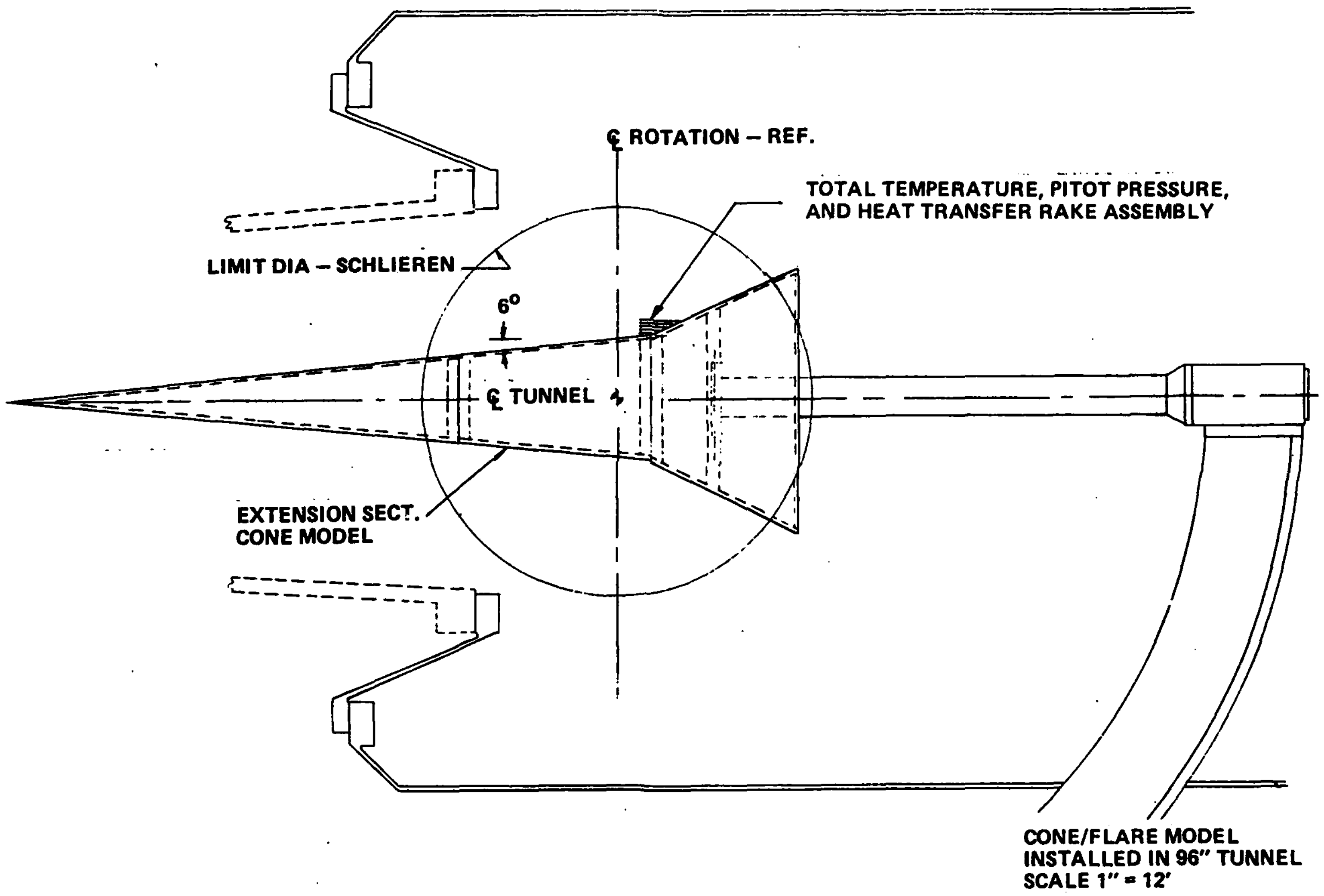
℄ ROTATION – REF.
TOTAL TEMPERATURE, PITOT PRESSURE, AND HEAT TRANSFER RAKE ASSEMBLY
LIMIT DIA – SCHLIEREN
6°
℄ TUNNEL
EXTENSION SECT. CONE MODEL
CONE/FLARE MODEL INSTALLED IN 96" TUNNEL SCALE 1" = 12'

Figure 2 INSTALLATION DRAWING OF CONE/FLARE MODEL

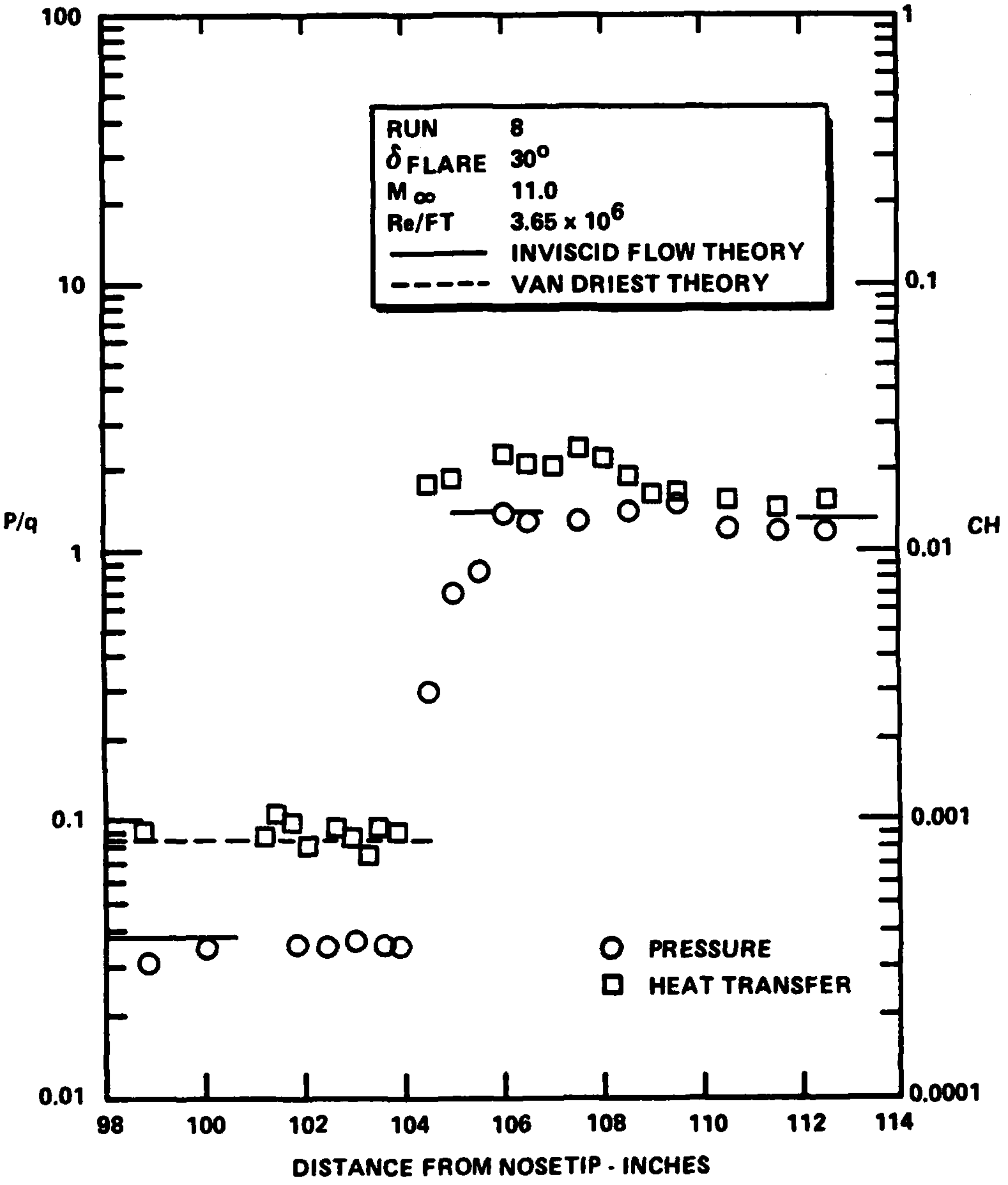

Figure 3 DISTRIBUTION OF PRESSURE AND HEAT TRANSFER IN ATTACHED FLOW OVER THE LARGE 6° CONE/30° FLARE CONFIGURATION

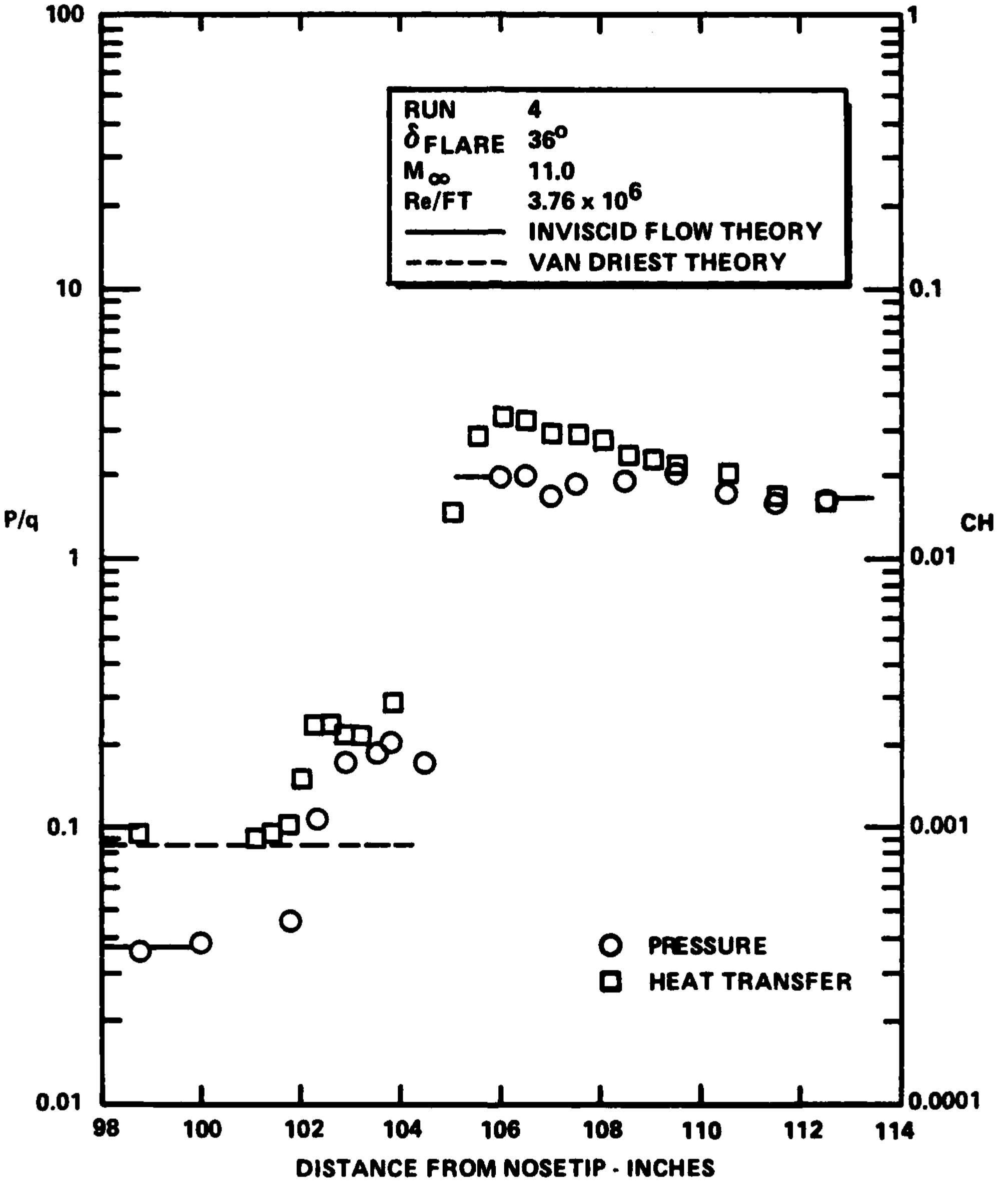

Figure 4 DISTRIBUTION OF PRESSURE AND HEAT TRANSFER IN ATTACHED FLOW OVER THE LARGE 6° CONE/36° FLARE CONFIGURATION

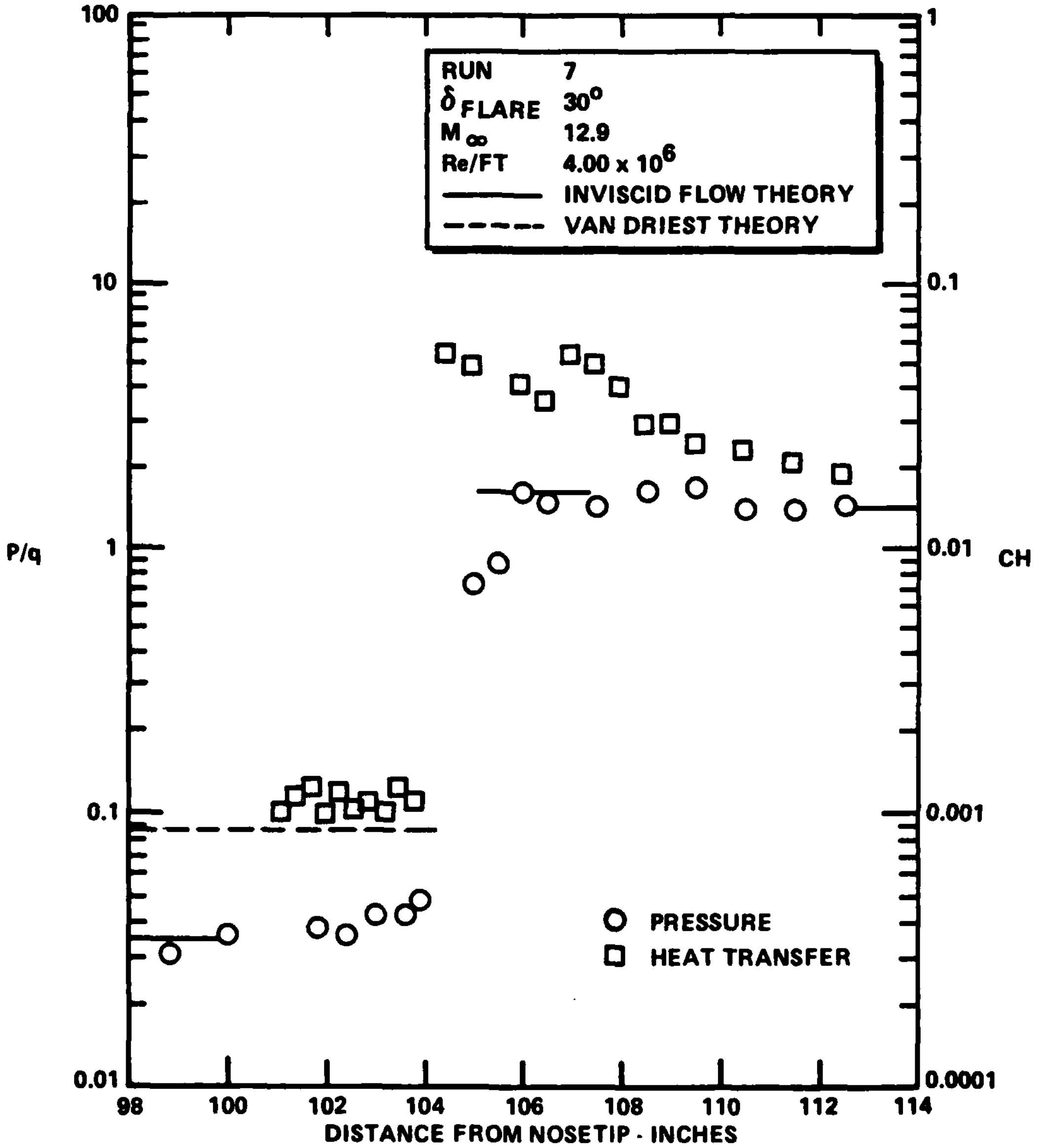

Figure 5 DISTRIBUTION OF PRESSURE AND HEAT TRANSFER IN ATTACHED FLOW OVER THE LARGE 6° CONE/30° FLARE CONFIGURATION

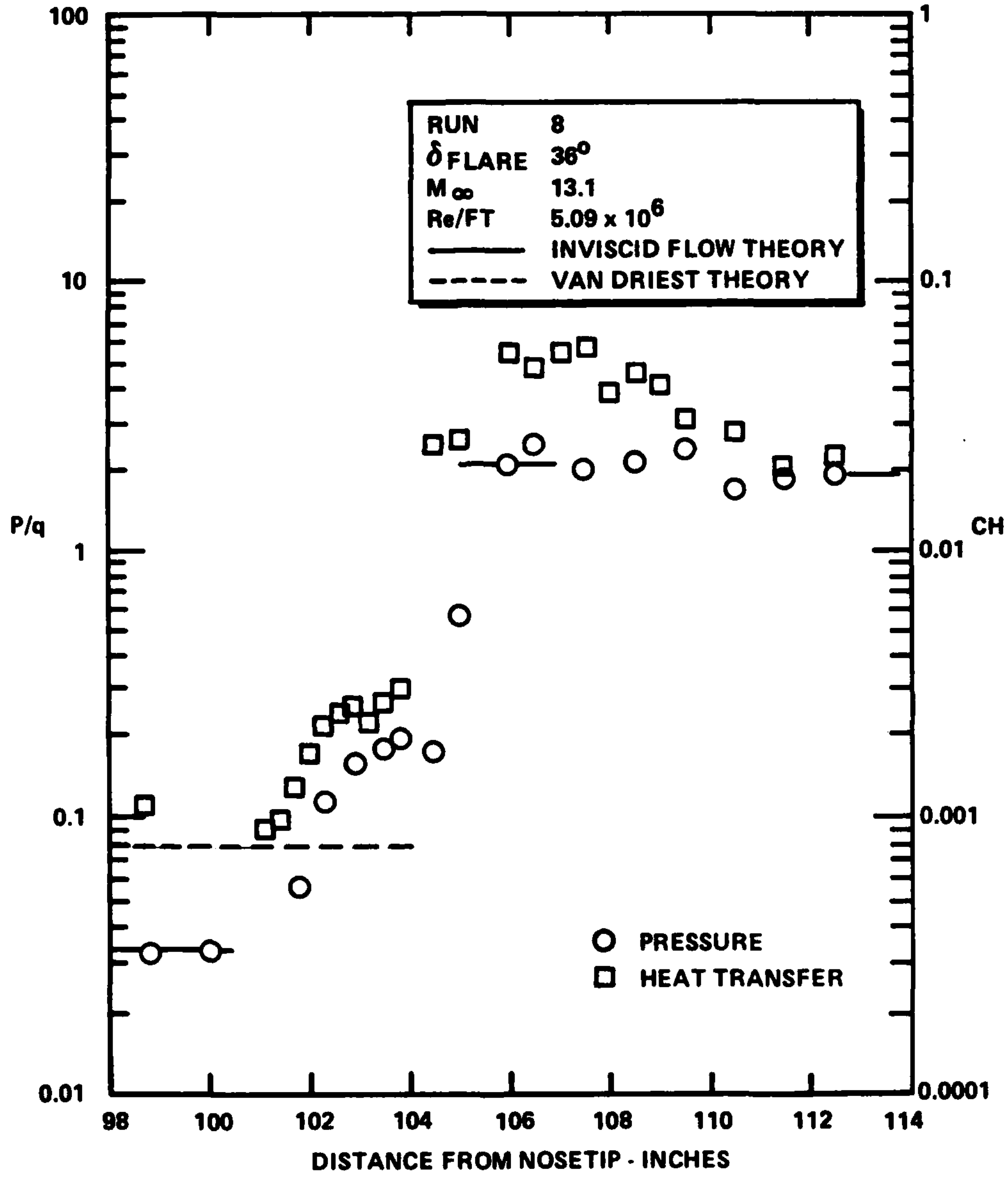

Figure 6 DISTRIBUTION OF PRESSURE AND HEAT TRANSFER IN SEPARATED FLOW OVER THE LARGE 6° CONE/36° FLARE CONFIGURATION

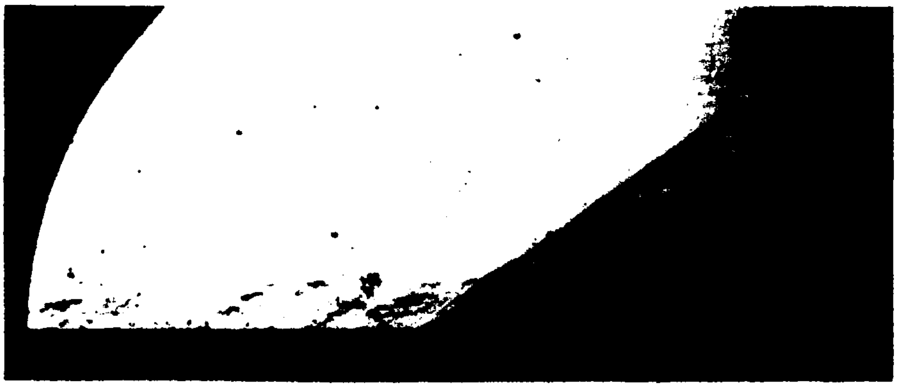

Figure 7a ATTACHED FLOW OVER CONE/FLARE CONFIGURATION, M = 11

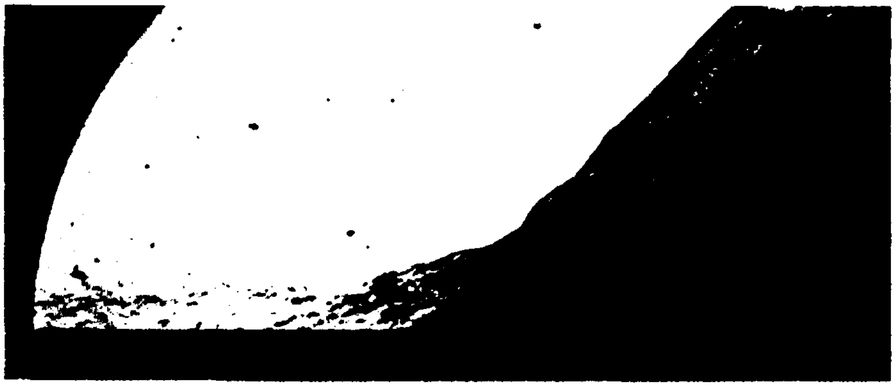

Figure 7b SEPARATED FLOW OVER CONE/FLARE CONFIGURATION, M = 11

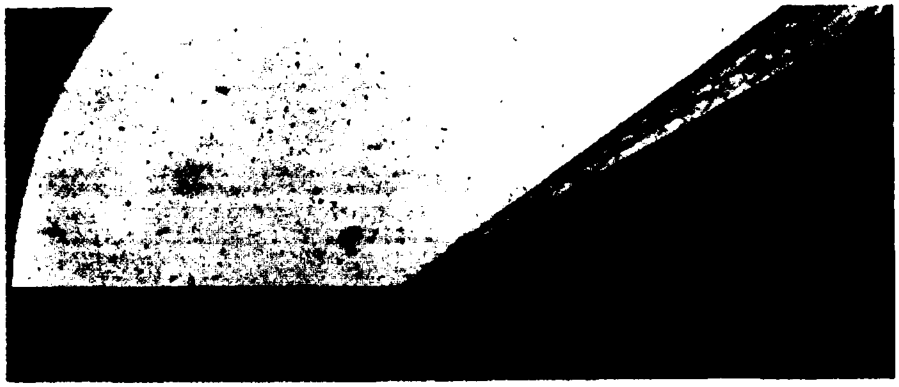

Figure 8a ATTACHED FLOW, M = 13

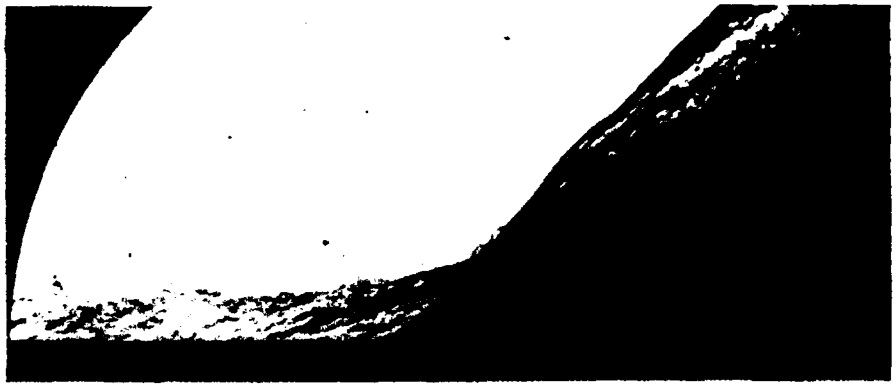

Figure 8b SEPARATED FLOW, M = 13

of study. The platinum thin-film probes shown in Figure 9 were used, in conjunction with the total temperature instrumentation, to examine the structure of the turbulent boundary layer and shear layer.

4.2.2 Pitot and Static Pressure Instrumentation

We used Calspan piezoelectric pressure transducers mounted in pitot pressure rakes, beneath orifices in the model surface, to obtain the mean pitot pressure through the boundary layer and along the surface. The pitot pressure gages had .030 orifices and were staggered as shown in Figure 9 to achieve a transverse spacing of .010 at the base of the boundary layer.

4.2.3 Total Temperature Instrumentation

A significant effort was devoted to the design and development of a total temperature gage which responded within 3 milliseconds, withstood the large static and dynamic pressures generated in regions of shock/boundary layer interaction in the shock tunnel flows, and was small enough to resolve the total temperature in the wall layer. The result of this development was a gage .030 inches in diameter which used a .0005 butt-welded iron/constantin thermocouple in the arrangement shown schematically in Figure 10. The typical response of one of these gages (Figure 11) clearly shows we have adequate time to obtain accurate measurement. A small (~2%) radiation is applied and this factor is checked for measurements in the freestream where the total temperature is known accurately. The gages are deployed in a staggered array (see Figure 9) similar to that employed for the pitot pressure gages.

4.2.4 Test Conditions and Model Configurations

The experimental studies were conducted at Mach 11, 13 and 16 for Reynolds numbers from 30 x 10^6 to 80 x 10^6. Under these conditions, the boundary layer is fully turbulent well upstream of the cone/flare junction and, as discussed in following sections, the measurements of heat transfer were in good agreement with prediction techniques based on a large amount of measurements on highly-cooled walls in high Reynolds number hypersonic flows. The test conditions at which the studies were conducted are listed in Table 2.

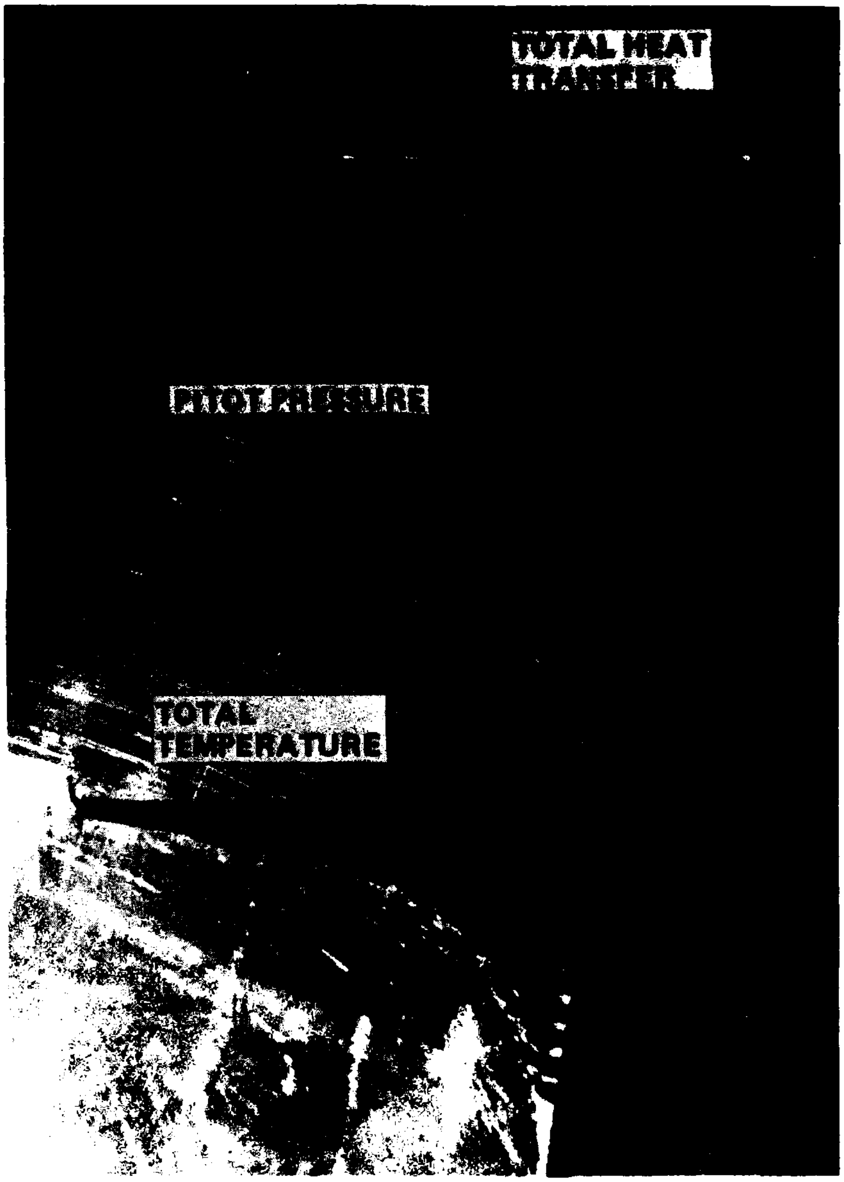
TOTAL HEAT TRANSFER
PITOT PRESSURE
TOTAL TEMPERATURE

Figure 9 RAKE ASSEMBLY

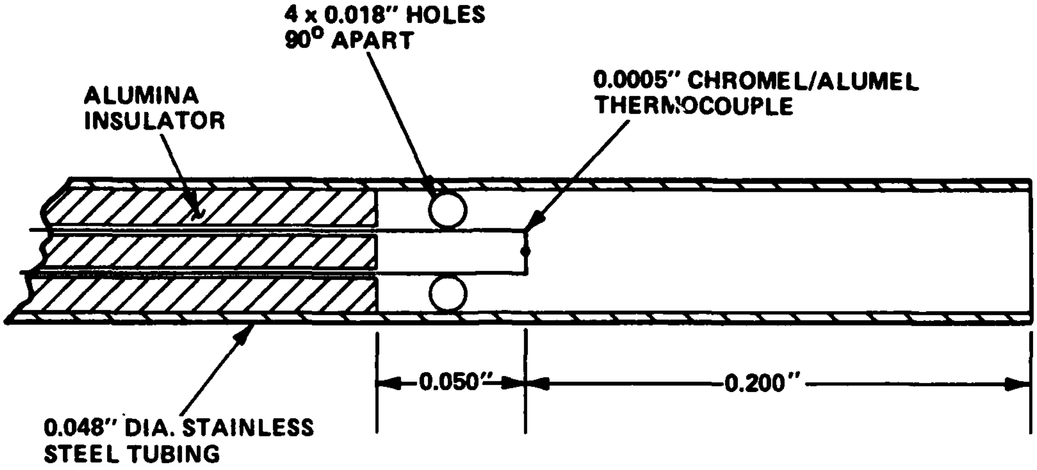
4 x 0.018" HOLES
90° APART
ALUMINA
INSULATOR
0.0005" CHROMEL/ALUMEL
THERMOCOUPLE
0.050"
0.200"
0.048" DIA. STAINLESS
STEEL TUBING

Figure 10 SCHEMATIC DIAGRAM OF TOTAL TEMPERATURE GAGE

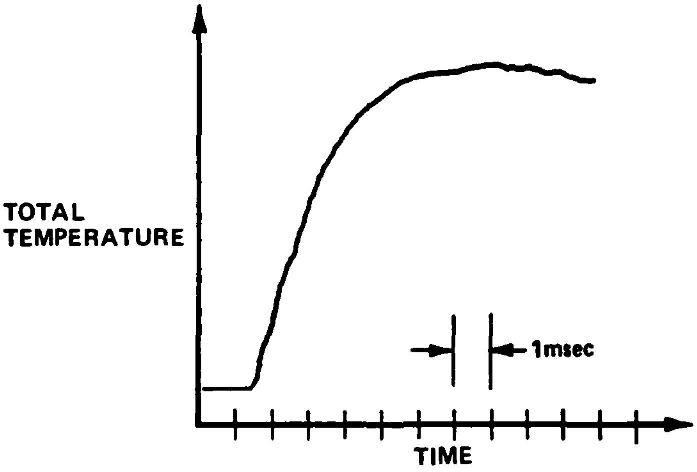

Figure 11 TYPICAL RESPONSE OF TOTAL TEMPERATURE GAGE

Table 2

TEST CONDITIONS, LARGE 6° CONE

	AIR			N_2
RUNS	3,4,8	6,7	9	6-15
Mi	3.345E+00	3.633E+00	4.200E+00	2.635E+00
P0 PSIA	7.216E+03	1.760E+04	1.705E+04	5.430E+03
H0 FT^2/SEC^2	1.825E+07	2.147E+07	2.795E+07	1.287E+07
T0 $^{\circ}R$	2.717E+03	3.104E+03	3.875E+03	1.939E+03
M	1.096E+03	1.301E+01	1.543E+01	1.111E+01
U FT/SEC	5.922E+03	6.458E+03	7.404E+03	4.981E+03
T $^{\circ}R$	1.214E+02	1.026E+02	9.574E+01	8.065E+01
P PSIA	9.172E–02	7.345E-02	1.860E-02	6.698E-02
Q PSIA	7.721E+00	8.712E+00	3.104E+00	5.800E+00
RHO SLUGS/FT^3	6.340E-05	6.038E-05	1.631E-05	6.734E-05
Mu SLUGS/FT·SEC	1.021E-07	8.634E-08	8.054E-08	6.783E-08
RE/FT	3.680E+06	4.544E+06	1.499E+06	4.945E+06
PITOT PSIA	1.431E+01	1.619E+01	5.798E+00	1.070E+01

4.3 Results and Discussion

The experimental program had two objectives. First, we sought to generate a model and environment in which we could establish a thick, well-developed turbulent boundary layer that had developed under constant pressure conditions. We then sought to design, develop and use instrumentation to obtain profile measurements; first in the constant pressure boundary layer, and then in regions of strong adverse pressure gradient in regions of shock wave/boundary layer interaction generated at a cone/flare junction. We planned to use two cone/flare junctions, one (a 30 degree flare) which promoted a flow close to incipient separation, and a second (a 36 degree flare) which promoted a well separated flow.

The measurements of the heat transfer and pressure distributions over the two cone/flare configurations are shown in Figures 3, 4, 5 and 6. The corresponding schlieren photographs are presented in Figures 7 and 8. The measurements of the pressure along the entire length of the cone were in good agreement with predictions based on Sim's solutions for a sharp cone, and the pressures at the back of the flare were in good agreement with calculations based on an inviscid shock compression from the cone to the flare, as shown in Figures 4 and 5.

Based on comparisons with a large number of heat transfer and skin friction measurements made in flat plates and cones in the shock tunnels and other high Reynolds number hypersonic facilities, we have found that predictions based on the Van Driest(II) technique[34] are in best agreement for hypersonic flows over highly-cooled walls. The Van Driest method is based on a transformation to relate measurements in compressible flow to those in incompressible flow. Here the measured coefficient of local skin friction and heat transfer (C_f and C_H) are related to an equivalent quantity in an incompressible flow (C_{f_i} and C_{h_i}) through the relationship

$$C_{f_i} = F_c\left(M_e, \frac{T_w}{T_0}\right) C_f$$

$$C_{h_i} = F_c\left(M_e, \frac{T_w}{T_0}\right) C_h$$

The local Reynolds numbers based on the momentum thickness, θ , and distance from the virtual origin X_v , Re_θ and Re_x, respectively, are related to similar quantities in the incompressible plane through the relationships

$$F_c C_f = F_\theta Re_\theta$$

$$F_c C_t = F_x Re_x$$

We have assumed that the Karman-Schoenherr[35] relationship

$$\log_{10}\left(Re_{x_i} C_{F_i}\right) = \log_{10}\left(2Re_{\theta_i}\right) = 0.242\left(C_{F_i}\right)^{-\frac{1}{2}}$$

where the average skin friction C_{F_i} is related to the local skin friction C_{f_i} by

$$C_{f_i} = 0.242 \quad C_{F_i} \left[0.242 + 0.8686\left(C_{F_i}\right)^{\frac{1}{2}}\right]^{-1}$$

Van Driest's analysis is based on the Prandtl-Karman[36] mixing length model, together with a compressibility transformation, to describe the compressible turbulent boundary layer over a flat plate. From this analysis, the transformation or compressibility factors are

$$\left(F_c\right)_{VD} = r\, m_e \left(\sin^{-1}\alpha + \sin^{-1}\beta\right)^{-2}$$

$$\left(F_\theta\right)_{VD} = \frac{\mu_e}{\mu_w}$$

and and $F_x = F_\theta F_c^{-1}$

where $\alpha = \left(2A^2 - B\right)\left(4A^2 + B^2\right)^{-\frac{1}{2}}$ and $\beta = \left(\frac{B}{\left(4A^2+B^2\right)}\right)^{\frac{1}{2}}$

and

$$A = \left[r\, m_e\left(\frac{T_w}{T_e}\right)^{-1}\right]^{\frac{1}{2}} \text{ and } B = \left(1 + r\, m_e - \frac{T_w}{T_e}\right)\left(\frac{T_w}{T_e}\right)^{-1}$$

where $M_c = \frac{\gamma-1}{2} M_c^2$ and a recovery factor (r) of 0.89 was used.

To compare the prediction methods with the experimental measurements in the $C_f F_c - F_\theta Re_\theta$ plane, the momentum thickness, θ, must be calculated. We have used the relationship from the momentum equation $\theta = \int_0^x C_f/2\, dx$ to calculate this quantity. For our measurements in transitional and turbulent flows, we found that the Reynolds analogy factor was close to unity, as shown in Figures 12 and 13. Thus, when only heat transfer measurements were available, we calculated the momentum thickness from the expression $\theta = \int_0^x C_H\, dx$.

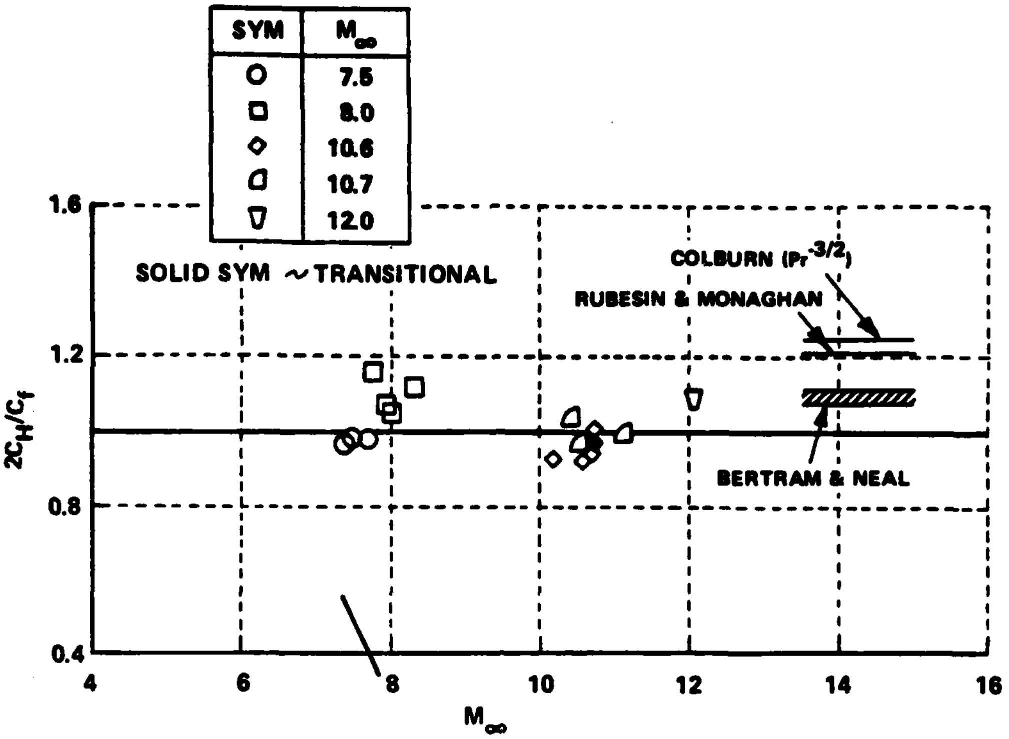

Figure 12 REYNOLDS ANALOGY FACTORS FOR TURBULENT HYPERSONIC BOUNDARY LAYERS

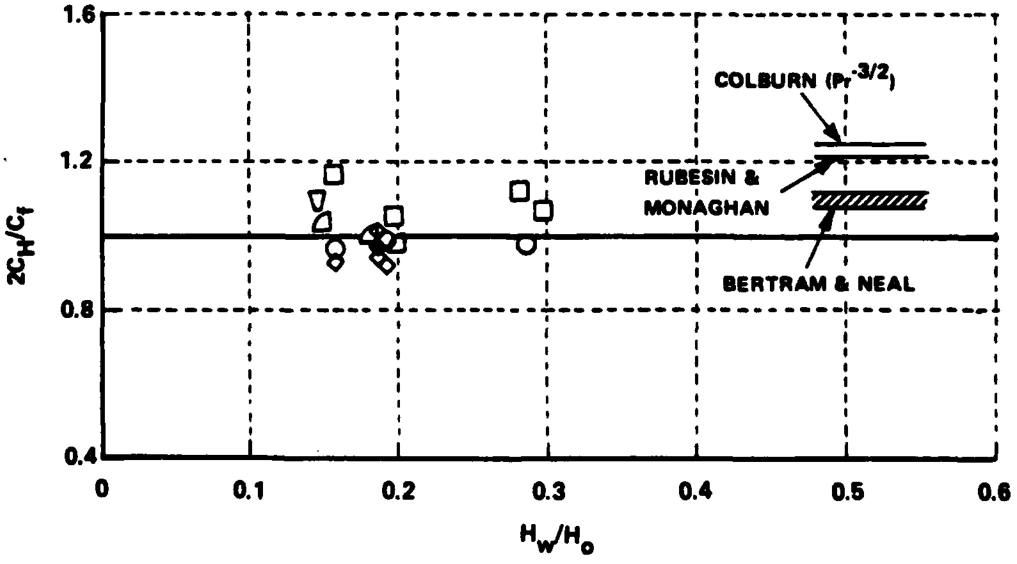

Figure 13 REYNOLDS ANALOGY FACTORS FOR TURBULENT HYPERSONIC BOUNDARY LAYERS

In correlating the measurements made on the conical models in the $F_C C_H - F_{Rx} Re_x$, we employed the Mangler[37] transformation in the form suggested by Bertran and Neal[38] to relate the measurements on the cones to an equivalent two-dimensional flow. For an equal distance from the virtual origin of the turbulent boundary layer on flat plates and cones, the local Stanton number on the cone would be larger than that on a flat plate by the ratio

$$\frac{\left(C_H\right)_{cone}}{\left(C_H\right)_{fp}} = \left(\frac{2m-1}{m-1}\right)^{\frac{1}{m}} \left[\left(\frac{1+R_{xv}}{R_x}\right) - \frac{R_{xv}}{R_x} \left[\frac{\frac{R_{xv}}{Re_x}}{1+\left(\frac{R_{xv}}{R_x}\right)} \right]^{\frac{m}{m\ 1}} \right]^{-\frac{1}{m}}$$

By employing the above equation, the measurements on the conical bodies were transformed into the equivalent two-dimensional compressible plane and subsequently to the incompressible plane by the transformations given above.

A typical comparison between a large body of heat transfer measurements obtained earlier and the Van Driest approach is shown in Figure 14. Thus, the good agreement between the heat transfer measurements on the large cone and the Van Driest prediction technique suggests that at both Mach 11 and 13 (shown in Figures 12 and 13) the boundary layers are well developed.

Flow field surveys were made to determine the distribution of pitot pressure, total temperature and total heat at a number of stations through the interaction region at each of the flow conditions described above. Figures 15 and 16 show the measured pitot and total temperature measurements for the Mach 11 condition with a 30 degree flare. The profiles which were obtained at 2, 1.2, 0.8, and 0 inches ahead of the cone/flare junction indicate that there is very little upstream influence at this condition. (A similar set of measurements for the 36 degree flare are shown in Figures 17 and 18.)

$$\frac{P_{rake}}{P_{meas.\,cone}} = \left[\frac{(\gamma+1)Mb^2}{2}\right]^{\frac{\gamma}{\gamma-1}} * \left[\frac{\gamma+1}{2\gamma Mb^2-(\gamma-1)}\right]^{\frac{1}{\gamma-1}}$$

$$\frac{u_b}{u_e} = \frac{M}{M_e}\sqrt{\frac{T_{o_b}}{T_{o_e}}}\ \sqrt{\frac{1+\left(\frac{\gamma-1}{2}\right)M_e^2}{1+\left(\frac{\gamma-1}{2}\right)M_b^2}}$$

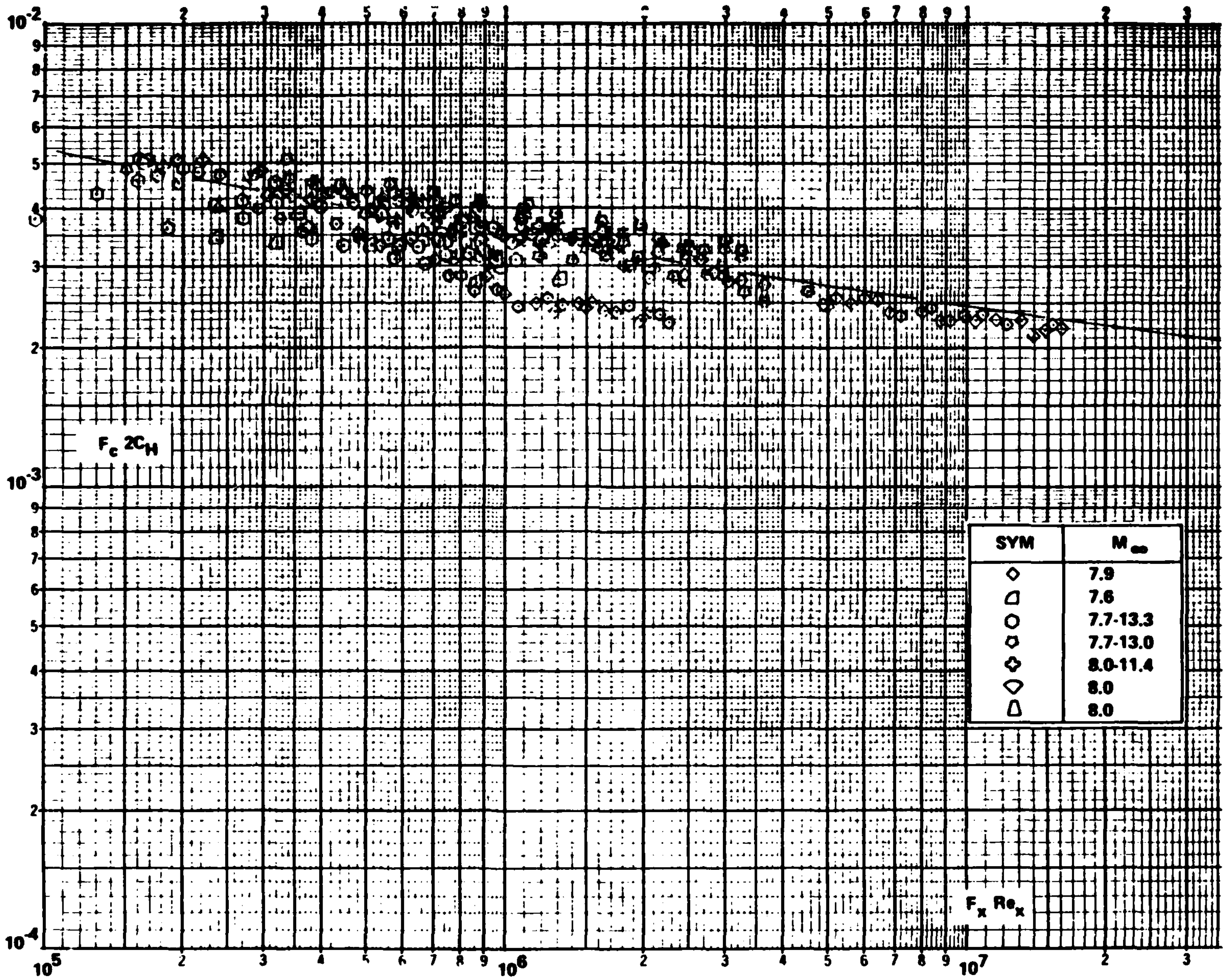

Figure 14 COMPARISON BETWEEN THE MEASURED HEAT TRANSFER AND THE THEORY OF VAN DRIEST ON SHARP CONES ($\Theta_V = \Theta_B + \Theta_{BE/2}$)

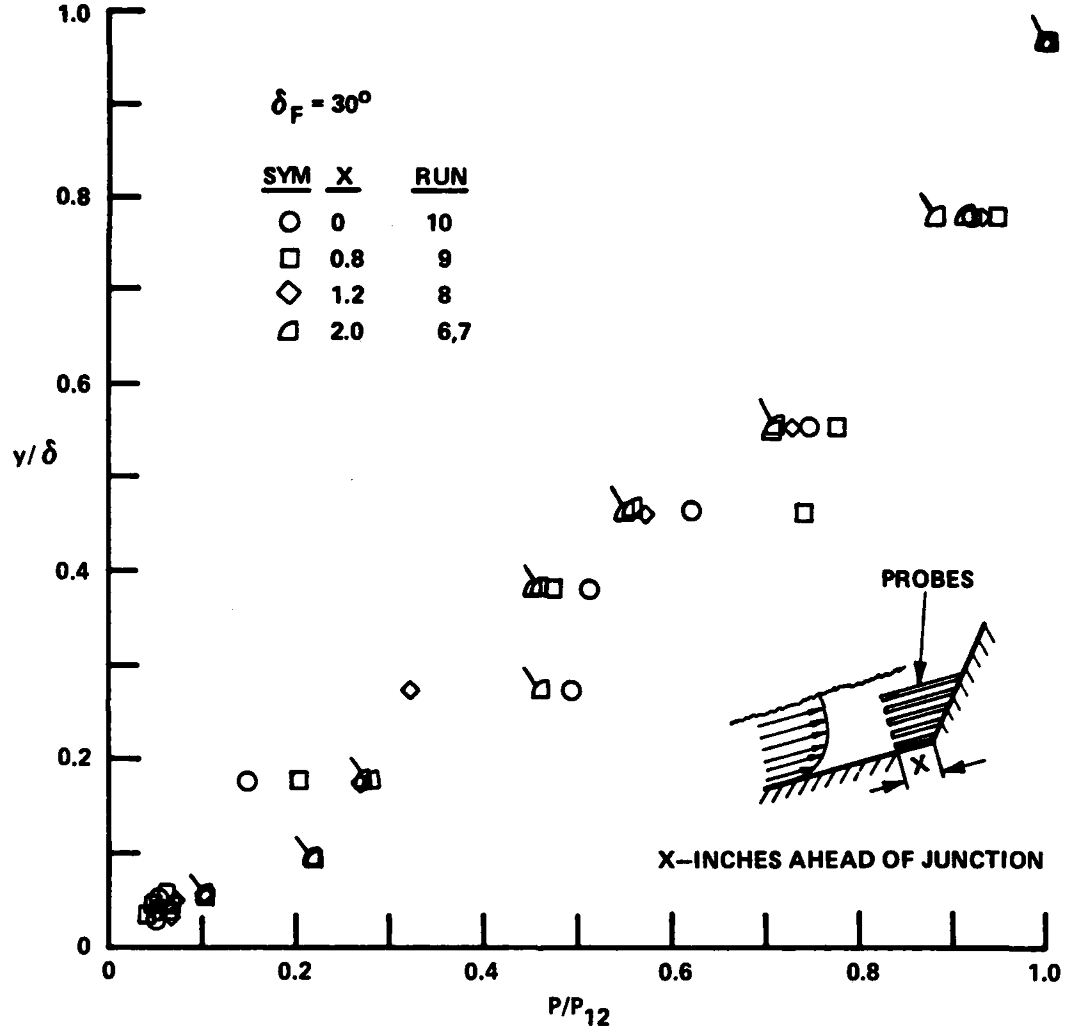

Figure 15 DISTRIBUTION OF PITOT PRESSURE ACROSS BOUNDARY LAYER UPSTREAM OF CONE/FLARE JUNCTION

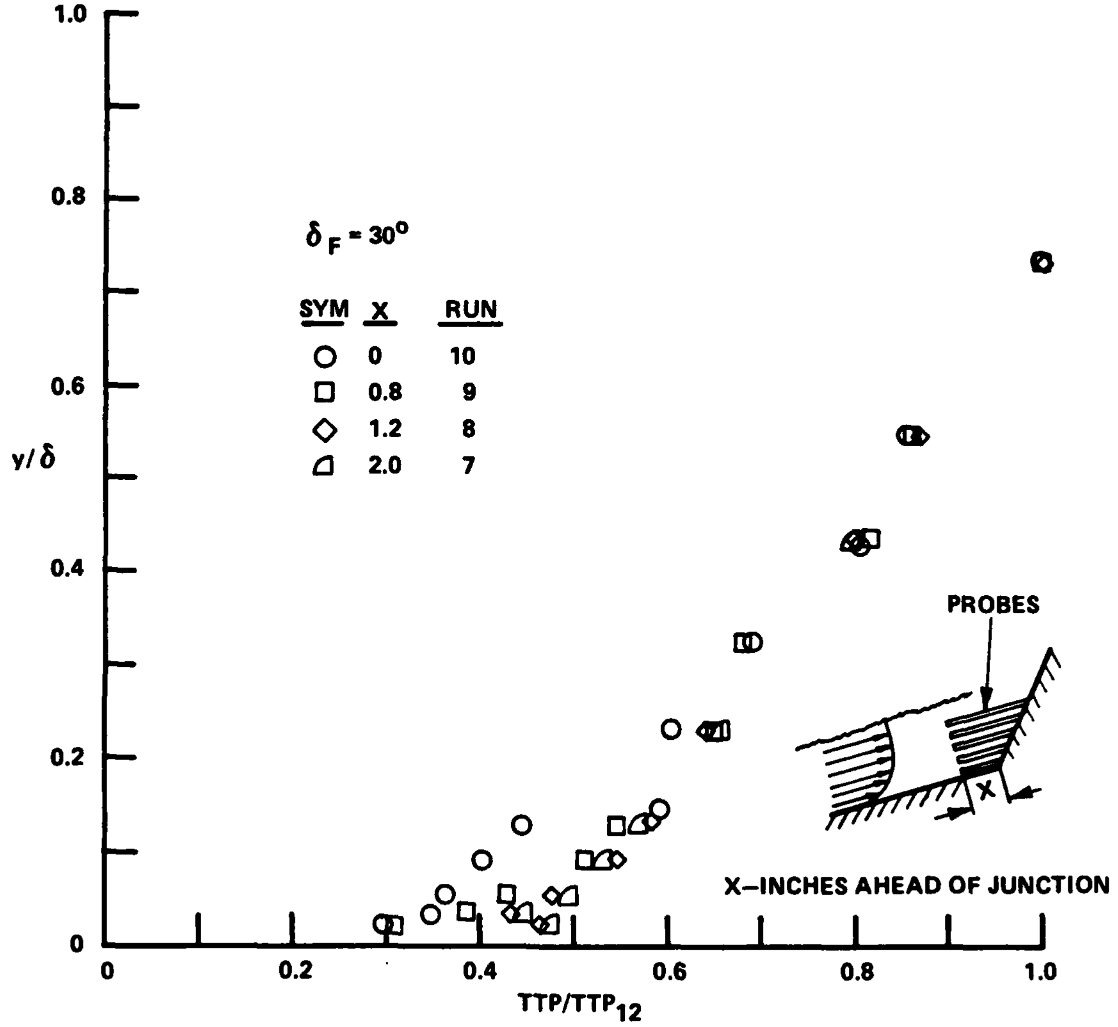

Figure 16 DISTRIBUTION OF TOTAL TEMPERATURE ACROSS BOUNDARY LAYER UPSTREAM OF CONE/FLARE JUNCTION

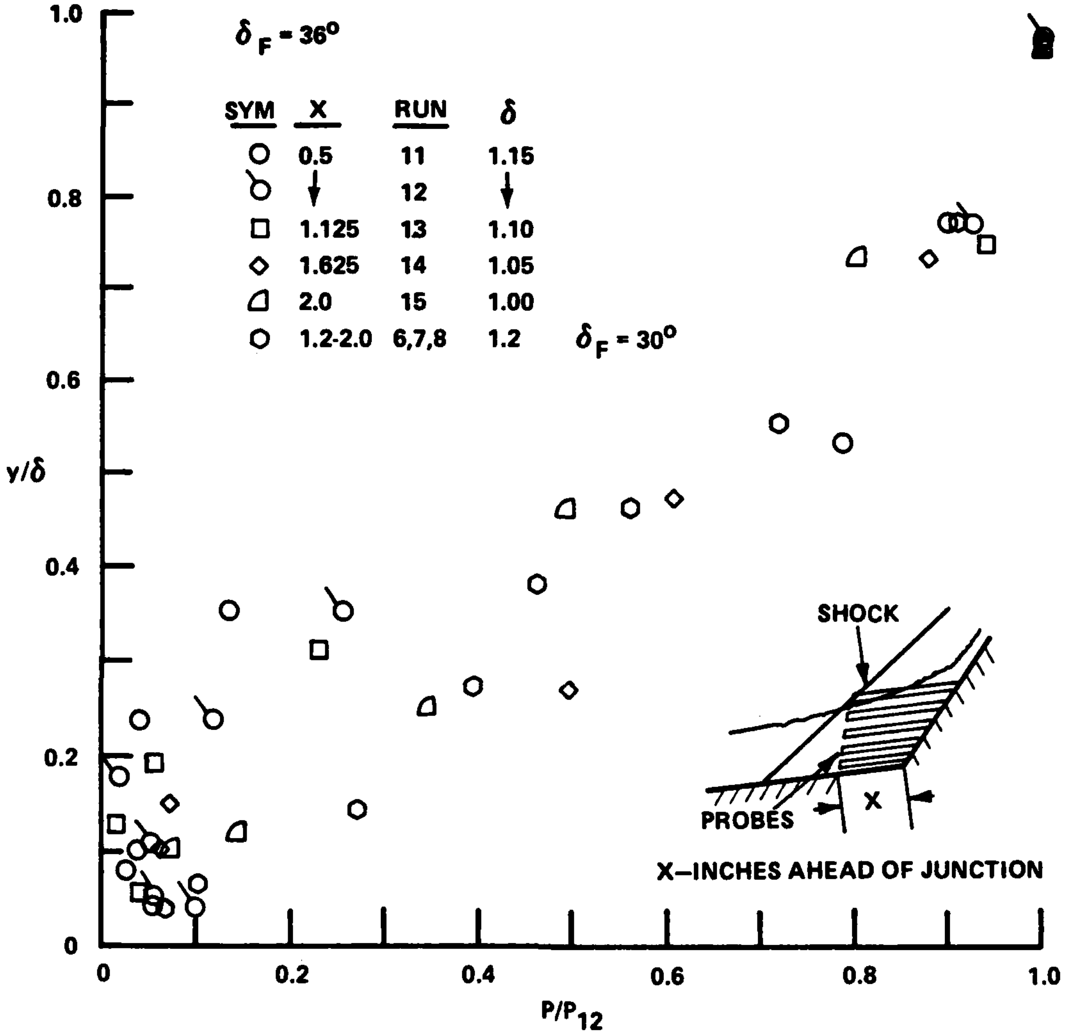

Figure 17 DISTRIBUTION OF PITOT PRESSURE ACROSS BOUNDARY LAYER UPSTREAM OF CONE/FLARE JUNCTION

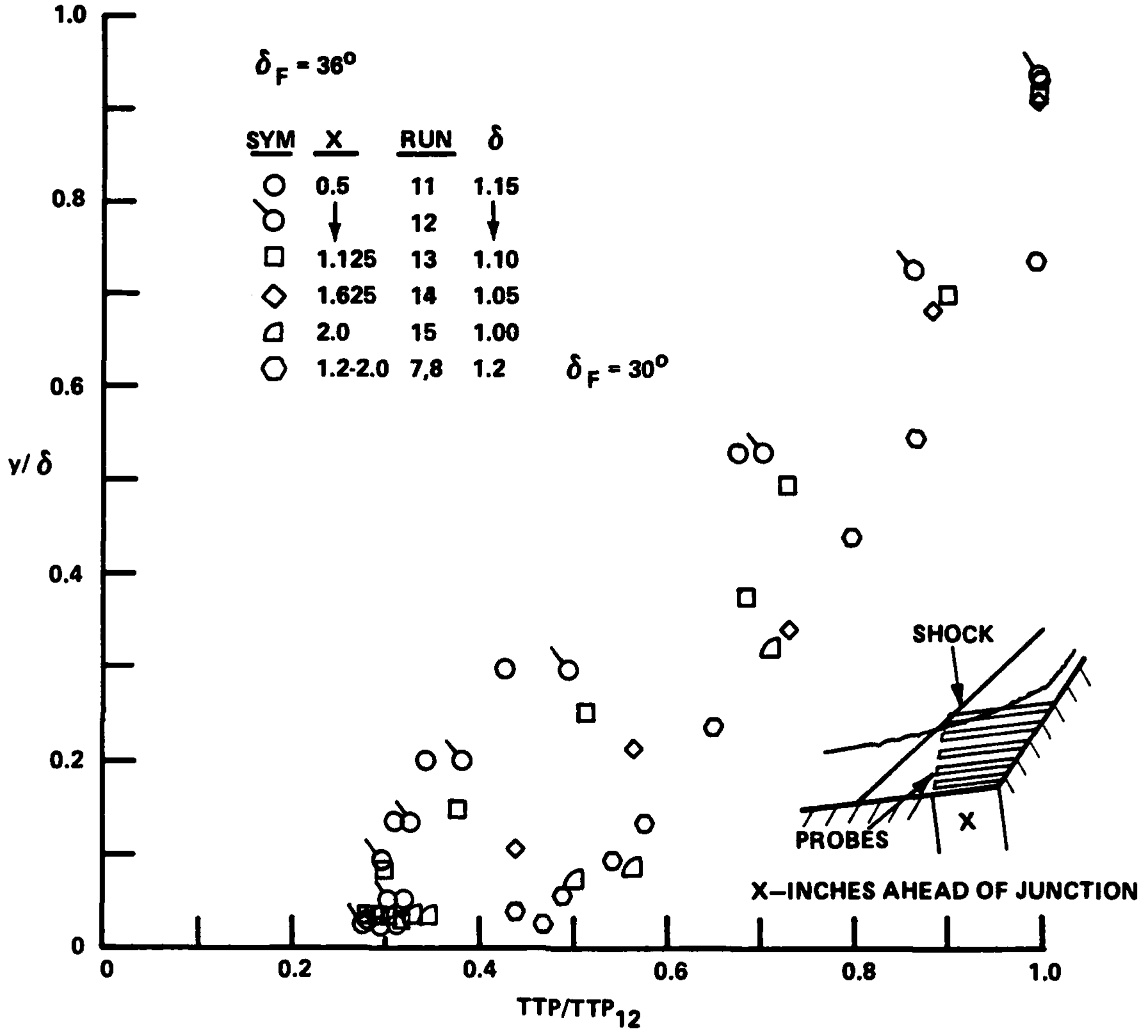

Figure 18 DISTRIBUTION OF TOTAL TEMPERATURE ACROSS BOUNDARY LAYER UPSTREAM OF CONE/FLARE JUNCTION

These measurements are compared with the Crocco relationship between enthalpy and velocity in Figure 19. It is clear that our measurements follow a parabolic relationship

$$\frac{T}{T_w} = 1 + \left[\left(1 - C_t\right)\left(1 + \left(\frac{\gamma - 1}{2}\right) M_e^2\right)\frac{T_e}{T_w} - 1\right]\frac{u}{u_e} + \frac{T_e}{T_w}\left[C_t\left(\frac{1 + \left(\frac{\gamma - 1}{2}\right) M_e^2}{\left(\frac{\gamma - 1}{2}\right) M_e^2}\right) - 1\right]\left(\frac{\gamma - 1}{2}\right) M_e^2 \left(\frac{u}{u_e}\right)^2$$

$0.5 < C_t < 1$; $C_t = 1$ for Crocco, $C_t = 0.5$ for quadratic

rather than Crocco's linear relationship

$$\frac{T_d}{T_w} = 1 + B\left(\frac{u}{u_e}\right) - A^2\left(\frac{u}{u_e}\right)^2$$

where:

$$A = \left[r\left(\frac{\gamma - 1}{2}\right) M_e^2 \frac{T_e}{T_w}\right]^{0.5}$$

$$B = \left[\left(1 + r\left(\frac{\gamma - 1}{2}\right) M_e^2\right)\frac{T_e}{T_w} - 1\right]$$

In the past it has been assumed that the "fuller than Crocco" velocity profile obtained in studies over tunnel walls was associated with turbulent non-equilibrium effects associated with the strong favorable pressure gradient upstream on the nozzle wall, however, no such explanation can be advanced to explain our results.

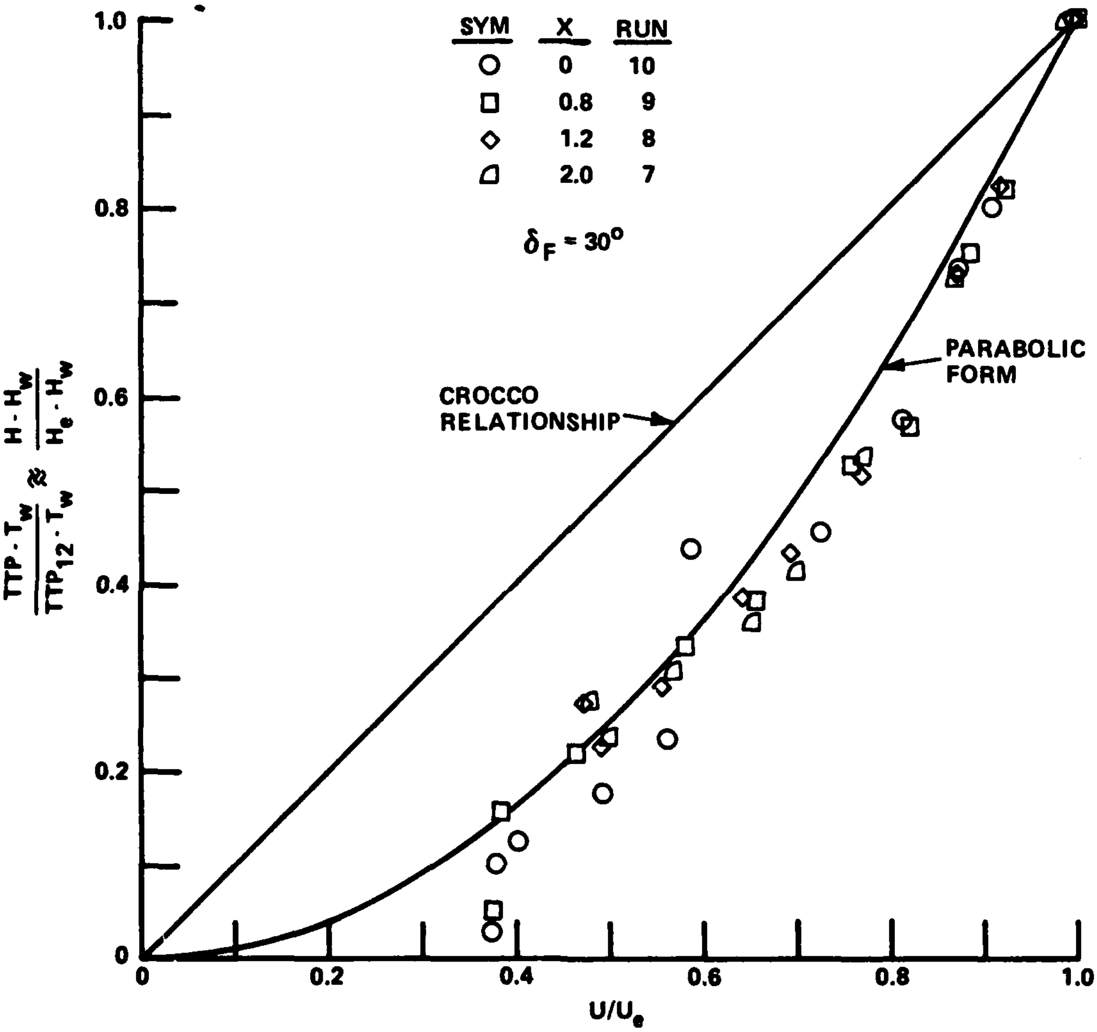

Figure 19 TOTAL TEMPERATURE AND VELOCITY MEASUREMENTS PRESENTED IN CROCCO FRAMEWORK

This page intentionally blank.

Section V. CONCLUSIONS

This report summarizes the research conducted under the current contract to investigate fundamental problems associated with flight at hypersonic speeds with particular emphasis on those related to the aerothermal effects of viscous/inviscid interactions and boundary layer transition.

The experimental study conducted under the current contract was directed toward obtaining detailed flow field measurements in a separating boundary layer over a large cone/flare model. In this study, the structure of the separating boundary layer was examined with pitot, total temperature and laser holography measurements. These measurements suggest that the total temperature/velocity relationship in the cone boundary layer is quadratic rather than the usually assumed linear form suggested by Crocco. The Van Driest transformation which has been used successfully in supersonic flows over adiabatic walls to relate the measured velocity to similar measurements in subsonic flow is apparently not as effective in hypersonic flows over highly cooled walls. The measurements—the rapid change in the structure of the sublayer as separation takes place and the formation of strong shock waves in the turbulent shear layer.

173

Solutions have been obtained to Navier-Stokes equations for the laminar flow over the leading edge of a sharp flat plate in Mach 16 flow for highly-cooled wall conditions using a modified MacCormack/Shang fully explicit formulation. To obtain a stable converged solution it was necessary to reduce the grid size close to the leading edge to the order of the mean free path, and typically 20,000 time steps were required to achieve convergence. However, once obtained, the solution was a good agreement with experiment.

In addition to experimental studies of turbulent boundary layer separation in hypersonic flow, during the past year further analysis has been performed of measurements made during earlier studies for AFOSR. This work has resulted in four AIAA and one Ver Springer publications during the course of this current contract. Boundary layer transition plays a key role in the aerothermal design of hypersonic vehicles and we have performed a number of studies to examine some important characteristics of transitional flows over re-entry vehicles. The effects of "natural" and "tripped" asymmetric transition regions on the force and heat transfer characteristics of slender hypersonic vehicles have been examined in a number of experimental studies which were analyzed in greater detail and published recently (see Appendix A) under the present contract. When transition moves close to the stagnation point some wind tunnel and flight test measurements suggest that the stagnation point heating rate increases above the laminar value. The exact mechanism by which this increase occurs is not well understood, however, an analysis conducted under the present contract of a number of studies conducted in Calspans 48-Inch and 96-Inch Shock Tunnels at Calspan in which stagnation region heating was measured in the presence of transition, identified the disturbances generated by minute particles in the freestream as an important mechanism of stagnation region heating enhancement. The result of this work was published as an AIAA paper in June 1985 and will appear in the AIAA Progress Series in 1986.

Section VI. REFERENCES

1. Knight, D.D., "Problems in Reconciling Computation and Experiment," 1985 Princeton University Workshop on the Structure of High-Speed Turbulent Boundary Layers.

2. Knight, D., Horstman, C.C., Shapey, B., and Bogdonoff, S., "The Flowfield Structure of the 3-D Shock Wave Boundary Layer Interaction Generated by a 20 degree Sharp Fin at Mach 3" AIAA-86-343, Jan. 6-9, 1986.

3. Shang, J.S., Hankey, W.L., and Petty, J.S., "Three-Dimensional Supersonic Interacting Turbulent Flow Along a Corner," AIAA Paper 78-1210, July 1978; also AIAA Journal, Vol. 17, No. 7, July 1979, pp. 706-713.

4. Horstmann, C.C. and Hung, C.M., "Computations of Three-Dimensional Turbulent Separated Flows at Supersonic Speeds," AIAA Paper 79-2, January 1979.

5. Settles, G.S. and Hortsmann, C.C., "Flowfield Scaling of a Swept Compression Corner Interaction -- A Comparison of Experiment and Computation," AIAA-84-0096, 22nd Aerospace Sciences Meeting, January 9-12, 1984.

6. Holden, M.S., "Preliminary Studies of Shock Wave-Turbulent Boundary Layer Interaction in Hypersonic Flow," AIAA Paper 72-74, 17-19 January 1972, 10th Aerospace Sciences Meeting, San Diego, CA.

7. Chapman, D.R. "Computational Aerodynamic Development Outlook," AIAA Journal, Vol. 17, pp. 1293-1313, 1979.

8. Anderson, D.A., Tannehill, J.C., and Pletcher, R.H., Computational Fluid Mechanics and Heat Transfer, 1984, McGraw Hill.

9. Tennekes, H., and Lumley, J.L., A First Course in Turbulence, 1985, MIT Press.

10. Jones, W.P., and Launder, B.E., "The Prediction of Laminarization with Two-Equation Model of Turbulence," Int. J. of Heat Mass Transfer, Vol. 15, pp. 301-314, 1972.

11. Karvorkin, J., Cole, J.D., Perturbation Methods in Applied Mathematics, Spring-Verlag, 1981.

12. Rudman, S. and Rubin, S.G., "Hypersonic Viscous Flow over Slender bodies with Sharp Leading Edge," AIAA Journal, Vol. 16, pp. 1883-1889, 1968.

13. Cheng, H.K., Chen, S.Y., Mobley, R., Huber, C.R., "The Viscous Hypersonic Slender Body problem: A Numerical Approach Based on a System of Composite Equations," The Rand Corporation, Report No. RM-6193-PR, Santa Monica, CA, 1970.

14. MacCormack, R.W., "The Effect of Viscosity in Hypervelocity Impact Cratering," AIAA paper No. 69-354, Cincinatti, OH, 1969.

15. Beam, R.M., Warming, R.F., "An Implicit Finite-Differencing Algorithm for Hyperbolic System in Conservation Form," Journal of Computational Physics, vol.

22, pp. 87-110, 1976; and "An Implicit Factored Scheme for Compressible Navier-Stokes Equations," AIAA Journal, vol. 16, pp. 393-401, 1978.

16. MacCormack, R.W., Baldwin, B.S., "A Numerical Method for Solving the Navier-Stokes Equations with Applications to Shock-boundary Applications," AIAA paper No. 75-1, Pasadena, CA, 1975.

17. MacCormack, R.W., "Numerical Solution of the Interaction of Shock Wave with a Laminar Boundary Layer," Proceedings of the Int'l. Conference on Numerical Methods in Fluid Dynamics, Lecture Notes in Physics, vol. 8, Spring-Verlag, NY, NY, pp. 151-163 (1971).

18. Stwertson, K., "Multistructured Boundary Layers on Flat Plates and Related Bodies," Advances in Applied Mechanics, Academic Press, 1977.

19. MacCormack, R.W., "A Numerical Method for Solving the Equations of Compressible Flow," AIAA Paper No. 81-0110, St. Louis, MO, 1981.

20. Lombard, C.K., Oliger, J., Yang, J.Y., "Conservative Supra-Characteristic Method for Splitting the Hyperbolic Systems to Gasdynamics with Computered boundaries for Real and Perfect Gases," AIAA paper No. 82-0837, St. Louis, MO, 1982.

21. Lombard, C.K., Oliger, J., "Multi-Dimensional Formulation of CSCM - An Upwind Flux Difference Eigenvector Split Method for the Compressible Navier-Stokes Equations," AIAA paper No. 83-1895, Danvers, MA, 1983.

22. Lombard, C.K., Venkatapathy, E., Bardina, J., "Universal Single Level Implicit Algorithm for Gasdynamics," AIAA paper No. 84-1533, Snowmass, CO, 1984.

23. Stookesberry, D.C., and Tannehill, J.C., "Computation of Separated Flow on a Ramp Using the Space Marching Conservative Supra-Characteristics Methods," AIAA Paper No. 86-0564, Reno, NV, 1986.

24. Chakravarthy, S.R., Anderson, D.A., and Salas, M.D. , "The Split-Coefficient Matrix Methods For Hyperbolic System of Gasdynamic Equations," AIAA Paper 80-0268, Pasadena, California, 1980.

25. Steger and Warming, "Flux Splitting of the Inviscid Gasdynamic Equations with Application to Finite Difference Method," NASA TM D-78605, 1979.

26. Steger, "A Preliminary Study of Relaxation Methods for the Inviscid Conservative Gasdynamics Equations using Flux Splitting," NASA CR 3415, 1981.

27. Knight, D., "Improved Calculation of High-Speed Inlet Flows: Part I. Numerical Algorithm and Part III. Results," AIAA Journal, Vol. 19, pp. 34-41, 1972-179, 1980.

28. Knight, D., "A Hybrid Explicit-Implicit Algorithm for the Three-Dimensional Compressible Navier-Stokes Equations," AIAA Journal, vol. 22, pp. 1056-1063, 1983.

29. Hortsman, (1986), unpublished presentation.

30. Shang, J.G., "Numerical Solution of the Compressible Navier-Stokes Equations for a Three-Dimensional Corner," AIAA paper No. 77-169, Los Angeles, CA 1977.

31. Kumar, A., "Numerical Simulation of Flow through Scramjet Inlet Using a Three-Dimensional Navier-Stokes Code," AIAA Paper No. 85-1664, Cincinatti, OH, 1985.

32. Knight, (1986), unpublished presentation.

33. Baldwin, B.S., Lomax, H., "Thin-Layer Approximation and Algebraic Model for Separated Turbulent Flows," AIAA paper No. 78-257, Huntsville, AL, 1978.

34. Van Driest, E.R., "Problem of Aerodynamic Heating," Aeronautical Engineering Review, vol. 15, No. 10, October 1956.

35. Schoenherr, K.E., "Resistance of Flat Surfaces Moving Through a Fluid," Soc. of Naval Arch. and Marine Engrs. Trans., Vol. 40, pp. 279-313, 1932.

36. von Karman, T., "The Problems of Resistance in Compressible Fluids," GALCIT Pub. No. 75, 1936.

37. Howarth, L., "Modern Developments in Fluid Dynamics," Oxford University Press, NY, 1953, pp. 382-386.

38. Bertram, M.H., Neal, L. Jr., "Recent Experiments in Hypersonic Turbulent Boundary Layers," NASA Report No. TMX-56335, May 1965.

APPENDIX A

AIAA-85-0325

"Experimental Studies of the Effects of Asymmetric Transition on the Aerothermal Characteristics of Hypersonic Blunted Slender Cones"

AIAA 23rd Aerospace Sciences Meeting
January 14-17, 1985
Reno, Nevada

AIAA'84

AIAA-85-0325

Experimental Studies of the Effects of Asymmetric Transition on the Aerothermal Characteristics of Hypersonic Blunted Slender Cones

M.S. Holden, Calspan Advanced Technology Center,
Buffalo, NY

AIAA 23rd Aerospace Sciences Meeting

January 14-17, 1985/Reno, Nevada

For permission to copy or republish, contact the American Institute of Aeronautics and Astronautics
1633 Broadway, New York, NY 10019

EXPERIMENTAL STUDIES OF THE EFFECTS OF ASYMMETRIC TRANSITION ON THE AEROTHERMAL CHARACTERISTICS OF HYPERSONIC BLUNTED SLENDER CONES

M.S. Holden*
Calspan Advanced Technology Center
P.O. Box 400
Buffalo, NY 14225

ABSTRACT

An experimental study has been conducted to investigate the effects of asymmetric boundary layer transition on the aerothermal characteristics fo slender blunted cones at angle of attack in hypersonic flow. In this study, which was conducted at Mach 11 and 13 in Calspan's 96-Inch Shock Tunnel, simultaneous measurements of force, heat transfer, and pressure were made to examine the effects of asymmetric transition induced by angle of attack, and by roughness, steps and gaps in the frusta and nosetip, on the aerodynamic stability and asymmetric heating loads generated over the cones. Observations of the mechanisms of boundary layer transition in these studies, made with spark source photogrpahy, revealed the presence of ordered "wave-like" instabilities preceeding the massive breakdown of the laminar boundary layer. Our measurements of the Reynolds numbers at which boundary layer tranistion occurred were found to be in good agreement with those from flight tests and ballistic range studies. The current studies of the effects of asymmetric transition induced by angle of attack demonstrated that transition moved first onto the leeside fo sharp or slightly blunted cones inducing a destablishing effect, while for cones with bluntness ratio's (r/Rb) greater than 12% transition occurred first on the windward ray and resulted from "wind-fixed" transition resulted in C.P. movements of the order of 1%. The studies of "body-fixed" transition regions demonstrated that "wedge-shape" transition regions could be induced with relative ease by small gouges in the spherical nosetip, or surface roughness near the nosetip. In contrast, gaps in the surface of the frustum were not found to be effective trips. Our studies indicated that the magnitude of the destabilizing forces was relatively independent of the tripping mechanism. Typical forces and moments associated with such regions were $\Delta Cn=-1.8E-3$ and $\Delta Cm=6E-3$. Such force levels were are in general agreement with calculations based on the increased pressures and skin friction forces induced in the asymmetric transition regions.

INTRODUCTION

While hypersonic boundary layer transition has been studied extensively over the past two decades, only recently have strenuous efforts been made to determine the mechanism by which boundary layer transition influences the aerothermal characteristics of slender cones.

Flight test data indicate that perturbations occur to the trajectory of slender conical RV's which can be linked directly to destabilizing forces generated during boundary layer transition. At "high" altitude, this can be associated with asymmetric transition on the cone frustrum, while at "low" altitude asymmetric nose shaping is believed to be the underlying mechanism. The high altitude phenomenon is characterized by perturbations which build up and subside smoothly over several cycles. A net lateral velocity results from nonlinearities in the coning motion of the RV. In contrast, the perturbations observed at low altitudes can occur over a period of less than one cycle. Flight data suggests that the magnitude of the net lateral velocity, which results when frustum transition occurs, decreases with nose bluntness (r_n/R_b); whereas, the lateral perturbations at low altitude increase with increased bluntness ratio.

Studies of full-scale flight transition on slender RVs suggest that both "naturally developed" and tripped transition regions can develop. Surface discontinuities at the nose tip-cone junction and antenna windows have been suggested as potential sources of transition regions which appear "body-fixed" on spinning vehicles which are undergoing changes in angle of attack. Gouges and regions of roughness on the nose tip have also been cited as sources for tripped transition regions. However, most of the flight measurements and those on smooth bodies in ballistic ranges and wind tunnels suggest the onset of transition is relatively well ordered in terms of free stream properties and the preceding length of laminar run. Transition onset is also influenced by both angle of attack and nose tip bluntness on smooth non-ablating slender cones.

Objectives of the Current Studies

In the first part of this study we sought to measure the destabilizing/stabilizing forces associated with the movement of regions of wind-fixed transition onto the frustum of sharp and blunted slender cones and establish how these forces and the characteristics of the transition regions vary with bluntness ratio, angle of attack and freestream conditions. This study was followed by an investigation to examine the effectiveness of nose tip gouges, asymmetric frustum roughness, and steps and gaps in the frustum inducing body fixed transition regions. We also wanted to measure the destabilizing/stabilizing forces associated with the movement of regions of body-fixed transition onto the frustum of sharp and blunted slender cones and establish how these forces, and the geometry and characteristics of the transition regions, vary with the tripping mechanism and freestream conditions. The bluntness ratio ($0 < r_n/R_B < 0.21$) and the nose shape (sharp, spherical, and elliptical) of the cone were varied in these studies. The 6°-conical model was chosen because when it was tested at Mach numbers between 11 and 13 and Reynolds numbers from 20×10^6 to 5×10^6, there was good simulation of conditions of Mach number, Reynolds number and wall-to-freestream stagnation temperature ratio.

---

*Member, AIAA

This work was supported by the Air Force Office of Scientific Research under contract #F44620-76-C-003.

Models and Instrumentation

This experimental study was conducted in Calspan's 96-Inch Shock Tunnel. Since in the study of transition, one cannot guarantee that the transition region on two models of nominally the same dimensions and tested at nominally the same freestream conditions will be identical in size and properties, a key aspect of the current program was the simultaneous measurement of model forces and the pressure and heat transfer on the cone surface. The extremely small changes (0.001) in normal force (ΔC_N) and moments associated with boundary layer transition made highly accurate force measurements essential. The acceleration-compensated force balance used in this work, which was capable of making such measurements, was essentially two balances mounted in one model, a six-component strain gage balance and a six-component accelerometer balance. These balances were linked through a small analog computer in such a way that the electrical signals generated by the strain gage balance as a result of acceleration loads on the model were cancelled out by signals generated by the accelerometer balance, leaving a balance output which is accurately related to the air loads on the model. By employing this acceleration-compensation force balance, the cone model could be extensively instrumented with 48 heat transfer gages and 22 pressure gages without sacrificing accuracy in the measurement of forces. A photograph of the models used in this program is shown in Figure 1.

Since we sought to measure small differences in frustum pressure resulting from asymmetric transition over the model, special electronic circuits were devised which, when connected to the pressure transducers on each side of the model, gave an output proportional to the difference in their pressure. We used Calspan's high frequency ($f_n > 100$ kHz) piezoelectric pressure transducers and thin film heat transfer gages in this study. The high frequency response of the thin film gages enabled us to sense transition from both the mean and fluctuating component of the gage output.

RESULTS AND DISCUSSIONS

OBSERVATIONS ON THE MECHANISM OF BOUNDARY LAYER TRANSITION

A typical photograph of the development of a transition region over a sharp slender cone at Mach 13 is shown in Figure 2. The first evidence of transition is provided by the appearance of a system of regular instabilities in the boundary layer, which subsequently breaks down into a random structure as transition proceeds. We observe transition as a growth of the boundary layer in the Schlieren photographs not only because the momentum thickness increases but also because the optical properties, particularly the position of the maximum density gradient, change. The heat transfer distribution in the transition region exhibits an intermittent character as illustrated in Figure 2 which shows records from the gages positioned along the model. The first indication of transition appears as "spikes" in the records as indicated at Station 1 in Figure 2. The magnitude and frequency of these "spikes" increase with downstream distance until at the end of the transition process they coalesce to give a larger heating rate with considerably less intermittency. The heat transfer measurements also suggest that secondary vortices are developed as the major disturbances move down the cone. Spatial and temporal correlations of these measurements suggest that close to their point of origin the disturbances are convected downstream at a little under half the freestream velocity, while toward the end of transition this figure has risen to approximately 85% of the freestream velocity. The regular instabilities which preceed transition can be seen more easily in Figure 3, taken under conditions where we lowered the Reynolds number to delay the start of transition. Close examination reveals that instabilities of this kind always preceed transition, and in some cases can be classified as turbulent bursts.

Our studies suggest that the instabilities originate at the edge of the boundary layer and we believe these disturbances are basically three-dimensional in character, possibly a streamwise vortex system, which breaks up into random motion as transition develops.

FACTORS INFLUENCING THE TRANSITION REYNOLDS NUMBER

Since the early studies of Osborne Reynolds[1], it has been recognized that the transition of boundary layers or free shear layers from laminar to turbulent flow is influenced by both the local Reynolds number and by the level of internally generated or background disturbance. Thus, experiments to define a specific transition Reynolds number, for a given model configuration and freestream conditions, are of little general value unless it can be shown that the instabilitiy modes of the boundary layer remain unexcited by disturbances in the freestream or respond to stronger disturbances generated, for example, by surface roughness. While the transition Reynolds number can be influenced by disturbances generated on the model or in the freestream, such disturbances do not appear to influence the basic mechanisms involved in the transition process. However, a high degree of background noise may trigger instability modes which "by-pass" the weaker modes such as the Tollmien-Schlichting[2] instability.

The studies of Pate and Schueler[3], and the extensive measurements made at NASA Langley[4], have demonstrated that in conventional supersonic wind tunnels, the Reynolds number at which transition occurs is strongly influenced by the fluctuating pressure level in the freestream. Pate and Schueler further demonstrated that the level of pressure fluctuation could be related to geometric features of the tunnels and the characteristic of the boundary layer on the tunnel walls. A direct result of Pate and Schueler's studies is that a decrease in tunnel size for the same freestream conditions should result in a decrease in the transition Reynolds number. Thus, when we compared our transition measurements obtained in the 96-Inch shock tunnel, equipped with a 24" diameter A nozzle, with those obtained in the same tunnel equipped with the 48" diameter D nozzle, we anticipated a significant difference. However, as demonstrated in Figure 4, where we have plotted the Reynolds number of the laminar boundary at the onset of transition (Re_θ) versus the freestream unit Reynolds number, the Pate and Schueler scaling does not appear to apply, even though a unit Reynolds variation is evident. It should be mentioned that the Calspan studies were conducted at Mach numbers and Reynolds numbers well above those used by Pate and Schueler. As a result, we believe that in our test environment, the magnitude of the noise radiated from the walls and its intensity on the tunnel axis was significantly less than those found in the experiments analyzed by Pate and Schueler. Transition Reynolds numbers of over 200×10^6 are predicted if the Pate and Schueler correlation is extrapolated to the tunnel configurations and freestream test conditions at which our studies were performed. Clearly, such values are well in excess of physical meaningful quantities. Thus, it was not surprising to find that the measurements made in the Calspan studies fall below the Pate and Schueler correlation as shown in Figure 5. These results suggest that in our studies, pressure fluctuations resulting from acoustic radiation from the tunnel walls may not be a dominant disturbance in the freestream. Thus, the position of transition on the model examined in the present study may be controlled by disturbances more complex than simple acoustic noise. It remains to be determined whether transition can be related to the fluctuating pressure level in the freestream, which, in turn, might be related to fluctuations in the reservoir conditions. However, because of the large expansion ratios in the A and D nozzles, we must look to fluctuations in the enthalpy in the reservoir, as opposed to velocity fluctuations, as a potential source of freestream disturbances.

One of the most successful formats that we have found for comparing and correlating the transition measurements made in the 48-Inch and 96-Inch-shock tunnels at Calspan with measurements from ballistic ranges and flight tests has been in terms of the Reynolds number based on local momentum thickness and the local Mach number M_{LOCAL}. A correlation of the transition measurements made on sharp cones and flat plates in the present and earlier studies at Calspan, flight measurements reported by TRW, and measurements in the ballistic ranges at AEDC and NSWC are shown in Figure 6. We see that there is relatively good agreement between the shock tunnel measurements and those obtained in free flight. A further comparison between our measurements and those made in the more recent studies of Reda[5], plotted in terms of the unit Reynolds number. Again, we find relatively good agreement between the two sets of measurements. In common with the studies of Potter[6], Sheetz[7], and Reda, we observe a unit Reynolds number effect as shown in Figure 7. The source and significance of the unit Reynolds number effect has been the subject of extensive debate. However, while the analysis of Morkovin[8] and Reshotko[9] have suggested that the unit Reynolds number effects may be traced to a sensitivity to the non-dimensional frequency (V_e/ν_e), or the wavelength of the disturbance (V_e/ν_e), in reality, the disturbance inducing transition may stem from a superposition of a number of different mechanisms.

Experimental studies of boundary layer transition on hypersonic flows have demonstrated that it is difficult to induce transition in such a manner that the boundary layer downstream of the trips approaches the characteristics of an "equilibrium" turbulent boundary layer in a distance significantly less than if a natural transition had been allowed to occur. The experimental studies of Morrisette, Stone and Carey[10] at Langley, and studies at Calspan[11], have suggested that while trips were found disturbing a highly-cooled laminar boundary layer on sharp cones, causing an increase in the local values of skin friction and heat transfer, the Reynolds number at the point where the boundary layer exhibited the characteristics of a "fully turbulent boundary layer" was almost identical to the value calculated for a natural transition. Further, Morrisette, et al., found trip-induced disturbances persisted well downstream of transition. Measurements of heat transfer for the tripped (with surface roughness) and untripped boundary layers over a sharp cone demonstrate that although roughness causes an increase in the heating rate immediately behind the trips, the heat transfer to the cone beneath the tripped and untripped boundary layer reaches the turbulent values at approximately the same distance downstream. This result suggests that in high speed/highly cooled flow, a turbulent boundary layer will develop only when the Reynolds number is large enough for the turbulence to be self-sustaining. Thus, following Bradshaw[12], we can examine the lowest Reynolds number where turbulence can be self-sustaining by comparing the energy or stress-producing eddy size with the dissipation-scale size. When these scale sizes are equal or overlap, production and dissipation can exist in equilibrium; however, if the Reynolds number is too low, then dissipation will dominate. This criteria can be expressed in terms of an eddy Reynolds number Re_λ which is derived by taking the ratio of the scale size of the energy containing eddies, $\lambda = ((\tau/\rho)^{3/2}/E)$, and the Kolmogoroff scale size, $(\nu^3/E^{1/4})$, which becomes $Re_\lambda = (u\lambda/\nu)$ and must exceed 30 for turbulent equilibrium flow. Our measurements suggest that transition is complete by $Re_\lambda \doteq 50$, and transition begins at approximately $Re_\lambda \doteq 25$. We observe that the magnitude of Re_λ is in good agreement with Bradshaw's figure, and this parameter appears independent of Mach number. However, as shown in Figure 8, a small unit Reynolds number effect remains.

INFLUENCE OF ANGLE OF ATTACK AND BLUNTNESS ON TRANSITION PATTERN

To understand when and how wind-fixed transition can influence the aerodynamic stability of slender sharp and blunted cones, we must first examine how the shape of the transition front varies with angle of attack and bluntness ratio. The effect of angle of attack is to increase the Reynolds number and decrease Mach number on the windward ray, and decrease Reynolds number and increase Mach number on the leeside ray. Cross flow effects act to decrease the momentum thickness on the windward ray and increase it on the leeside ray. Thus, depending on the angle of attack and bluntness ratio, the product of the unit Reynolds number and the momentum thickness on the windward and leeward rays Re_w and Re_L will undergo significant variation. In earlier experimental studies, it was observed that for small bluntness ratios, increasing nose tip bluntness caused an increase in the transition Reynolds number while at large bluntness ratios the opposite trend occurred. Nose tip bluntness influences the position at which transition takes place on the surface of the cone by influencing the local Mach number, Reynolds number and momentum thickness of the boundary layer, as well as the local streamwise pressure gradient. The studies of Stetson and Rushton[13] and others demonstrated that the position of boundary layer transition on the frustum of a blunted cone can be related to the distance to the point where the entropy layer is swallowed into the boundary layer. Plotted in this format, Stetson's and Rushton's measurements show the strong stabilizing effect of small bluntness on transition Reynolds numbers and a lesser effect for high bluntness conditions. Finson[14] has demonstrated that plotting such measurements in terms of the Reynolds number based on momentum thickness rather than the length Reynolds number gives a monotonic variation with non-dimensional transition distance, which demonstrates a continuous decrease in Reynolds number based on momentum thickness with bluntness ratio. For both sharp and blunt bodies, the Reynolds number based on local momentum thickness appears to be one of the most successful correlation parameters for correlating transition; thus, in correlating transition measurements on cones with angle of attack, this parameter would be a logical first choice.

In the present experimental studies measurements were made of both the mean and fluctuating components of the heating rates along the cone frustum and high-speed Schlieren photographs of the cone boundary layer were made to enable us to most accurately define the beginning and end of transition. While in the correlations presented here, we have used all three observations in determining transition, for consistency we have defined the beginning of transition as the point on the model surface from which there is a monotonic and uniform rise in the time-averaged heating rate (see Figure 9). In general, this coincides with the point at which Schlieren photographs show an irregular increase in the growth rate of the boundary layer. However, as noted earlier, we do observe turbulent bursts and the associated transients in the outputs from the thin film gages, which coincide with the presence of systematic "wave like" disturbances upstream of points at which Schlieren photographs show an irregular increase in the boundary layer thickness. However, the time averaged increase in heating rates beneath such bursts is small, and thus, we have noted their presence as a precursor to transition rather than a definition of it. Typical distributions of pressure and heat transfer along and around the surface of the cone obtained during these studies are shown in Figures 10 and 11.

The variation of the position of the beginning of transition on the windward and leeside rays with angle of attack for a sharp 6°-cone are shown in Figures 12 and 13, together with earlier measurements made on similar cones but at a lower Mach number. These measurements demonstrate that the transition point on the leeside of the cone moves forward with increasing angle of attack while the transition point on the leeside ray moves toward the base of the cone. The shapes of the transition point obtained in our studies with sharp cones are compared with similar measurements from earlier studies conducted at lower Mach numbers. A unique feature of the shape of the transition points determined in the present study was the position of the most aft transition point(s) which occurred on the 90° and 270°-rays rather than the windward ray as observed in the earlier studies.

The measurements of the variation of the position of transition on the windward and leeside ray with angle of attack made in the present and earlier studies with 6%-blunt cones are shown in Figure 14. Here we observe the transition moves toward the tip on the windward ray, while there is a rearward movement on the leeside ray. The shapes of the transition fronts on the cones with the 14% blunt nose tip are shown in Figure 15. These configurations show a relatively narrow wedge-like transition region extending forward on the windward ray with a relatively flat transition front extending from the 90° to the 270°-ray around the leeside of the body.

In the analysis of transition measure obtained on sharp flat plates and cones, we found that the Reynolds number based on the local momentum thickness (Re_{θ}) provided the best correlation of both wind tunnel and flight measurements in hypersonic flow over highly cooled walls. Thus, following Finson, we have plotted the measurements made in the present studies together with those from earlier work in terms of the Reynolds number local momentum thickness and the local Mach number for both sharp and blunt bodies Figure 16). The values of the momentum thickness used in these plots were determined from computer solutions using the GE-3DSAP and Adams codes together with measurements from the Schlieren photographs obtained in our studies. It can be seen that for both sharp and blunt configurations, that ($Re_{\theta} / Re_{\theta \alpha = 0}$) ($M_o/M$) is relatively independent of angle of attack. Thus, for sharp cones it may be observed that transition moves forward on the leeside ray principally because of the large increase in the momentum thickness, while on the windward ray the effects of crossflow and higher unit Reynolds number combine to cause a decrease in the momentum thickness. For the blunted cones, the entropy layer is swallowed more rapidly on the windward rays, and consequently, the Reynolds number based on momentum thickness is increased and transition moves forward relative to its position at 0° angle of attack.

Effects of Wind-Fixed Transition on Aerodynamic Stability

In this study, we found that the changes which occurred in the forces and moments, which were developed as boundary layer transition moved onto the cone frustum, while small, had a measureable effect on the aerodynamic stability of sharp and blunted cones. We attempted to place transition onset (by varying the unit Reynolds number of the freestream) on the sharp and slightly blunted cones such that it fell on the leeside ray just behind the center of pressure of the unperturbed cone. From our observations of the geometry of the transition front, it was anticipated that this configuration would provide the greatest destabilizing effect. On the 18% blunt configurations, we positioned the most rearward location of transition front (which occurred on the leeside ray) at the base of the cone.

As transition moves onto the frustum of the sharp and slightly blunted cones ($r_n/R_b = 0.6\%$), the small increase in surface pressure, which acts to reduce the normal force at the base of the cone, combined with the increase in skin friction to the leeside of the frustum, which created a positive pitching moment, produces a destabilizing pitching moment. Our pressure measurements suggest that the pressure rise through the transition region is less than 5% of the local cone pressure and the destabilizing moments resulting from the increments on pressure and skin friction are of comparable magnitude.

Transition moves first onto the windward surface of the 18%-blunt cone models and the local increase on pressure and skin friction combine to yield a negative or stabilizing pitching moment about the CG. Again, calculations in which the pitching moment associated with the increased skin friction was determined from the measured heat transfer rates (assuming a Reynolds analogy factor of 1) and transition patterns demonstrated that transition-induced increments in pressure and skin friction gave restoring moments of roughly equal proportions. Taking the force and moment measurements and determining the increments in the moment in the center-of-pressure resulting from transition, we obtain the results shown in Figure 17. Here we have selected cases where the transition region was positioned on the cone in an attempt to obtain the maximum destabilizing or stabilizing effects.

We observe, as discussed earlier, that boundary layer transition exerts a destablizing effect on the sharp and slightly blunted configurations, and this is manifest in the forward movement of the center of pressure ($\Delta X_{CP}/L$) of between 3% and 5%. Transition on the blunt configuration is stablizing, and incremental movements of the center of pressure as large as 5% were recorded. It should be reiterated that we have studied only the incremental changes in forces resulting from transition on non-ablating configurations, and it might be anticipated that the forces induced by the growth of a transition region enhanced and shortened by ablation could be significantly larger for the equivalent non-ablating body.

STUDIES OF ROUGHNESS-INDUCED BODY-FIXED TRANSITION REGIONS

Transition Induced by Roughness Strips

The first set of studies conducted in this segment of the experimental program were designed to examine the characteristics of the perturbations in cone forces induced by wedge-shaped transition elements. The roughness elements were constructed by bonding Carborundum grit particles with acrylic laquer to the frustum of the cone as illustrated in Figure 18. The shape of this element was selected from the measurements of the turbulent spreading rate made by Fischer[15]; we used a triangular-shaped pattern centered about the 180° ray with an included angle of 8°. Grit sizes of 4, 5, 8 and 13 mils were used in this triangular trip. The studies were conducted for nosetip bluntness ratios (r_n/R_B) of 6 and 12%. Typical distribution of heat transfer downstream of the 4 and 13 mil roughness wedges are shown in Figures 19a and 19b. We see that in both cases, we induced transition regions downstream of the trips. However, the measurements indicate that, whereas a relatively narrow wedge of turbulent flow was generated behind the 4 mil roughness, using 13 mil roughness with an identical trip planform geometry, we induced a significantly larger region of turbulent flow. The incremental forces and moments associated with the transition regions on the 12% spherical nose tip were typically $\Delta C_N = -1.6 \times 10^{-3}$ and $\Delta C_M = +7.5 \times 10^{-3}$, where the moments referred to the tip of the models.

In the second series of body-fixed studies, we switched to a 6% blunt configuration and performed measurements with model incidences of 0 and 1°. At 0° incidence, the flow over the smooth configurations was fully laminar, as can be seen in Figure 20. We had little problem in tripping transition and obtaining wedge-shaped transition at 0° incidence, as indicated in Figure 21. It is extremely difficult to determine from the measured pressure data the magnitude of the pressure rise which occurs through the transition process. However, typical transition regions induce increments of -1.6×10^{-3} and $+6 \times 10^{-3}$ in the normal force and moment coefficient (ΔC_N and $\Delta C_{M_{NT}}$). We found it more difficult to induce transition on the leeside of the 6% blunt nose tip at 1° angle of attack. However, by increasing the trip roughness to 8 mils, we were able to generate the wedge shape transition region as shown by the transition pattern heat transfer distributions in Figure 22. Here we see that the spreading rate is slightly larger than predicted from Fischer's correlation; however, the leeward meridian is fully turbulent over two-thirds of the length of the cone. The average values for the measurements of ΔC_N and $\Delta C_{M_{NT}}$ were found to be -1.8×10^{-3} and 10.3×10^{-3}, respectively. This compares with a value of $\Delta C_N = -0.00685$, calculated by King[16] for this case.

Transition Produced By Nosetip Gouges

One of the most interesting results from the studies of body-fixed transition was the finding that small gouges or grooves in the nose tip could induce large wedge-shaped regions of frustum transition, which in turn were found to induce small but significant destabilizing forces.

We began our studies of the downstream effects of nose tip gouges by examining the flow downstream of the shallow wedge configuration, which was reconstructed from the incipient gouge generated in earlier studies conducted by Aerotherm. The heat transfer measurements of this configuration are shown in Figure 23 and the pressure measurement is given in Figure 24. We observe that a transitional flow is developed downstream of the gouge that generates a wedge-shaped transition region. The pressure measurements through the transition region on the tripped and untripped side of the model for this run, nondimensionalized by the pressure measurements made on the smooth configuration, are shown in Figure 24. It can be seen that in the transition region, the pressure is approximately 5% greater than the pressure in the laminar boundary layer. This incremental force and moments induced by the asymmetric transition region were $\Delta C_N = -0.0016$ and $\Delta C_M = +0.0068$, figures similar to those obtained earlier with roughness tripped transition.

The remaining studies to investigate nose tip gouge-induced transition were conducted using the 12% ablated elliptical replica of the 30 megawatt nose tip. As discussed earlier, we filled in the major gouges in this nose tip, retaining first a pair of small adjacent gouges, and then one of these gouges. An experiment was also run with the pitted nose tip. The heat transfer distribution and transition pattern on the cone behind the single gouge configuration is shown in Figure 25. Here the region of transition extended the full length of the cone and was confined to within a narrow wedge of dimensions similar to those predicted from Fischer's measurements. For this flow configuration, we measured incremental normal forces ($\Delta C_N = -0.0023$) which were significantly larger than those reported above. However, when we induced a larger region of turbulent flow over the model, as we achieved when transition was tripped with the pair of incipient gouges examined in Run 32, the incremental normal force was reduced to $\Delta C_N = -0.0016$ and $\Delta C_M = +0.0048$. We see from Figure 26 that not only is the boundary layer fully turbulent behind the pair of gouges, but transition has extended to the 90° meridian. The characteristics of this region were similar to those induced by frustum roughness. A comparison between the pressure measurement on the tripped and untripped sides of the model, shown in Figure 27, again demonstrated that when the boundary layer became fully turbulent, we observe little difference in the pressure between the tripped and the untripped side of the model.

"Body-Fixed" Transition Regions Developed Behind Asymmetric Steps and Gaps

In the previous two sections, we discussed the forces and the boundary layer properties developed over the cone surface as a result of tripping with asymmetric regions of roughness and with gouges in the nose tip. Each of these transition sources were effective in generated body-fixed transition regions which induced force perturbations which were significant from the viewpoint of lateral dispersion. However, nose tip gouging and the development of asymmetric roughness on the frusta of RV's is not well understood, and there is a high degree of speculation in the specification of such disturbances. Steps and gaps do, however, arise in the fitting of the nose tip and antenna windows onto the frustum. Because of such surface discontinuities and the differential ablation between nose tip frustum and antenna windows, three- dimensional disturbances which can induce asymmetric transition can be generated. In the present studies, we examined the effects of circumferential gaps placed on the cone surface to simulate antenna windows and step-downs in the cone frustum to simulate a mismatch in surface dimensions between nose tip and the frustum.

We obtained the measurements with a single circular groove and with the groove filled in, leaving a small open segment to simulate antenna windows and gaps at the nosetip cone junction. Similar measurements were obtained with a symmetrical two-groove configuration and an asymmetric configuration based on this model with the grooves filled in, leaving two windows as shown in Figure 18. Transition measurements were also made with the asymmetric step-down model also shown in Figure 18.

The first set of studies was designed to investigate transition induced by circumferential symmetrical and asymmetric grooves in the frustum. Typical heat transfer distribuitons to the smooth configuration with the grooves filled in, to the configuration with a single symmetric groove, and to a configuration where the groove was refilled, leaving a small gap, are depicted in Figures 28, 29 and 30, respectively. We see that the boundary layer in the absence of the groove (Figure 28) is completely laminar. Adding a single symmetric groove induced a symmetric transition region beginning 14 inches from the tip of the nose. Finally, with the single rectangular gap, we obtained an asymmetric transition front. It can be seen that despite the sizeable gap in the surface of the cone, we induce only a small transition asymmetry. We increased the magnitude of the disturbance by introducing a second groove, testing first the symmetric, two-groove configuration and then the two-gap configuration. The heat transfer distribution behind the symmetric two-groove configuration indicated that a symmetric transition front was induced with the transition occurring 10 inches from the top of the model. The two-gap configuration induced a wedged-shaped transition region of significant proportions as shown in Figure 31. As shown in Figure 32, we can detect a small pressure rise (5% P_{CONE}) associated with the transition region. The incremental forces associated with the asymmetric transition regions induced by the gaps were typically $\Delta C_N = -1.4 \times 10^{-3}$ and $\Delta C_M = 4.8 \times 10^{-3}$, which are similar to those obtained by tripping with nose tip gouges and frustum roughness.

We had considerable difficulty generating asymmetric transition with the fairly radical step-down model. The heat transfer distribuiton (see Figure 33) shows some evidence of tripping, but this region is very small compared with the effects which can be induced by very small indentations in the nose tip. In general, very large steps and gaps were required to induce asymmetric regions of significant proportions. However, on a flight vehicle, discontinuities in the surface are also accomplished by changes in the surface material, which produces regions of differential ablation. Studies in the ballistic range have indicated that differential blowing is a much stronger stimulation to transition than a simple, geometric change. Hence, we feel that to simulate the flight vehicle correctly, we should introduce blowing form a relatively smaller gap region. However, as shown in Figure 34 our studies with the different methods of tripping transition provide a range of destabilizing forces and moments that appear relatively independent of the tripping mechanism. While additional studies with differential blowing should be made, the measurements made in the present series provide a good indication of the forces and moments one might expect during the asymmetric, body-fixed transition process at high altitudes.

CONCLUSIONS

In this research program, we investigated a number of aero-thermodynamic phenomena which influence the stability of slender reentry vehicles. The first phase of this study was an investigation of aerodynamic mechanisms which can perturb the stability of slender conical vehicles when transition moves, first onto the frustum, and then onto the nose tip "wind-fixed transition". Simultaneous measurements of cone force and the distribution of heat transfer and pressure were made to determine the influence of angle of attack and bluntness ratio on the characteristics of the frustum transition region and the associated perturbations in cone forces. Measurements of the characteristics of the transition regions are presented, together with correlations with earlier range and wind tunnel measurements. These measurements demonstrate that transition moved first onto the leeside of sharp or slightly blunted cones inducing a destabilizing effect; while, on blunter bodies ($0.1 < r/R_B < 0.2$) transition occurred first on the windward ray, resulting in a stabilizing effect. On both sharp and blunt configurations, the incremental forces and the corresponding movements of the center of pressure associated with such "wind-fixed" transition regions were small ($\Delta XCP/L_{cone} \approx 1\%$).

In the second phase of this study, we found that wedge-shaped regions of "body-fixed" transition could be induced over the conical models with relative ease. The incremental forces associated with such regions were typically $\Delta C_N = -1.8 \times 10^{-3}$ and $\Delta C_{M_{NT}} = 6 \times 10^{-3}$. We found that, whereas asymmetric frustum transition could be induced with relative ease by small gouges in the nose tip, large discontinuities were required in the frustum to induce comparable effects. Our studies indicated that the magnitude of the destabilizing forces induced by transition was relatively independent of the tripping mechanism. Thus, the measurements made in the present series should give a good indication of the forces and moments associated with body-fixed transition over a non-ablating body. Additional studies, in which the differential blowing associated with an ablating vehicle is simulated, are required.

REFERENCES

1. Reynolds, O., "An Experimental Investigation of the Circumstances Which Determine Whether the Motion of Water Shall be Direct or Sinuous and of the Law of Resistance in Parallel Channels," Trans. Roy. Soc. (London) A174, 1883 pp. 935-982 Sci. Papers 2:51.
2. Schlicting, H., Boundary Layer Theory, 4th Edition, McGraw Hill Book Co., New York, NY, 1960.
3. Pate, S.R. and Schueler, C.J., "An Investigation of Radiated Aerodynamic Noise Effects on Boundary-Layer Transition in Supersonic and Hypersonic Wind Tunnels," AIAA Paper No. 68-375, April 1968.
4. Stainbeck, P.C., Fischer, M.C. and Wagner, R.D., "Effects of Wind-Tunnel Disturbances on Hypersonic Boundary Layer Transition," AIAA 10th Aerospace Sciences Meeting, San Diego, California, 17-19 January 1972.

5. Reda, D.C., "Boundary-Layer Transition Experiments on Sharp, Slender Cones in Supersonic Freeflight," AIAA Paper 78-1129, July 1978.

6. Potter, J.L., "Boundary-Layer Transition on Supersonic Cones in an Aeroballistic Range," AIAA Journal, Vol. 13, No. 3, March 1975, pp. 270-277.

7. Sheetz, N.W., Jr., "Free-Flight Boundary Layer Transition Investigations at Hypersonic Speeds," AIAA Paper No. 65-127, 2nd Aerospace Sciences Meeting, New York, N.Y., Jan. 1965.

8. Morkovin, M.V., "Instability, Transition to Turbulence and Predictability" Keynote Address to AGARD Symposium on Laminar-Turbulent Transition, Technical University of Denmark, Copenhagen, Denmark, 2-4 May 1977.

9. Reshotko, E., "Boundary-Layer Stability and Transition," Annual Review of Fluid Mechanics, Vol. 8, 1976, pp. 311-349.

10. Morrisette, E.L., Stone, D.R., and Cary, A.M., "Downstream Effects of Boundary Layer Trips in Hypersonic Flow," Langley Symposium on Compressible Turbulent Boundary Layers, NASA SP 216, December 1968.

11. Holden, M.S., "Shock Wave-Turbulent Boundary Layer Interaction in Hypersonic Flow," AIAA 10th Aerospace Sciences Meeting, San Diego, California, 17-19 January 1972.

12. Bradshaw, P., "A Note on Reverse Transition," JFM (1969), Vol. 35, Part 2, pp. 387-390.

13. Stetson, K.F. and Rushton, G.H., "Shock Tunnel Investigation of Boundary-Layer Transition at M = 5.5," AIAA Journal, Vol. 5, No. 5, May 1967, pp. 899-906.

14. Finson, M., "Frustum Transition Modeling," Proceedings of the ABRES Accuracy Review, 8, 9, November 1977.

15. Fischer, M.C., "Spreading of a Turbulent Disturbance," AIAA Journal 10, pp. 957-959, July 1972.

16. King, H.H., "Lateral Motion Due to Frustum Transition (U)," 4th Joint Strategic Sciences Meeting of AIAA, Volume 1, pp. 2-38, September 1978 (SECRET).

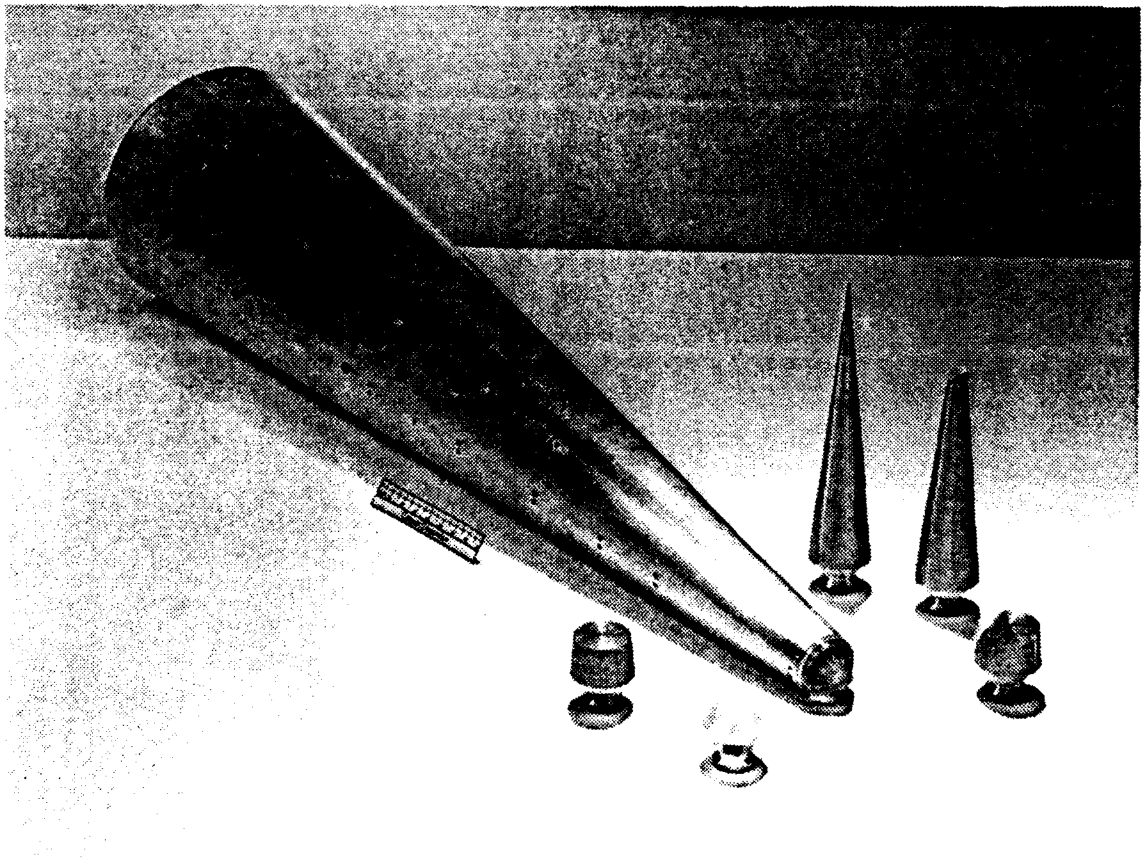

Figure 1 Cone Model With Interchangeable Nose Tips

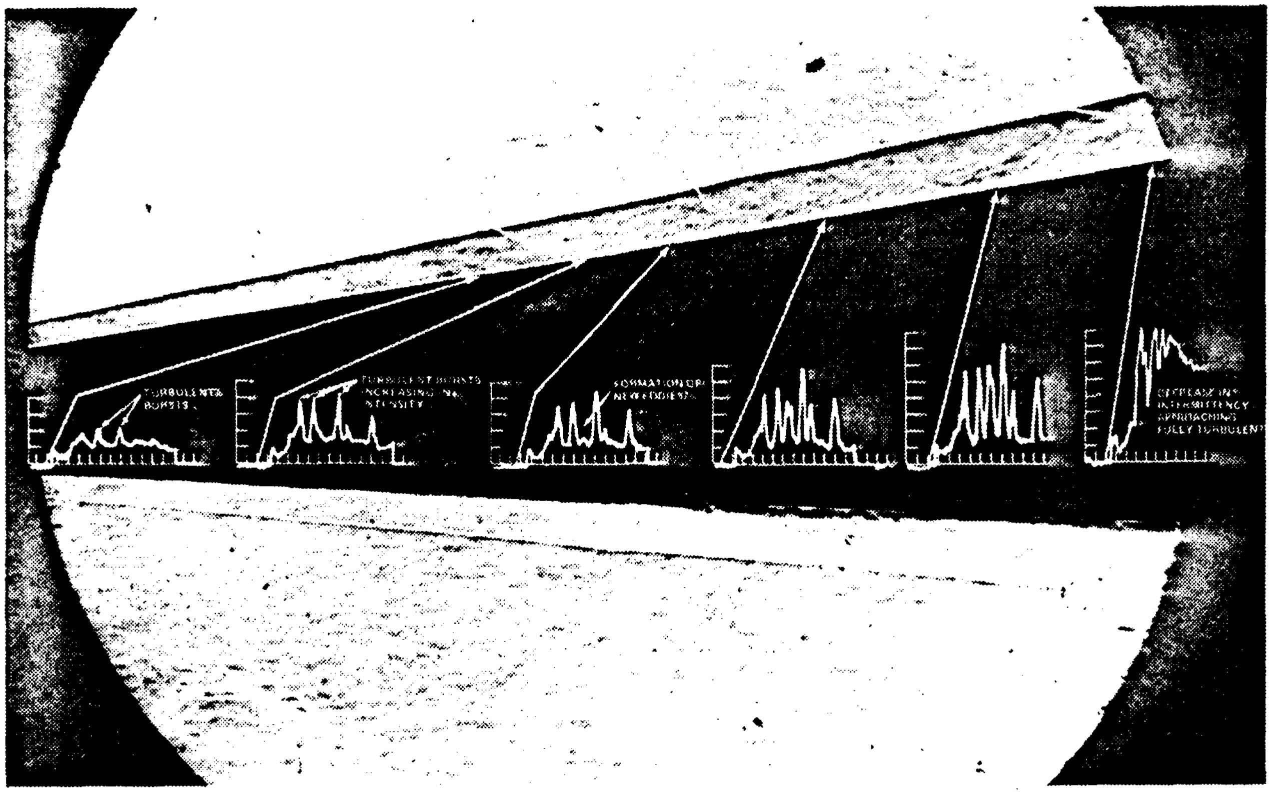
TURBULENT BURSTS
TURBULENT BURSTS INCREASING IN INTENSITY
FORMATION OF NEW EDDIES
DECREASE IN INTERMITTENCY APPROACHING FULLY TURBULENT

Figure 2 SCHLIEREN PHOTOGRAPH SHOWING DEVELOPMENT OF TRANSITION OF A CONICAL BOUNDARY LAYER IN HYPERSONIC FLOW

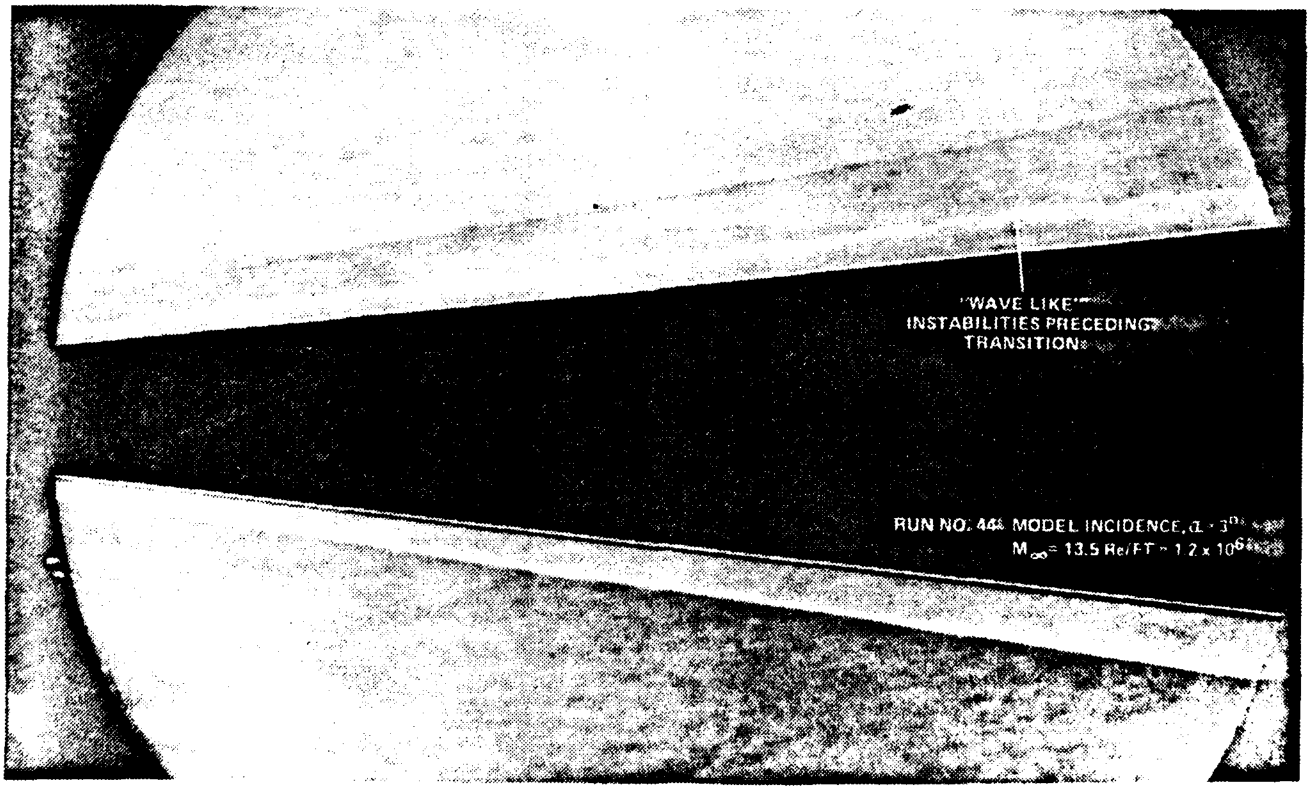
"WAVE LIKE" INSTABILITIES PRECEDING TRANSITION
RUN NO. 44 MODEL INCIDENCE, α = 3°
M∞ = 13.5 Re/FT = 1.2 x 10^6

Figure 3 FORMATION OF "WAVE LIKE" INSTABILITIES AT THE EDGE OF THE BOUNDARY LAYER PRECEDING THE GROSS INSTABILITIES

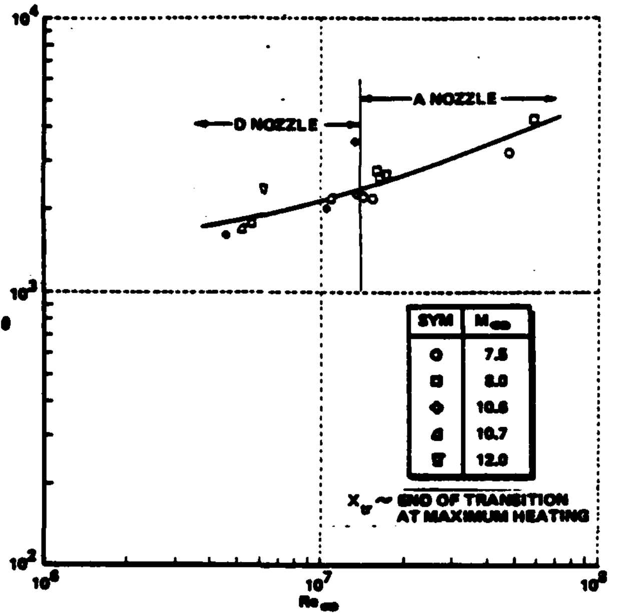

Figure 4 Correlation of Transition Showing the Effects of Tunnel Size

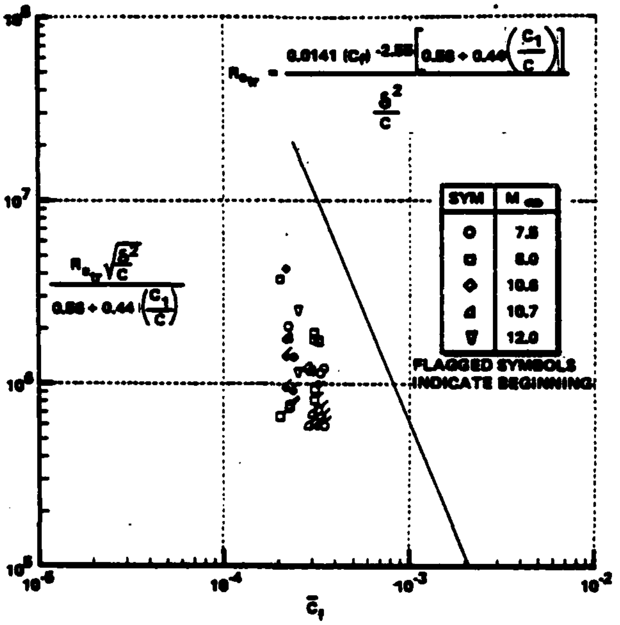

Figure 5 Correlation of the Flat Plate Transition Data in Terms of the Parameters Suggested by Pate and Schueler

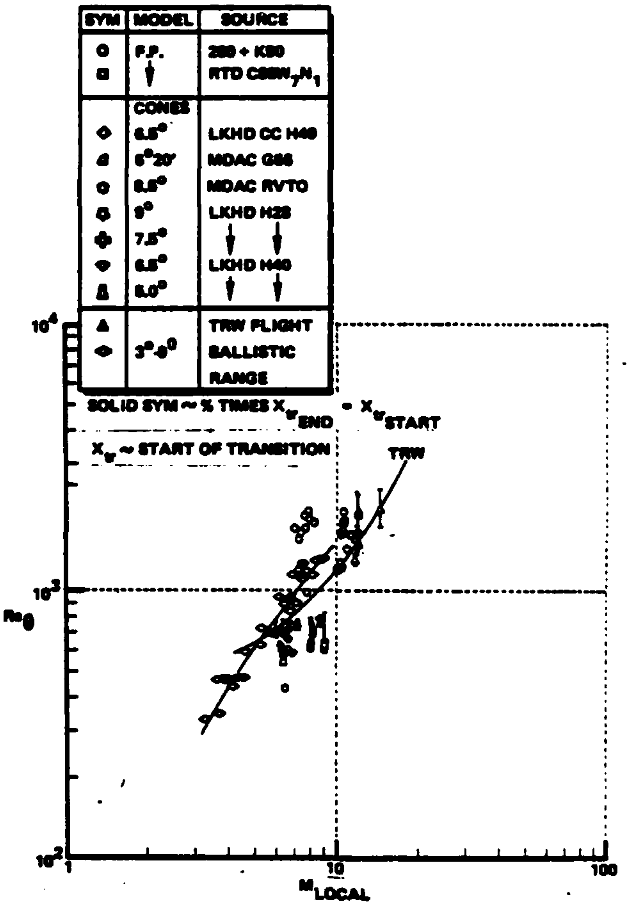

Figure 6 Correlation of Transition Measurements in the Calspan Shock Tunnels with Ballistic and Downrange Measurements

SOURCE	SYM	Θ_c	M_∞	M_e	$(T_W/T_{aw})_e$	U_e^2/ν_e, 1/SEC	FACILITY
REDA	○	5°	4.4	4.2	.22	.20 - 1.80 × 10^{11}	RANGE
KROGMANN	— — — ———	5°	5.0	4.7	.70 - .87	.08 - 0.42 × 10^{11}	LUDWIEG TUBE
STETSON	□ ◇ ▲ ○	8°	5.5	4.9	.17 - .23 .28 - .37 .42 - .50 .57	.11 - 0.30 × 10^{11} .09 - 0.30 × 10^{11} .14 - 0.17 × 10^{11} 0.10 × 10^{11}	SHOCK TUNNEL
PRESENT STUDY	◓	5°	13.2	10.2-10.6	.148	.41 × 10^6	SHOCK TUNNEL

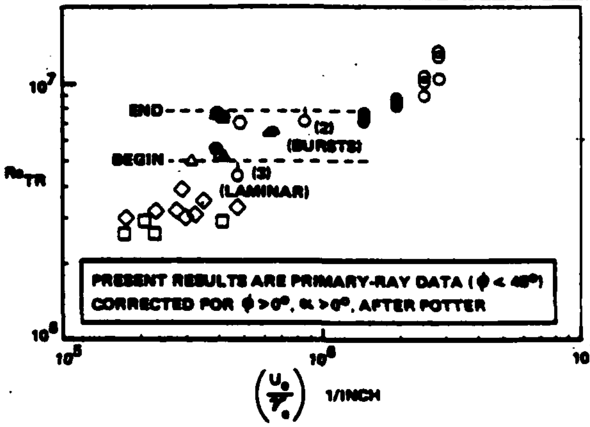

Figure 7 Transition Reynolds Number Vs. Unit Reynolds Number; Present Data Vs. Krogmann and Stetson

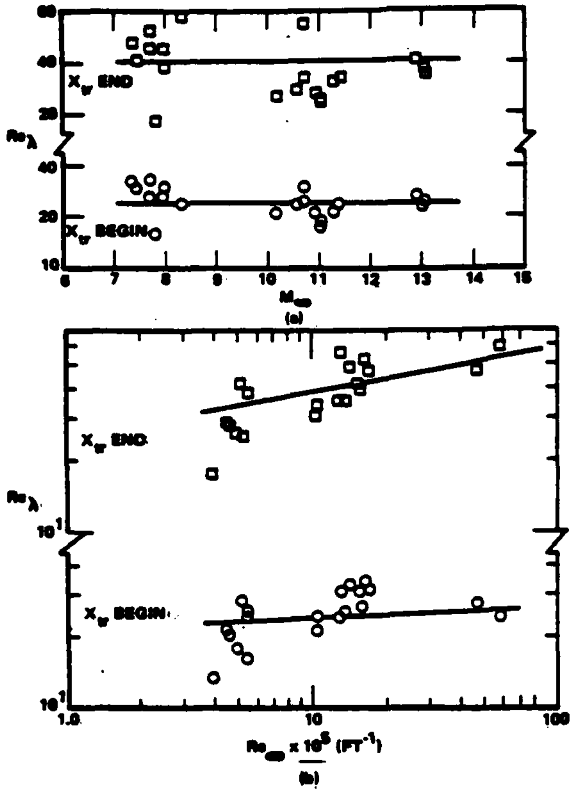

Figure 8 Correlation of the Eddy Reynolds Number with Transition Measurements on the Flat Plates

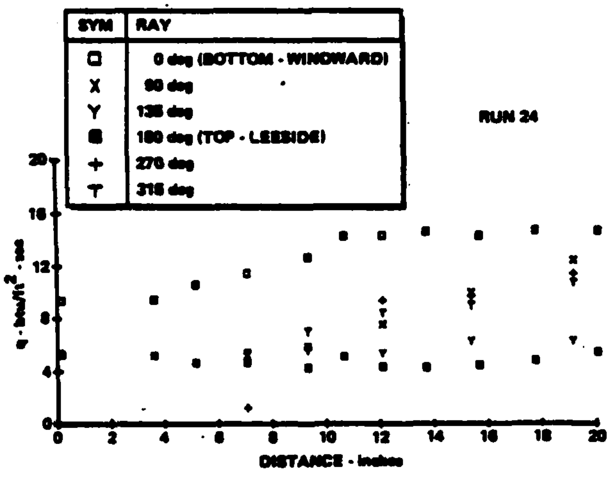

a. HEAT TRANSFER DISTRIBUTION

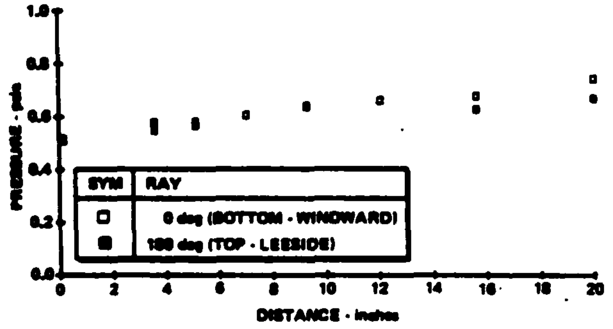

b. PRESSURE DISTRIBUTION

Figure 10 Measurements on 6° Cone Model for 6%, 0° Blunt Nose Configuration – M_∞ = 11.3, Re/FT = 1.0 x 10^7, α = 0° 5′

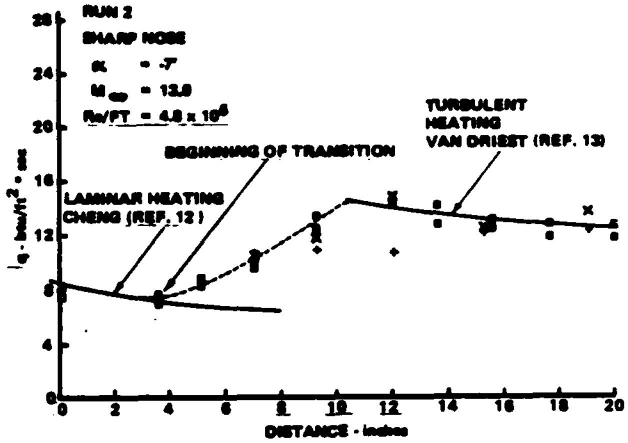

Figure 9 The Distribution of Heat Transfer Through a Transition Region on the Surface of a 6° Cone in Hypersonic Flow

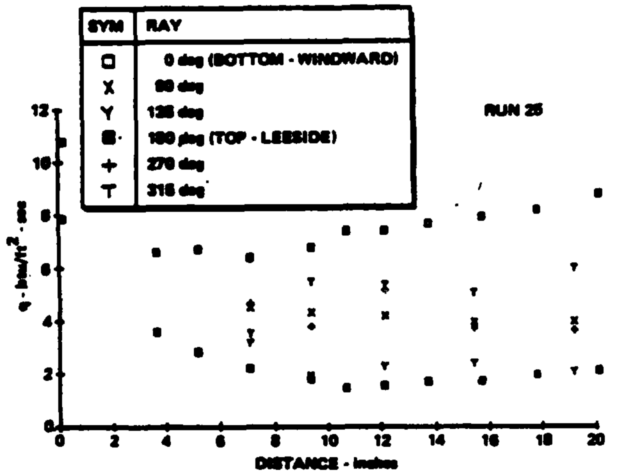

a. HEAT TRANSFER DISTRIBUTION

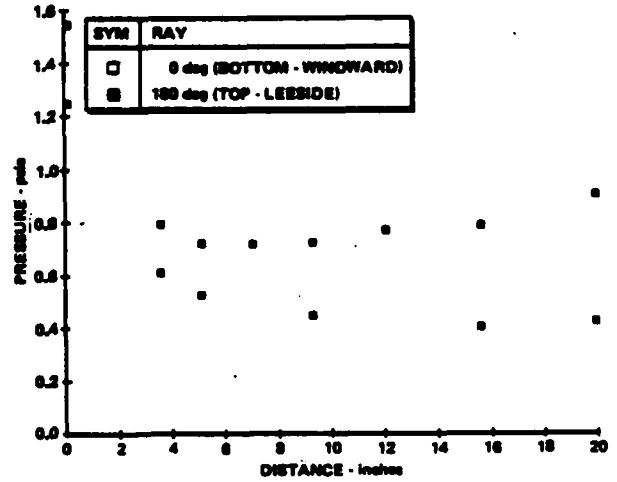

b. PRESSURE DISTRIBUTION

Figure 11 Measurements on 6° Cone Model for 21% Spherical Nose Configuration – M = 11.4, Re/FT = 1.0 x 10^7, α = 2° 5′

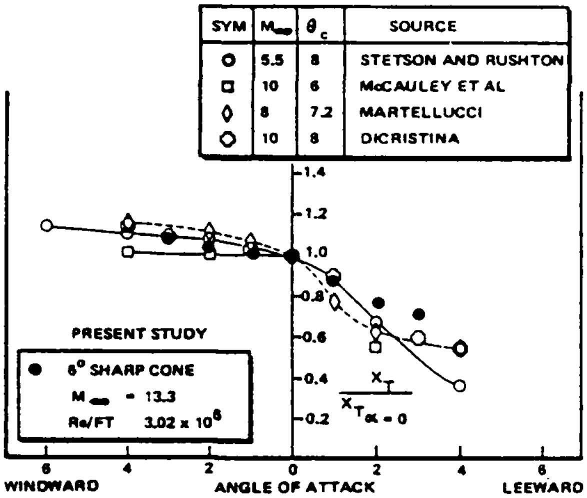

Figure 12 Variation of Nondimensional Transition Front Location on Sharp Cones with Angle of Attack

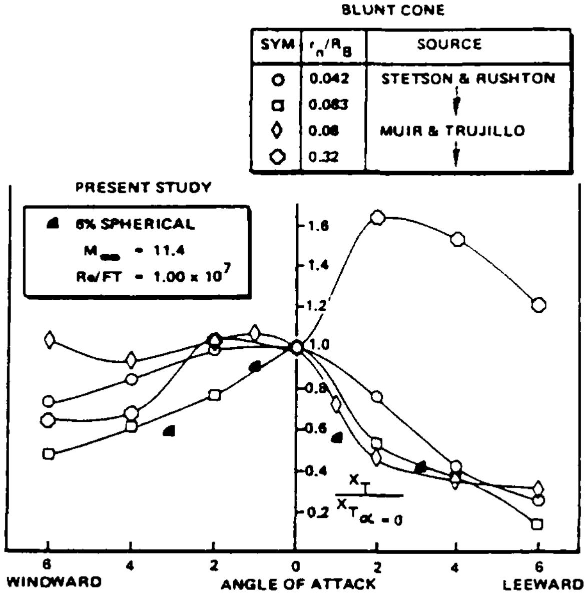

Figure 14 Variation of Transition Front Location on Slightly Blunted Cones with Angle of Attack

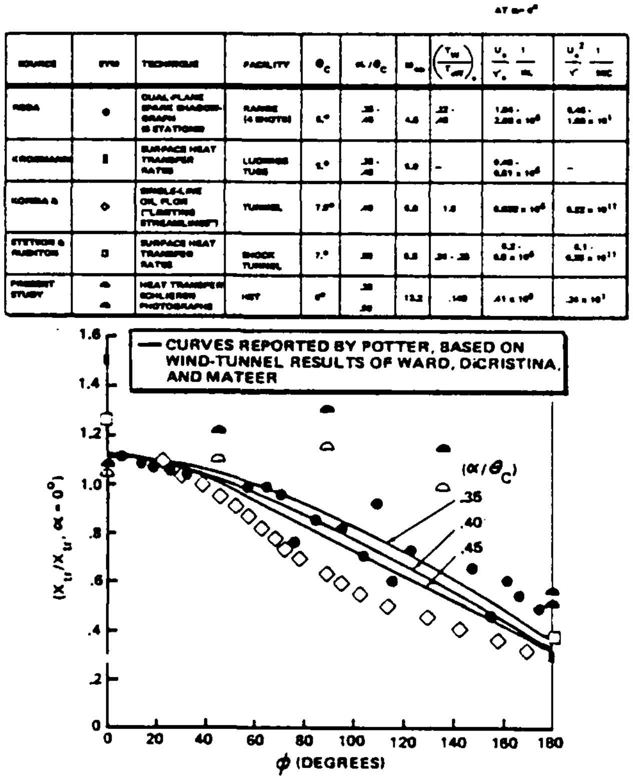

Figure 13 Transition Zone Asymmetry; Comparisons with Other Data, $0.35 \le (\alpha/\theta_c) \le 0.50$

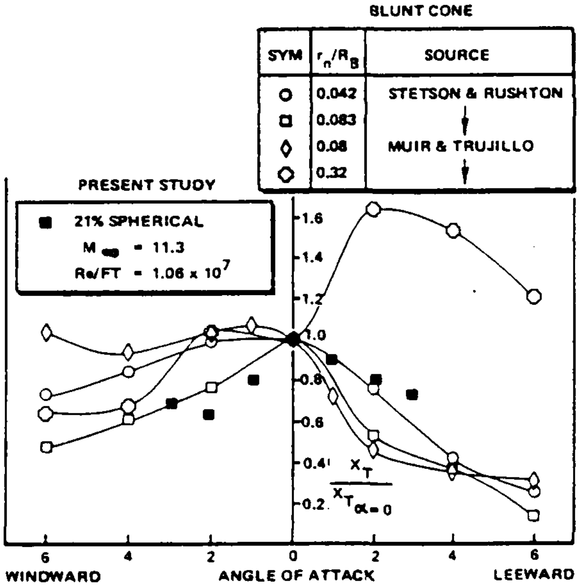

Figure 15 Variation of Nondimensional Transition Front Location on Blunt Cones with Angle of Attack

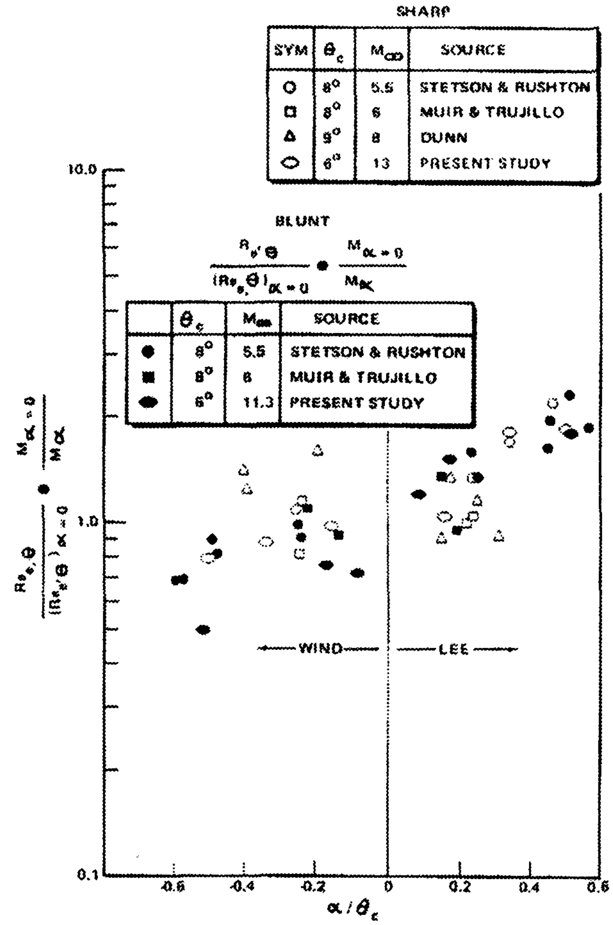

Figure 16 Correlation of Transition Front Locations on Sharp and Blunt Slender Cones at Angle of Attack

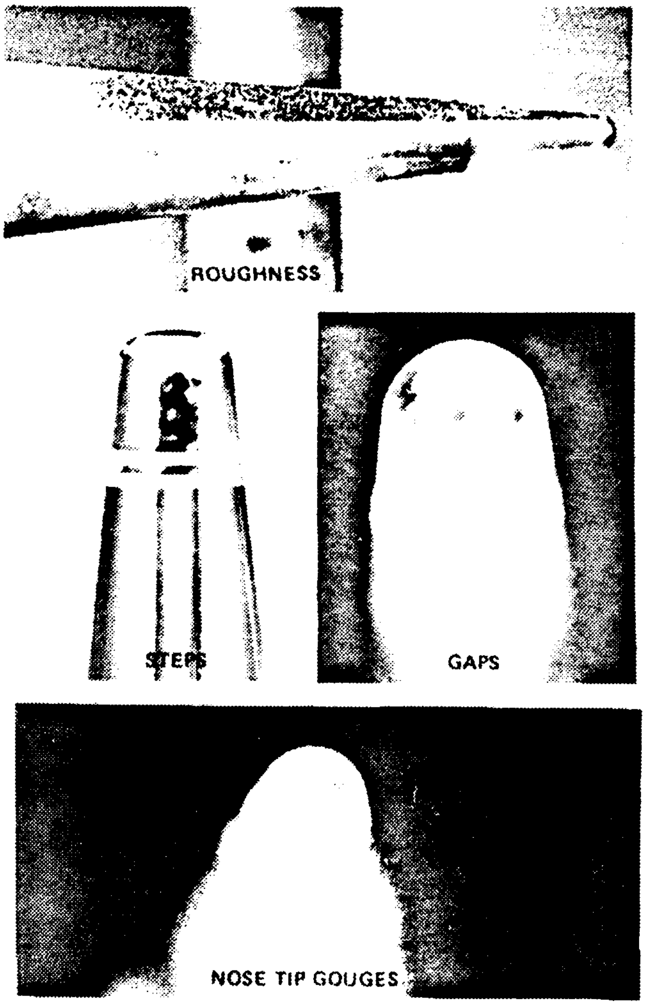

Figure 18 Body-Fixed Transition Sources

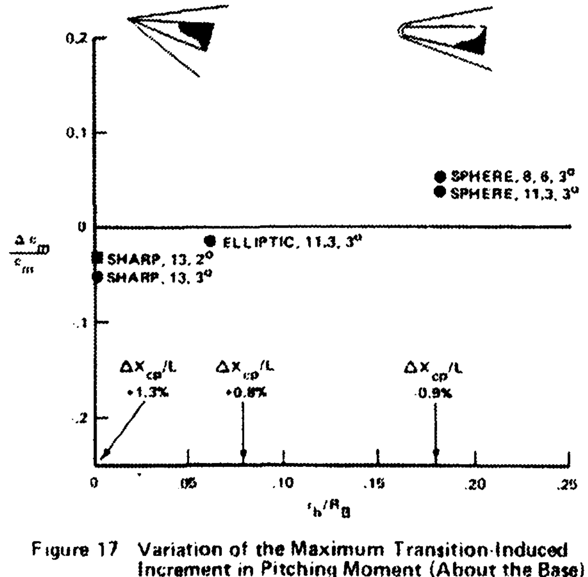

Figure 17 Variation of the Maximum Transition-Induced Increment in Pitching Moment (About the Base) with Bluntness Ratio for a 6° Cone

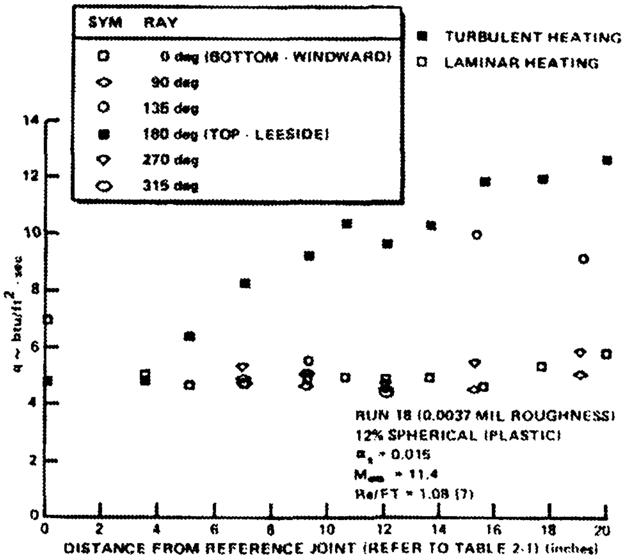

Figure 19a Asymmetric Boundary Layer Transition Tripped by a Triangular Roughness Strip Containing 3.7 Mil Roughness

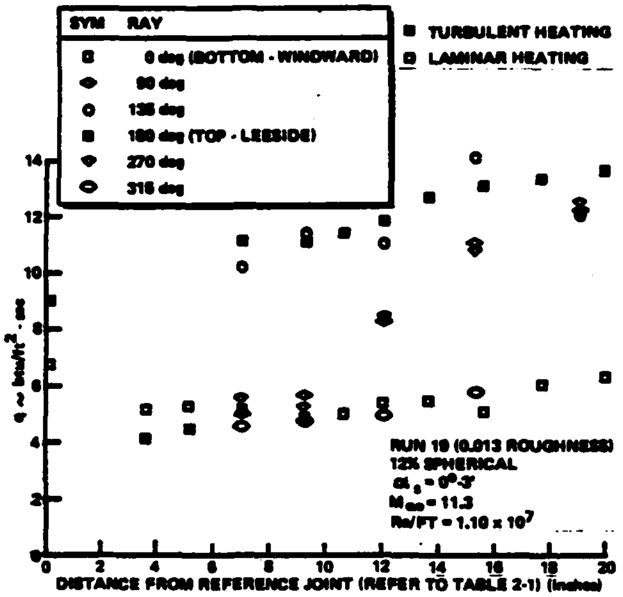

Figure 19b Asymmetric Boundary Layer Transition Tripped by a Triangular Roughness Strip Containing 13 Mil Roughness

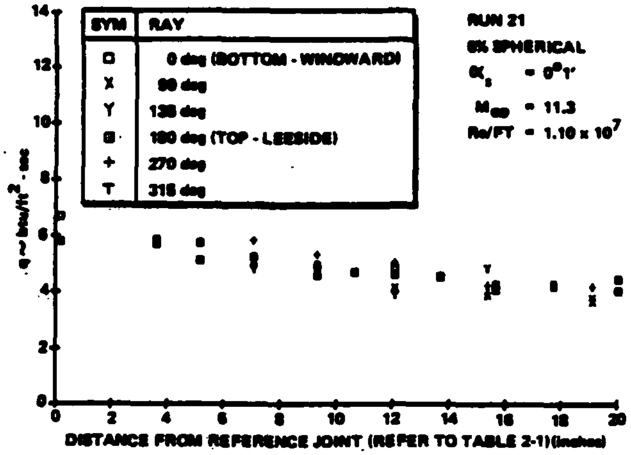

Figure 20 Body Fixed Transition Heat Transfer for 6% Spherical Cone, Re/FT = 1.10 x 10^7

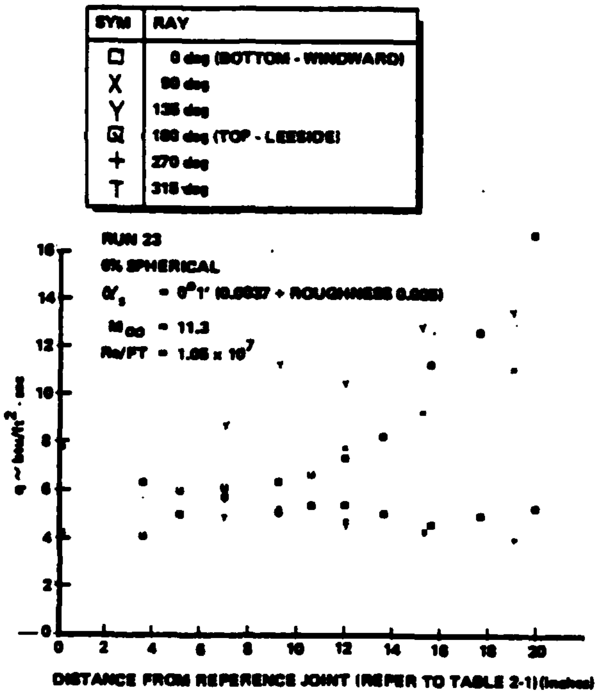

Figure 21 Body Fixed Transition Heat Transfer for 6% Spherical Cone, Re/FT = 1.05 x 10^7

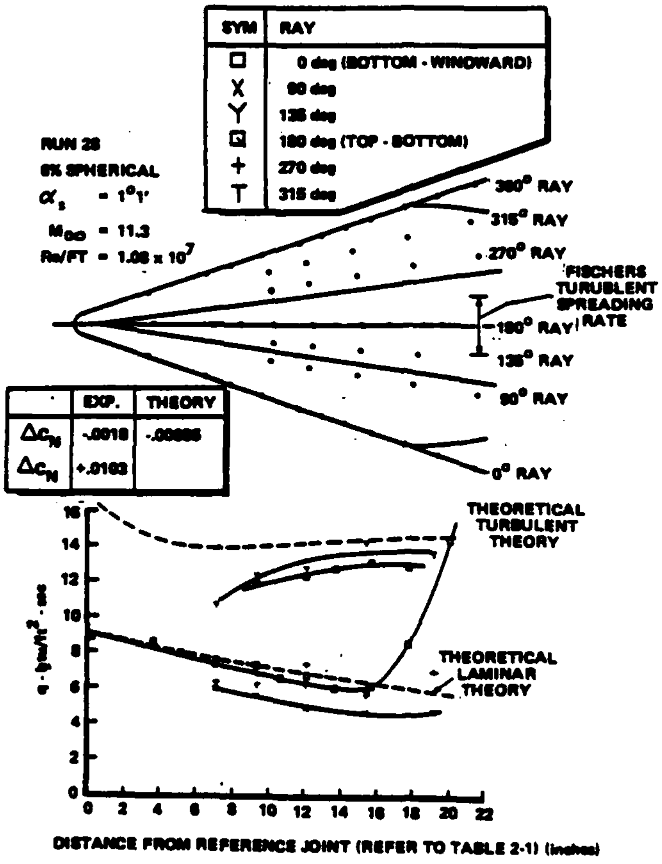

Figure 22 A Body-Fixed Transition Region Induced by Surface Roughness

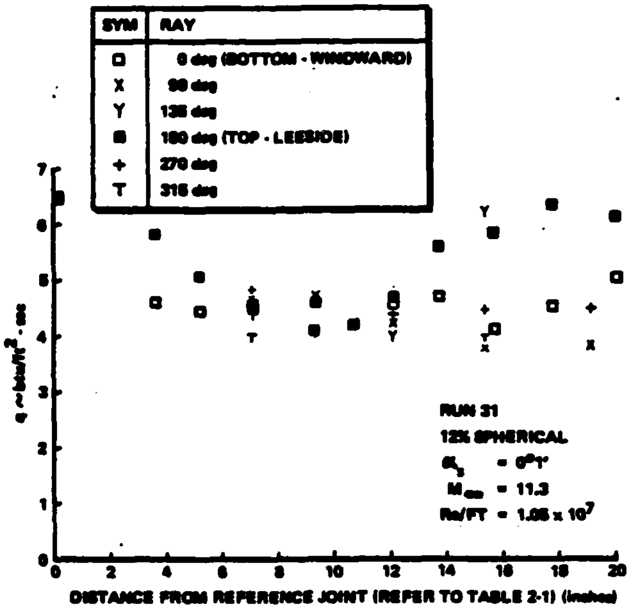

Figure 23 Heat Transfer Distribution to the 6° Cone in Asymmetric Transitional Flow Induced by the Incipient Gouge Reconstructed from the Aerotherm Nosetip

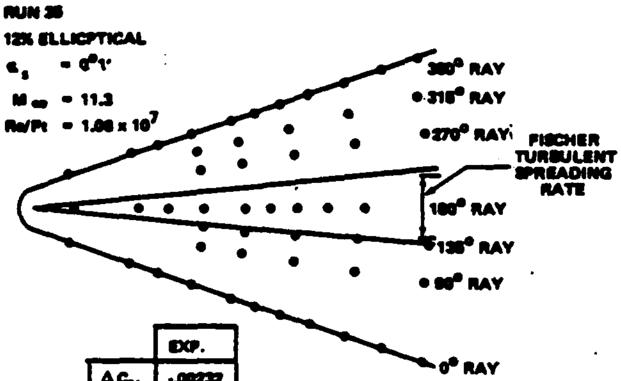
RUN 35
12% ELLICPTICAL
α_s = 0°1'
M_∞ = 11.3
Re/Ft = 1.06 x 10^7
360° RAY
315° RAY
270° RAY
FISCHER TURBULENT SPREADING RATE
180° RAY
135° RAY
90° RAY
0° RAY

	EXP.
ΔC_N	-.00232
ΔC_N	+.00715

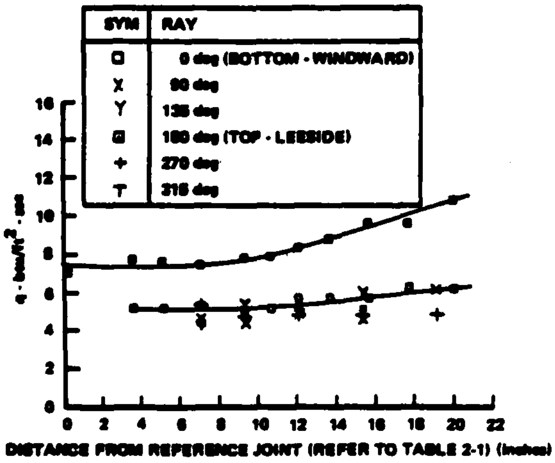

Figure 25 Body-Fixed Transition Induced by a Small Gouge in the Nose Tip

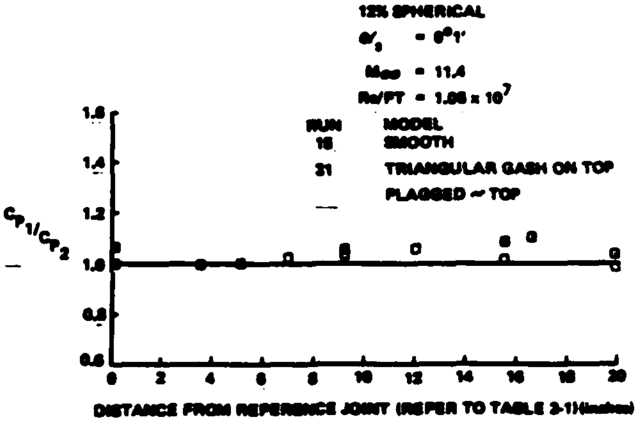

Figure 24 Normalized Pressure Distribution Showing the Influence of Gouges in the Nose Tip

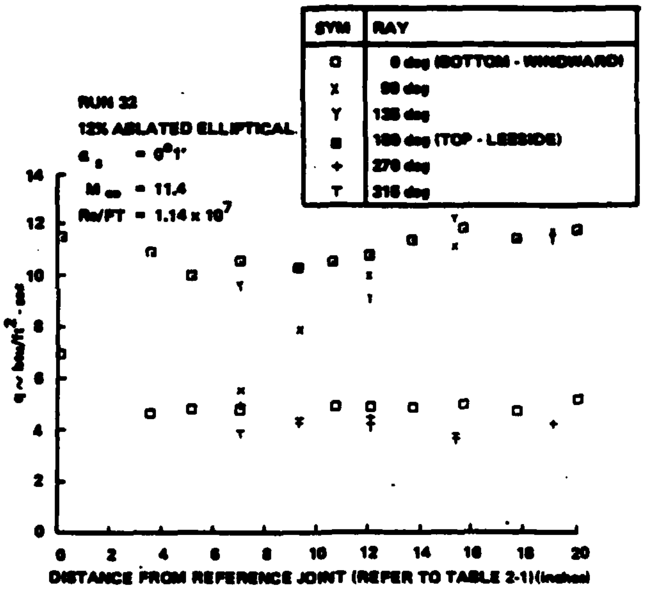

Figure 26 Heat Transfer Distribution to the 6° Cone in Asymmetric Transitional Flow Induced by Two Adjacent Gouges in the Elliptical Nose Tip

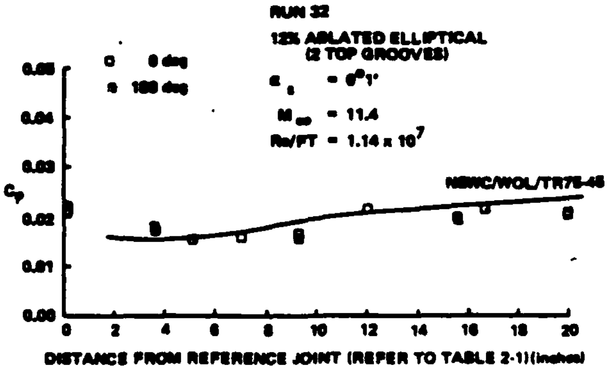

Figure 27 Pressure Distribution on the 6° Cone Capped with the Elliptical Nose Tip Modified with Two Gouges in the Nose Tip

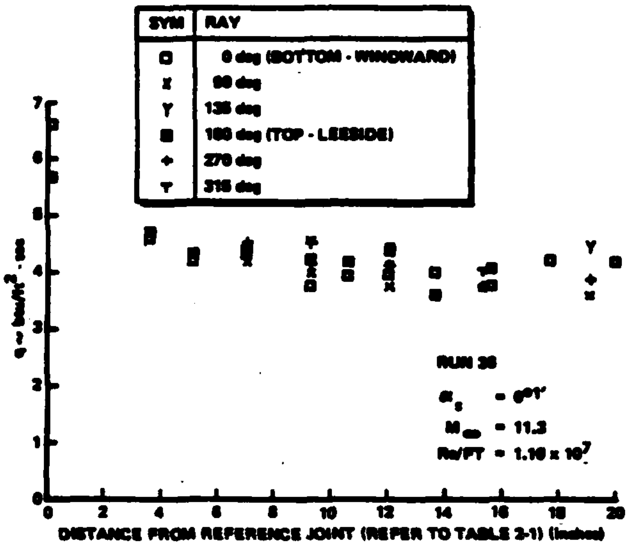

Figure 28 Heat Transfer Distribution to the Smoothed Model Configuration

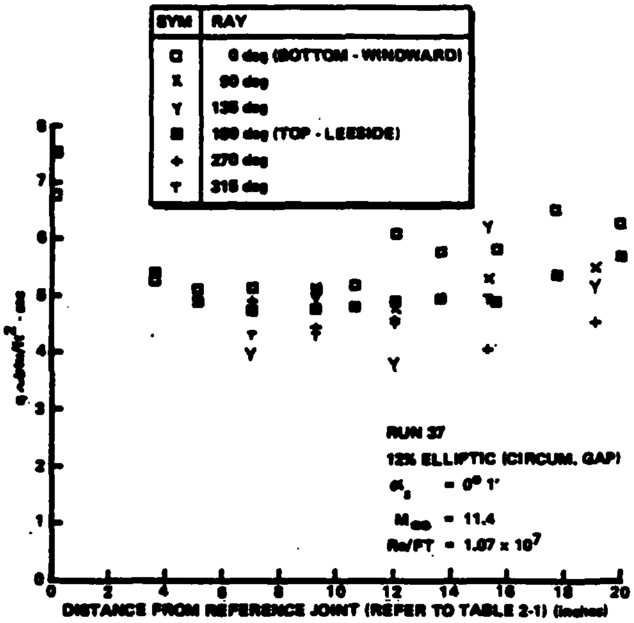

Figure 30 Heat Transfer Distribution to the Model with the Nose Tip Configuration with Single Gap in Circumferential Grove

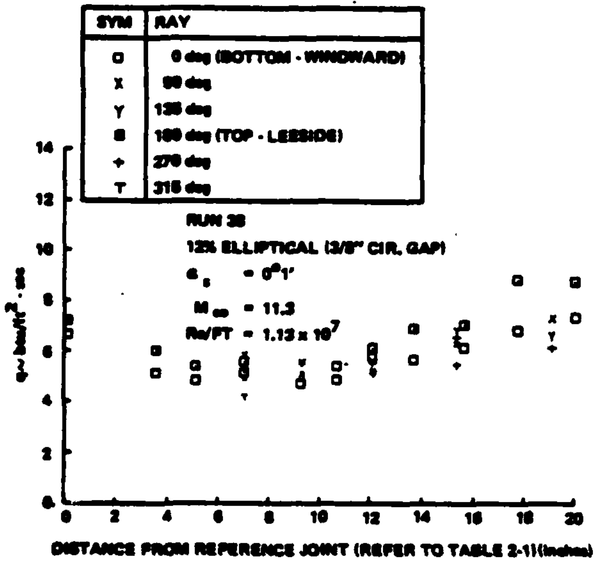

Figure 29 Heat Transfer Distribution to Model with Single Circumferential Gap

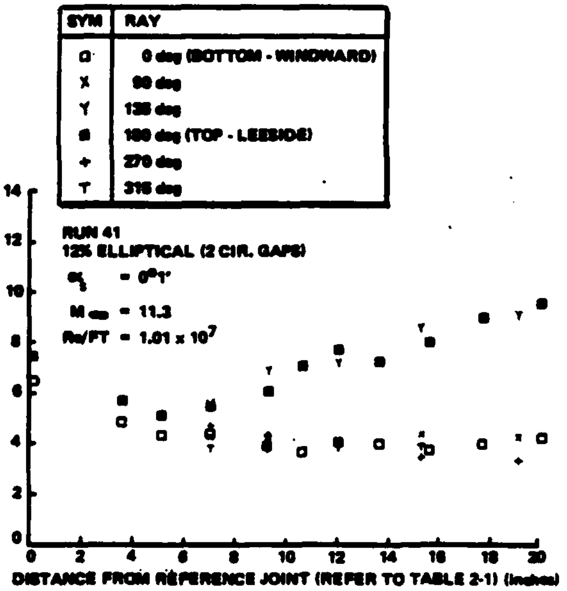

Figure 31 Heat Transfer Distribution to the Model with the Nose Tip Configuration Shown in Figure 2-31

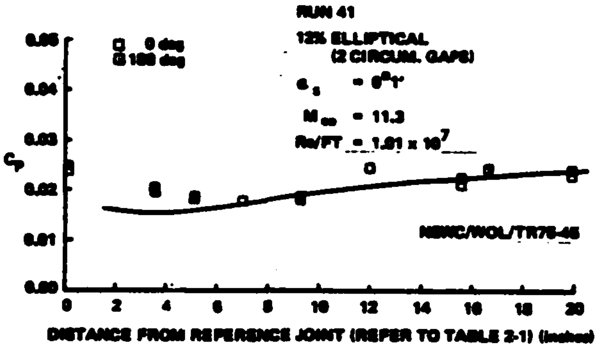

Figure 32 Pressure Distribution on the Frustum of the 6° Cone Downstream of Two Circumferential Gaps

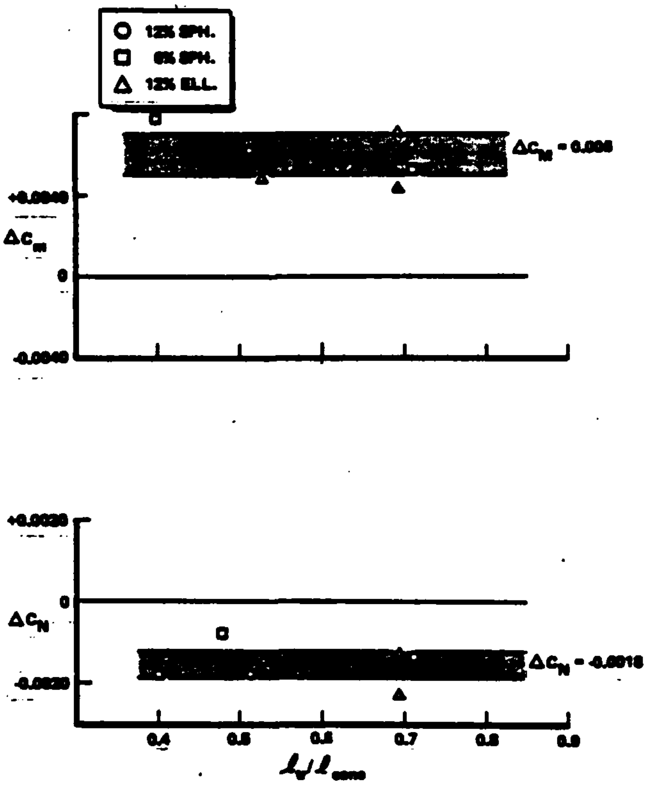

Figure 34 Incremental Force and Moment Measurements Resulting from Regions of Body-Fixed Transition

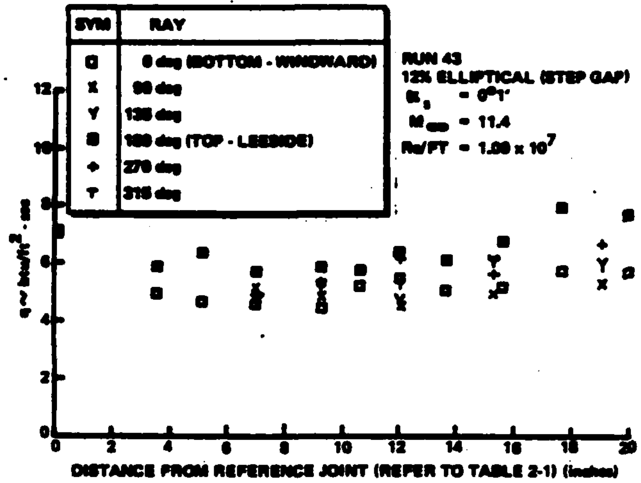

Figure 33 Heat Transfer Distribution Downstream of the Stepped Nose Tip Configuration Shown in Figure 2-28

APPENDIX B

"Aerothermal Problems Associated with Viscous/Inviscid Interaction Over Hypersonic Flight Vehicles"

IUTAM Symposium on "Turbulent Shear-Layer/Shock-Wave Interactions"

September 9-12, 1985
Palaiseau, France

This page intentionally blank.

AEROTHERMAL PROBLEMS ASSOCIATED WITH VISCOUS/INVISCID INTERACTION OVER HYPERSONIC FLIGHT VEHICLES

IUTAM Symposium
on "Turbulent
Shear-Layer/
Shock-Wave
Interactions",
Sept. 9-12,
Palaiseau, France

Michael S. Holden
Calspan/UB Research Center
Buffalo, New York 14225

1. Introduction

In recent years, there has been a resurgence of interest in the development of hypersonic vehicles whose designs are significantly more sophisticated than the essentially ballistic re-entry vehicles which have been constructed and flown to date. In assessing the prediction techniques associated with the design of systems like the trans-atmospheric vehicle (TAV), the orbital transfer vehicle (AOTV), and a number of vehicles designed to be highly maneuverable at hypersonic speeds, it has become evident that there are a number of important aerothermal problems which must be addressed. Such problems include the prediction of low density non-equilibrium flows in the transition regime, the transition to turbulence at hypersonic speeds, turbulent boundary layer and shear layer development in strong pressure gradients, and the development of turbulent reacting boundary layers over ablating and transpiration-cooled surfaces. However, in both laminar and turbulent flows, the classes of problems associated with viscous/inviscid interaction or shock/boundary layer interaction represent those which create the most serious aerothermal load problems and, at the same time, are the most difficult to compute with accuracy.

While in supersonic flows, regions of shock wave/boundary layer interaction have their largest impact on the aerodynamic loads; in hypersonic flow, it is the large thermal loads and gradients generated in turbulent shock interaction regions that are of greatest concern. Of course, the large dynamic loads associated with the intrinsic unsteadiness of these flows also remain a principal concern. Since the severe heating loads on certain key components mandate the use of ablative- or transpiration-cooled thermal protection systems, the effects of surface roughness and blowing on the characteristics of shock/boundary layer interaction over such components is an important and, as yet, an unresolved problem. Although the aerothermal heating loads associated with regions of shock wave/turbulent boundary layer interaction will present significant problems in hypersonic flight at low altitudes, it may be the laminar viscous/inviscid interaction and flow separation, which occurs in high altitude hypervelocity flight, which provides fundamental limitations on the performance of maneuvering hypersonic vehicles, and in particular those employing airbreathing propulsion systems. In the high altitude regime, the effectiveness of jet interaction and flap control systems, and intakes and combustors of hypersonic ram jets may be seriously reduced as the surfaces are in essence "faired-in" by viscous/inviscid interaction and flow separation as discussed in Reference 1. This paper reviews some of the important aerothermal problems associated with viscous/inviscid interaction over hypersonic flight vehicles.

2. Interacting Flows Over Transitional Nose Shapes

The shaping of ablative leading edges as boundary layer transition spreads over the surface can be strongly influenced by regions of shock wave/boundary layer interaction. The development of concave or idented nose shapes has been observed in both ground and flight test studies. The heating in the transition region near the sonic point causes the initial indenting (which is often three-dimensional in character) and the induced shock/boundary layer interaction subsequently enhances the indenting process. The large heating rates, which are generated at the base of the shocks formed on such indented nose shapes (Figure 1), coupled with roughness-enhanced heating, can induce heating many times those recorded at the stagnation point.

In hypersonic flows, the shock pattern and distribution of properties over blunt nose shapes are relatively independent of Mach number. However for flows over indented noseshapes, where embedded shocks and separated flows are generated in the flow field, this "Mach number independences principal" is invalid. This point is illustrated in Figures 2 and 3, where schlieren photographs and heat transfer measurements over an indented configuration are shown for Mach numbers of 11 and 13. It can be seen that the size of the separated region is reduced and the magnitude of the reattachment heating is nearly doubled as the Mach number is increased. Surface roughness, which is an intrinsic feature of an ablating nosetip, can also play an important role in controlling the flow field and the distribution of heating over indented nose shapes as illustrated in Figures 4 & 5.

It can be seen that adding surface roughness increased the size of the separated region and almost doubled the heating rate in the reattachment compression region. Notice that roughness does not have as great an effect upstream of the interaction, because it occupies a relatively smaller fraction of the thickness of the boundary layer in this region. While the configurations shown above are idealized axisymmetric representations of a transitional ablated nose shape, in reality, such a nose shape may be far from axisymmetric, as shown in Figure 1 (see Ref. 2 & 3).

The Nosetip Recovery Vehicle (NRV) was one of the few nosetips which has been recovered from a flight test during the part of re-entry where boundary layer transition was spreading over the nosetip. The nosetip is intrinsically three-dimensional in shape, and it is clear from the size of the indentations that large embedded separated regions were formed in the streamwise flutes. The schlieren photograph of the flow over the nosetip shown in Figure 1 clearly shows the flow features typical of embedded shock interaction regions over indented nosetips. The flow over the top of the model separates downstream of the spherical cap forming counterrotating longitudinal vortices in the flow between the grooves. A reattachment shock is formed as the compression waves formed at the back of the cavity coalesce. On the lower half of the model, the flow is basically attached. However, a recompression region is formed on the afterbody and a walljet is formed. The measurements of heat transfer shown in Figure 6 indicate that the boundary layer remains laminar over the spherical cap of the model with transition occurring in the free shear layer, downstream of the shoulder expansion. The heat transfer rates in the recompression region of the model can rise to three times the stagnation point heating value. It is clear that the prediction of these flows, which in reality are also influenced by surface roughness and blowing, is far from simple. However, unless such complex phenomena are modeled in some way in the prediction techniques, little progress will be made in describing such flows.

3. Hypersonic Interacting Flows Over Two- and Three-Dimensional Compression Surfaces

The complexity of the flow field in regions of shock wave/turbulent boundary layer interaction is such that it is unrealistic to expect to describe such regions in any detail within the framework of the boundary layer equations. Indeed their are some who would question whether the time or mass averaged Navier-Stokes equations capture the basic fluid mechanics associated with the intrinsically unsteady nature of separated regions. In hypersonic flows the effects of compressibility on the structure and development of turbulence must also be considered.

While there have been strenuous efforts to obtain predictions of two-dimensional and three-dimensional turbulent interaction regions, it is currently recognized that "successes" with "Navier-Stokes" code in describing some three dimensional turbulent interactions regions is a result of the dominance of the pressure and inertial terms in these flows. In these latter comparisons (References 4, 5, 6) it was found that the modeling of turbulence could be changed without significantly changing the numerical solution. For two dimensional interactions it appears the modeling of turbulence is more critical. To obtain good agreement for these latter flows, some very gross assumptions must be made in the turbulence model. Shang and Hankey[7], for example, chose to apply an empirical relationship (selected by matching the length of the separated region) to rapidly decrease the turbulent scale size through the interaction region, as shown in Figure 7. Horstmann[8], however, found the best agreement with Settles[9] measurements in wedge-induced separated regions using a two equation model for turbulence scale size and vorticity, as shown in Figure 8. Working with this same turbulence model, however, Horstmann was unable to predict the occurrence of separation on two incident shock/turbulent boundary layer configurations studied by Holden at Mach 11.2. As shown in Figure 9 these flow fields are clearly separated and yet the numerical solution fails to predict the characteristic plateaus in either the heat transfer or pressure distributions. The modeling of turbulence in separated interaction regions at hypersonic Mach numbers should account for the effects of compressibility and the generation of turbulence by the unsteady movement of the incident and induced shocks as they traverse and interact with a major region of the turbulent boundary layer. Clearly, further detailed experimental work on insightful theoretical modeling is required to develop numerical prediction techniques which are capable of describing turbulent interaction regions in detail.

Corner Interaction Studies

Studies with the emphasis on the heating in swept-shock interaction regions have been conducted by Newmann and Burke[10], Law[11], Token[12], and Scuderi[13] and Holden[14]. At low Mach numbers (M = 2→4) and for adiabatic surfaces, a large body of data exists on the mean characteristics of swept-shock interactions. Strangely, this body of three dimensional data has been found to be in better overall agreement with the Hung and MacCormack[15] Horstmann[8] Shang and Hankey[7] Settles and Horstmann[6] solutions to the Navier-Stokes equations than the relatively less complex two-dimensional flow separation over a flat plate/wedge. These results are not as sensitive to the turbulence model and suggest that the gross features of the flows are controlled principally by inviscid effects. In a recent experimental study at Mach 11, Holden[14] used the incipient formation of a plateau in the heat transfer distribution, together with a marked increase in the fluctuation levels in the output of the thin film instrumentation, as marking the onset of flow separation. As shown in Figure 10, Holden's measurements indicated that in hypersonic flow over highly-cooled surfaces, the turbulent boundary is more tenacious in resisting boundary layer separation than predicted by the methods derived by McCabe[16] and Korkegi.[11] The measurements of the peak pressure ratio through the interaction and the plateau pressure rise are in better agreement with calculations based on an inviscid flow model in the two dimensional theory of Reshotko and Tucker[17] than the correlations of Scuderi[13], as shown in Figure 11. In was found that, as in the studies of two-dimensional separated interaction regions, the peak heating can be related to the overall pressure rise by a simple power law relationship as shown in Figure 12. Figure 12 shows that the maximum pressure rise through the interaction region can be calculated with good accuracy from inviscid flow relationships. While there appears to be merit for the development of simple prediction methods in describing the flow in terms of the normal flow Mach number, this is clearly a gross oversimplification and it should be noted that the plateau pressure measurements obtained in Holden's study were relatively independent of $M_0 \sin \theta$.

Swept Wedge and Skewed Shock/Boundary Layer Interaction

Another approach to exploring flow separation in regions of three-dimensional shock wave/boundary layer interaction is to begin with a two-dimensional or axisymmetric interaction and sweep this interaction (or introduce angle of attack for the axisymmetric case) to progressively introduce crossflow into the interaction region. Experimental studies of this type have been conducted by Ericsson, Reding and Guenther[18], Settles and Perkins[19], and Settles and Teng[20]. Settles, who studied the interaction region over swept and unswept flat plate/wedge configurations in an adiabatic Mach 3 airflow, found that introducing crossflow increased the scale of the separated interaction region. Considerable effort was expended in this latter study to determine the Reynolds number scaling, and the length from the upstream tip of the wedge for the flow to become quasi-two-dimensional. However, the effect of changing the overall spanwise scale of the model on the scale of the interaction was not examined explicitly. The measurements of surface and pitot pressure through the interaction regions were in good agreement with solutions to the Navier-Stokes equations obtained by Horstman[8]; however, some key features of the flow were poorly predicted. It is known that agreement with pressure data is not the most definitive of tests. More recently Holden[14] performed studies of crossflow effects on the size and properties of the interaction region induced by a swept-oblique-shock incident on a turbulent boundary layer over a flat plate at Mach 11 and $R_{e_L} = 30 \times 10^6$. Experiments were conducted for two strengths of incident shock, the first ($\theta_{SG} = 12.5^o$) to generate a separated condition close to incipient separation, and the second ($\theta_{SG} = 15^o$) to generate a well-separated flow. Distributions of heat transfer and pressure as well as schlieren photographs of the unswept or two-dimensional flow condition and the 30 degree swept condition are shown in Figures 14 and 15. It is clear from the well defined plateau regions in the distributions of pressure and heat transfer, as well as the well defined separation shock in the schlieren photograph, that a well separated region, extending two inches in length, is induced beneath the stronger incident shock. The measurements made of the distribution of heat transfer and pressure beneath the well separated flow induced by both the 12.5 degree and the 15 degree shock generators swept at angles of 0 and 30 (shown in Figures 14 and 15) indicated that the induced crossflow has little effect on the size and characteristics of the interaction regions. If there is a perceptible effect, it is a decrease in the length of the separated region with increased crossflow. The significant differences between Holden's and Settles' measurements of the variation of interaction length with sweep angle and those obtained in these studies are shown in Figure 16. While Settles finds an almost threefold increase in separation length at sweep angles of 40 degrees, Holden found 10 percent reduction in this length. Further studies are required to resolve this issue.

4. Concluding Remarks

Boundary layer transition and transitional flows are ever present factors in hypersonic flows, and (as shown inadvertently in many experimental studies) have significant effects on the size and properties of separated interaction regions. The prediction of transition at hypersonic (or even supersonic) speeds is best describe as an art, and this, coupled with an inability to describe (even empirically) the characteristics of transitional interactions, probably represents the largest gap in our predictive capabilities.

While, in the absence of real gas effects, a number of the salient characteristics of shock wave/turbulent boundary interaction regions in hypersonic flow can be predicted using semi-empirical techniques. A numerical solution to Navier-Stokes equations has yet to be obtained to successfuly describe such flows. A fundamental problem associated with obtaining such a solution is, of course, the generation of a technique for modeling the turbulence in these flows; however, correctly gridding the interaction region is not a trivial matter. Correctly selecting a turbulence model which will describe the generation of turbulence at the base of the boundary layer as separation occurs, and its restructuring as the boundary layer undergoes radical thinning through the strong reattachment compression process, is central to the correct description of separation and reattachment in any speed range. Also, it remains to be determined whether the unsteady flow phenomena observed in separated flows at any speed can be described in the framework of the time- or mass-averaged Navier-Stokes equations. In hypersonic flow, however, the effects of compressibility on the generation and development of turbulence cannot be ignored. Only through carefully directed and conducted experimental studies can the insight and information be generated to resolve the issues raised above. An intrinsic problem which faces the experimentalist studying turbulent boundary layer separation in hypersonic flow is that the wall layer, within which separation first occurs and the properties of which are required to define the characteristics of both the attached and separated boundary layer, is very thin--typically five percent of the boundary layer thickness, making the accurate probing of this layer difficult. Thus, to obtain the required resolution, measurements must be made on very large models or on tunnel walls, with no intrusive techniques or miniature but robust flow field instrumentation. In the past, mostly because of difficulties in designing equipment robust enough to survive enough not to disturb interaction regions in high Reynolds number hypersonic flows, only mean surface measurements have been made. In many cases, only surface pressure measurements were obtained, and such measurements have little value in the evaluation of prediction techniques. In future experimental studies, every attempt must be made to obtain both mean and fluctuating flow field, and surface skin friction and heat transfer measurements to provide necessary to correctly model the development of turbulence generated in these flows.

References

1. Holden, M.S., "Studies of the Heat-Transfer and Flow Characteristics of Rough and Smooth Indented Noseshapes Part 1. Steady Flows," AIAA-86-0384, January 6-9, 1986, Reno, NV.

2. Holden, M.S., "A Review of Aerothermal Problems Associated with Hypersonic Flight," AIAA-86-0267, January 6-9, 1986, Reno, NV.

3. English E.A., "Nosetip Recovery Vehicle Postflight Development Report" SAND75-8059, Sandia Laboratories, Livermore, CA, January 1976.

4. Knight, D.D., "Prolems in Reconciling Computation and Experiment" 1985 Princeton University Workshop on the Structure of High-Speed Turbulent Boundary Layers.

5. Knight, D., Horstmann, C.C., Shapey, B., and Bogdonoff, S., "The Flowfield Structure of the 3-D Shock Wave Boundary Layer Interaction Generated by a 20 degree Sharp Fin at Mach 3" AIAA-86-343.

6. Horstmann, C.C. and Hung, C.M., "Computations of Three-Dimensional Turbulent Separated Flows at Supersonic Speeds," AIAA Paper 79-2, January 1979.

7. Shang, J.S., Hankey, W.L., and Petty, J.S., "Three-Dimensional Supersonic Interacting Turbulent Flow Along a Corner," AIAA Paper 78-1210, July 1978; also AIAA Journal, Vol. 17, No. 7, July 1979, pp. 706-713.

8. Settles, G.S. and Horstmann, C.C., "Flowfield Scaling of a Swept Compression Corner Interaction--A Comparison of Experiment and Computation," AIAA-84-0096, 22nd Aerospace Sciences Meeting, January 9-12, 1984.

9. Settles, G.S., Bogdonoff, S.M., and Vas, I.E., "Incipient Separation of a Supersonic Turbulent Boundary Layer at Moderate to High Reynolds Numbers," AIAA Paper 75-7, 1975.

10. Newmann, R.D. and Burke, G., "The Influence of Shock Wave-Boundary Layer Effects on the Design of Hypersonic Aircraft," AFFDL-TR-68-152, USAF Flight Dynamic Laboratory, 1968.

11. Law, H.C., "Three-Dimensional Shock Wave Turbulent Boundary Layer Interactions at Mach 6," ARL TR-75-0191, June 1975.

12. Token, K.H., "Heat Transfer Due to Shock Wave Turbulent Boundary Layer Interactions on High-Speed Weapon Systems," AFFDL-TR-74-77, April 1974.

13. Scuderi, L.F., "Expressions for Predicting 3D Shock Wave-Turbulent Boundary Layer Interaction Pressures and Heating Rates," AIAA Paper 78-162, January 1978.

14. Holden, M.S. "Experimental Studies of Quasi-Two-Dimensional and Three-Dimensional Viscous Interaction Regions Induced by Skewed-Shock and Swept-Shock Boundary Layer Interactions" Calspan Report No. 7018-A-2 Report Covering Period 15 January 1982 - 31 July 1984.

15. Hung, C.M. and MacCormack, R.W., "Numerical Solutions of Supersonic and Hypersonic Laminar Flows Over a Two-Dimensional Compression Corner," AIAA Paper 75-2, January 1975.

16. McCabe, A., "The Three-Dimensional Interaction of a Shock Wave with a Turbulent Boundary Layer," Aeronautical Quarterly, Vol. XVII, August 1966, pp. 231-252.

17. Reshotko, E., and Tucker, M., "Effect of a Discontinuity on Turbulent Boundary Layer Thickness Parameters with Application to Shock Induced Separation," NACA TN3454, 1955.

18. Ericsson, L.E., Reding, J.P., and Guenther, R.A., "Effects of Shock-Induced Separation," Lockheed Missiles and Space Co., Sunnyvale, CA, L-87-69-1, July 1969.

19. Settles, G.S., and Perkins, J.J., "Upstream Influence Scaling of 2D & 3D Shock/Turbulent Boundary Layer Interactions at Compression corners," AIAA-81-0334, 19th Aerospace Sciences Meeting, January 12-15, 1981.

20. Settles, G.S. and Teng, H.Y., "Flow Visualization of Separated 3D Shock Wave/Turbulent Boundary Layer Interactions," AIAA-82-0229, 20th Aerospace Sciences Meeting, January 11-14, 1982.

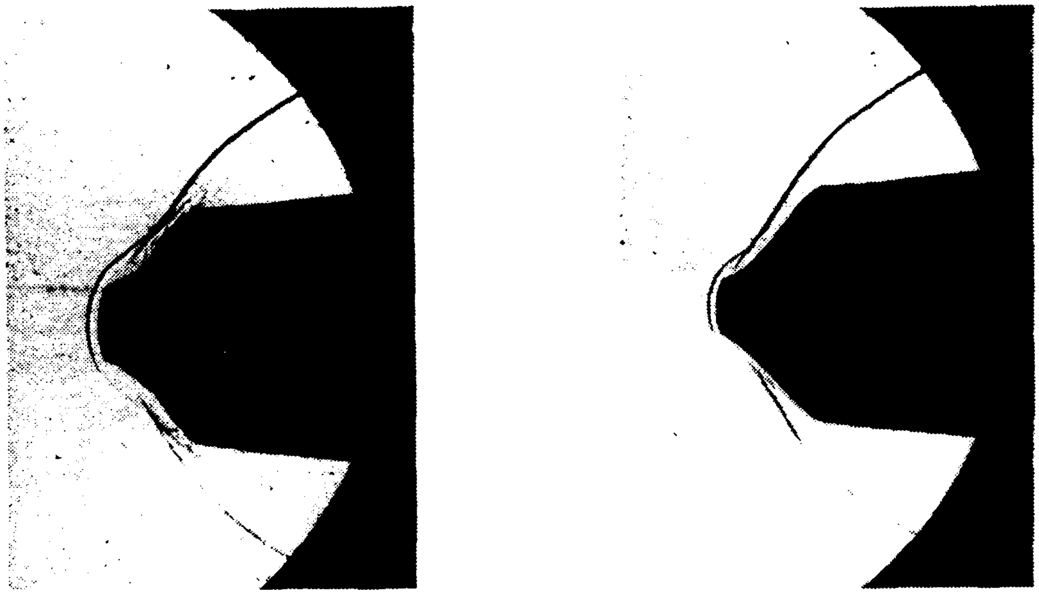

NRV NOSETIP

RTE NOSETIP

Fig. 1 Schlieren photographs of the flow over the NRV and RTE nosetips exhibiting regions of body shock – boundary layer interaction.

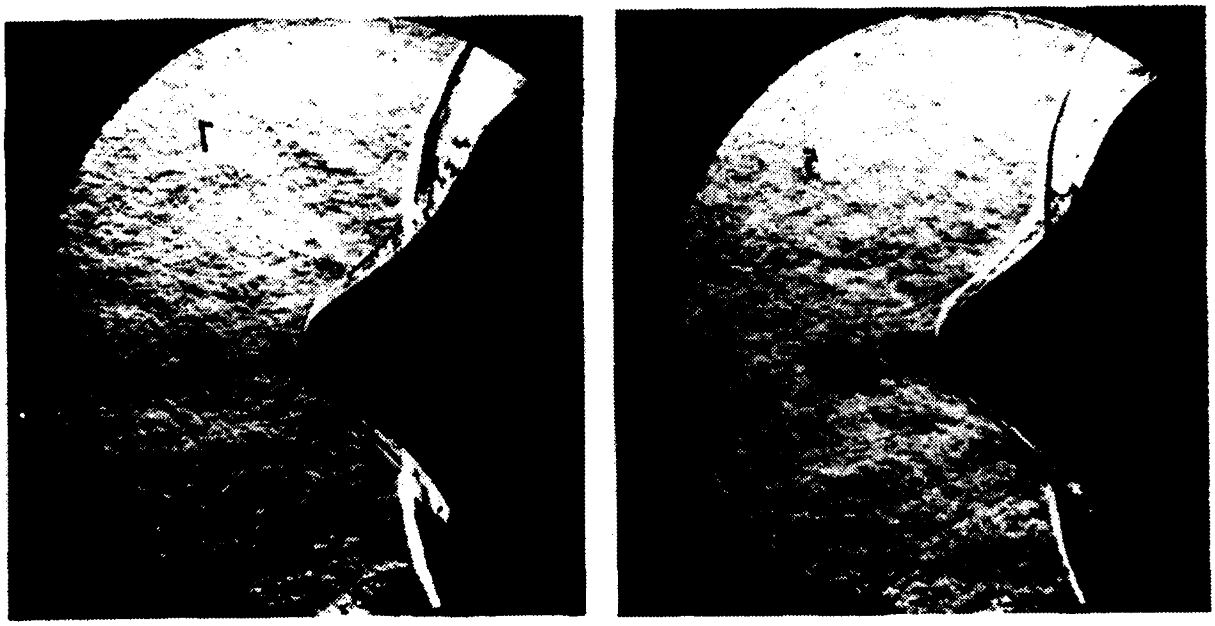

(a) MACH 11

(b) MACH 13

Fig. 2 Effects of Mach number on flow pattern over the indented nosetips (K = 15 MILS).

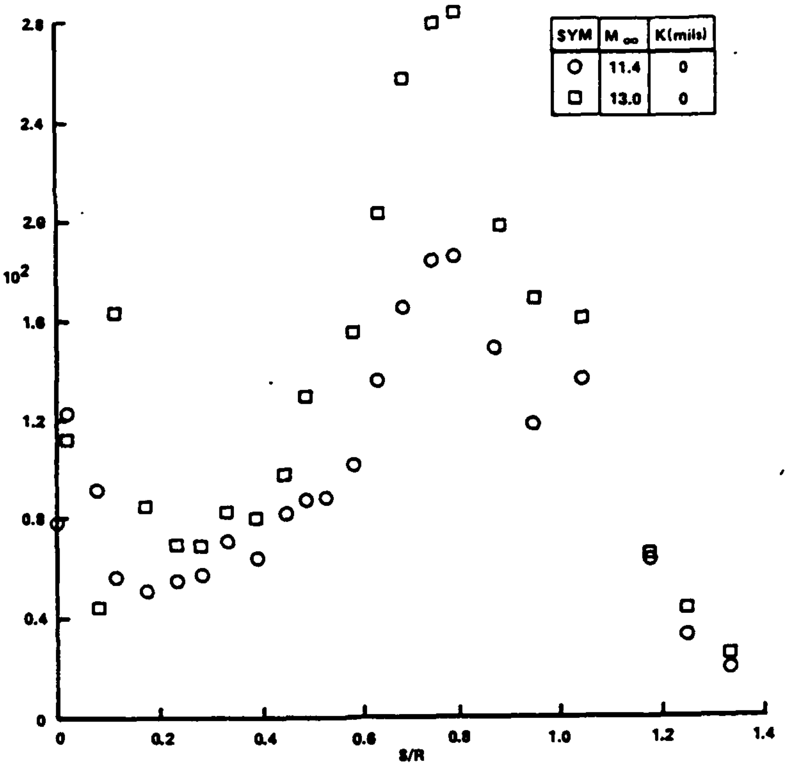

Fig. 3 Influence of mach number on the distribution of heating to the smooth model.

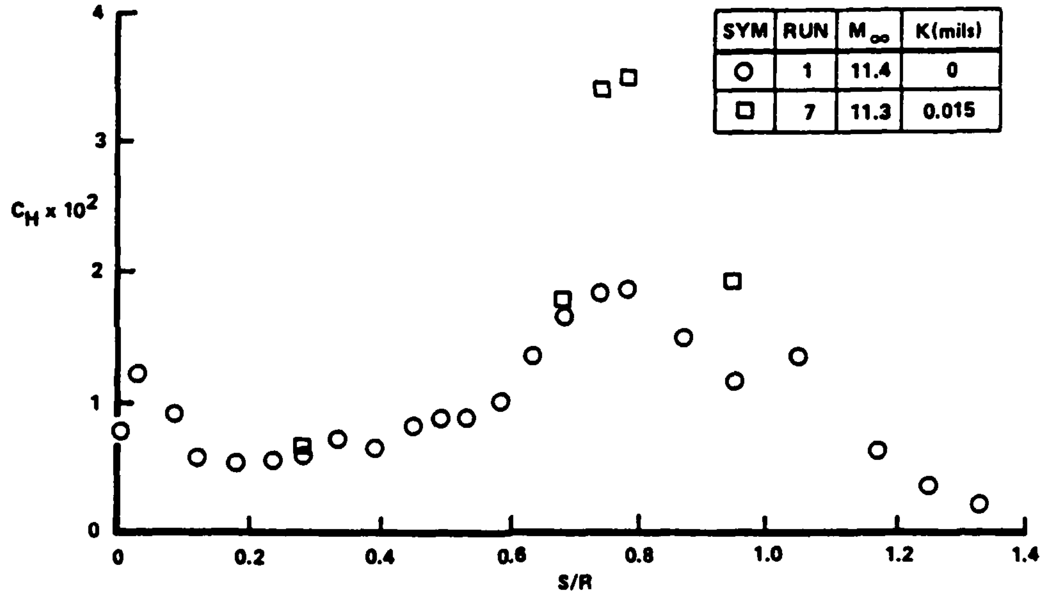

Fig. 4 Influence of surface roughness on the heating distribution. (M = 11.4 $Re_D = 12 \times 10^6$)

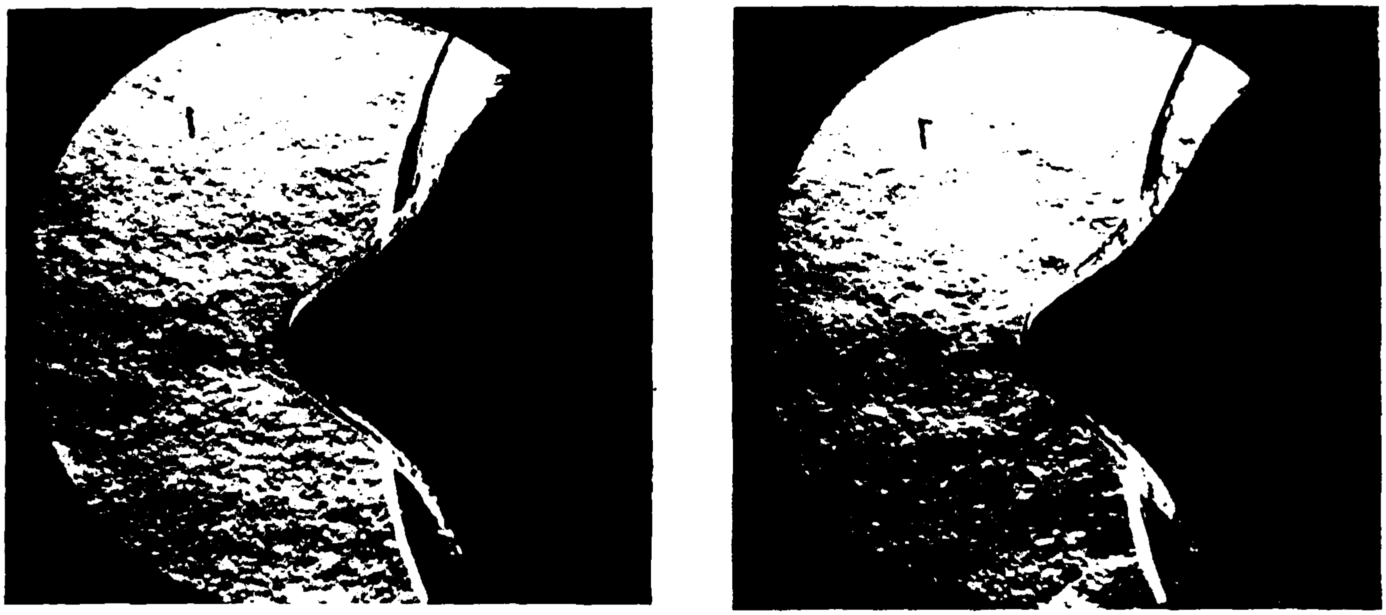

(a) K = 0

(b) K = 15 MILS

Fig. 5 Influence of surface roughness on the flow field on indented nosetips.

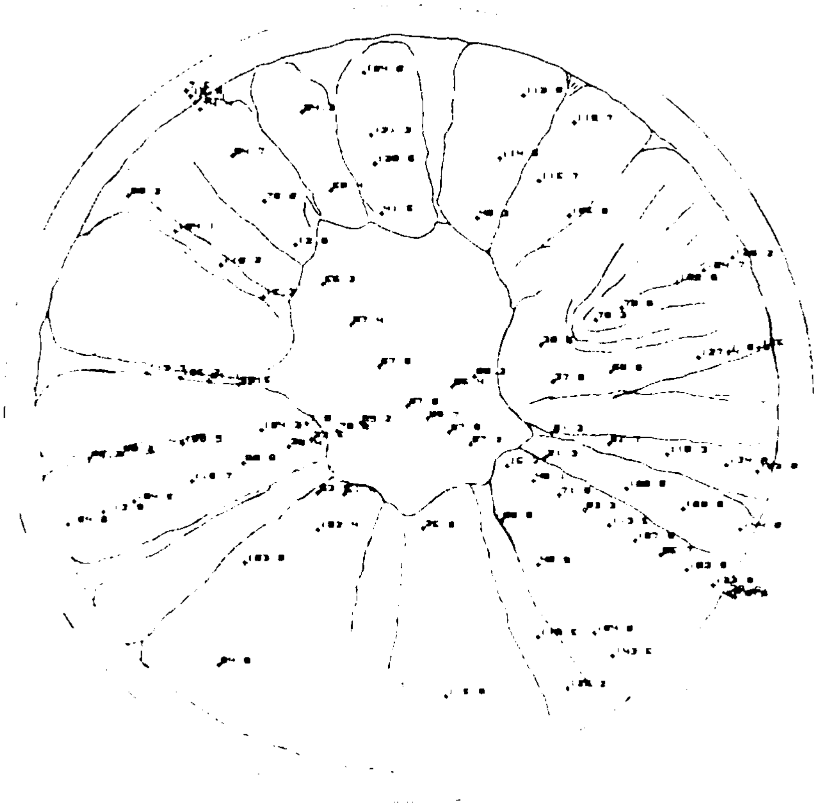

Fig. 6 Heat transfer distribution over the NRV configuration. M = 11 Re/Ft = 10 x 10^6

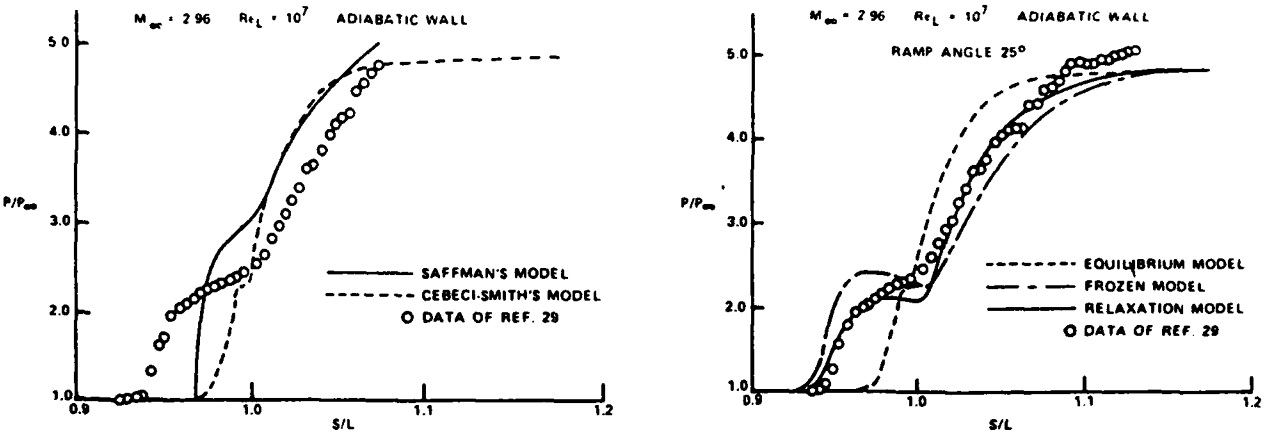

(a) (b)

Fig. 7 Comparison of different turbulent models with experiment. Ref. 7.

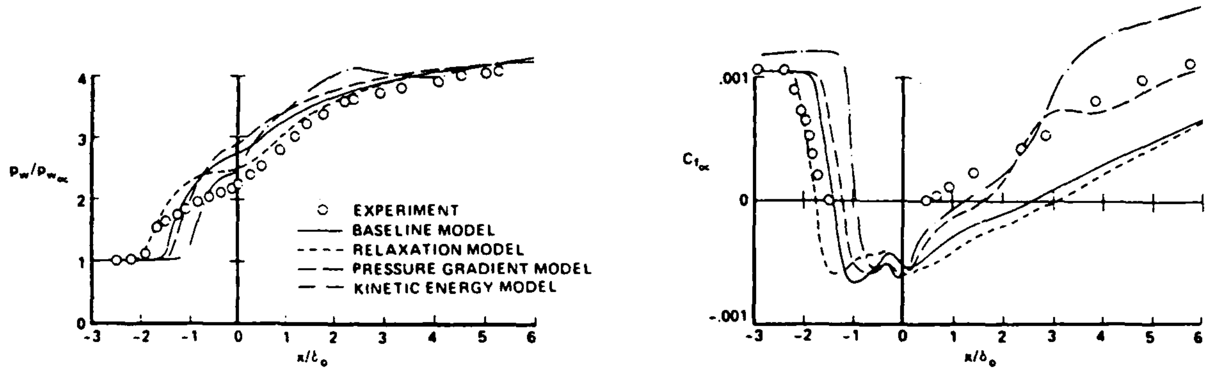

Figure 8 Comparison of computations and surface measurements; $\alpha = 24^{\circ}$, Ref. 8.

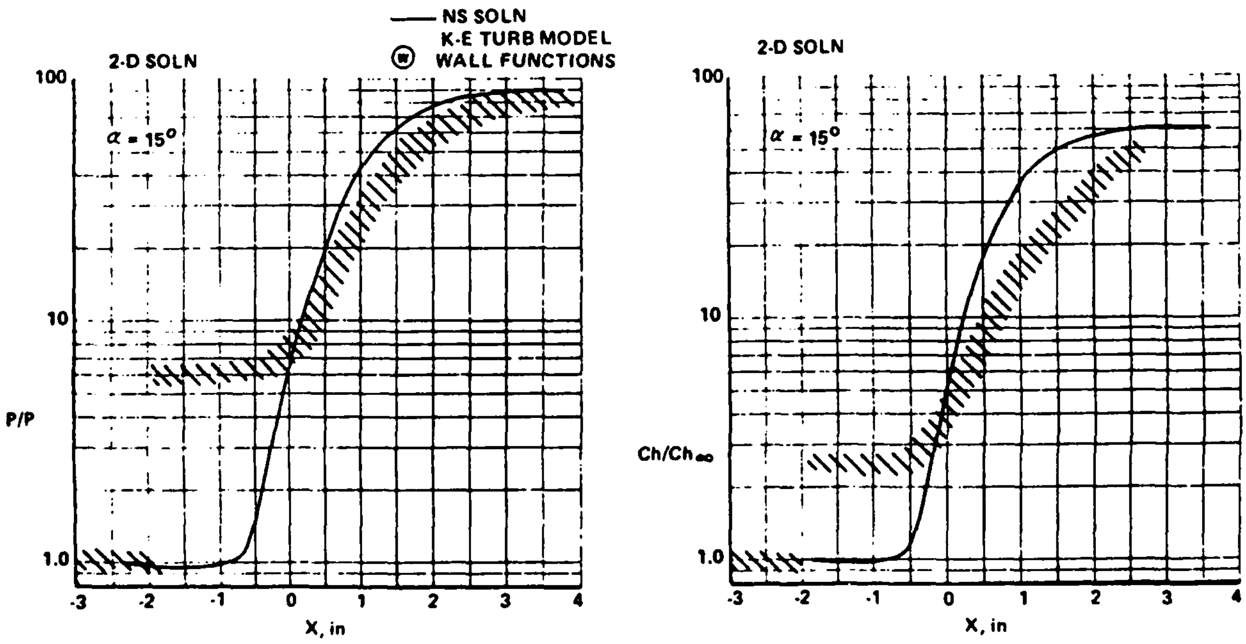

Fig. 9 Comparison between Navier-Stokes solution and experiment for a well separated flow.

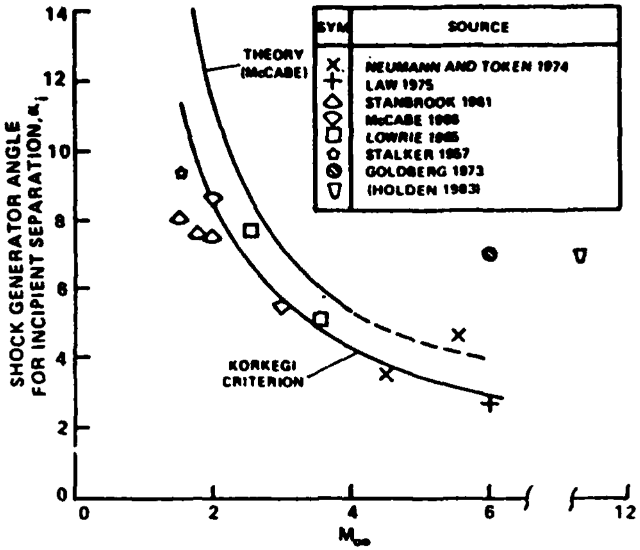

Fig. 10 Variation of shock generator angle to induce incipient separation with mach number.

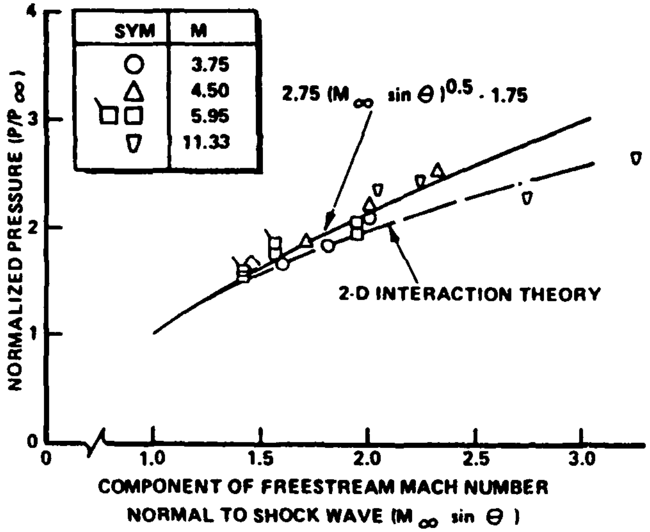

Fig. 11 Correlation of plateau pressure measurement from swept-shock interaction studies.

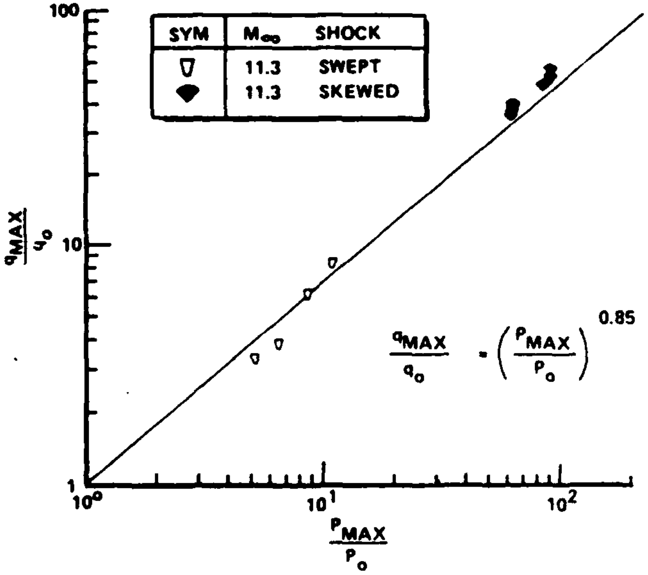

Fig. 12 Correlation of peak heating rates in skewed- and swept-shock interaction regions.

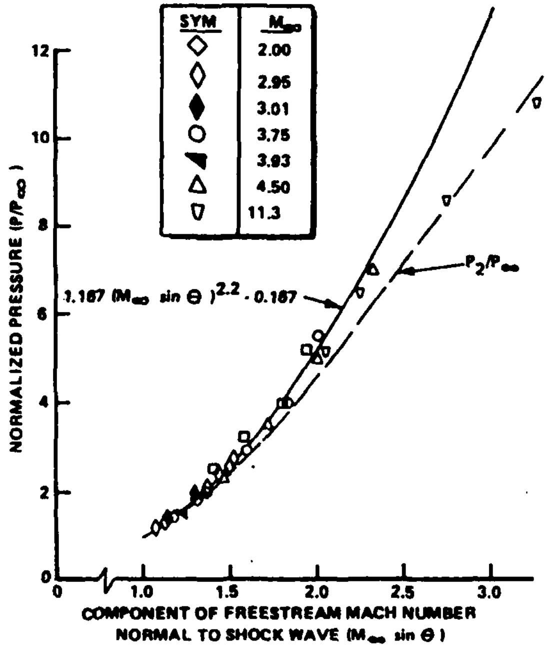

Fig. 13 Correlation of maximum pressures recorded in swept-shock interaction regions.

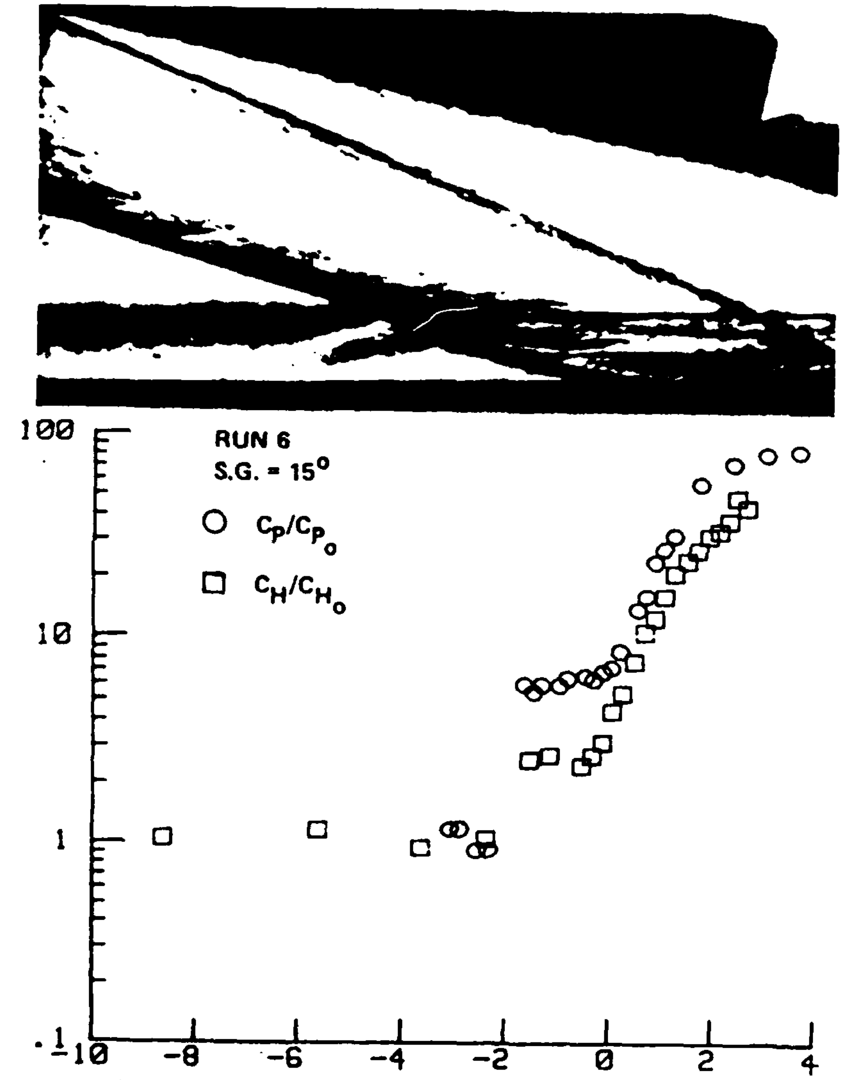

Fig. 14 Streamwise distributions of heat transfer and pressure through skewed-oblique-shock boundary layer interaction (θ = 15° ψ = 0°)

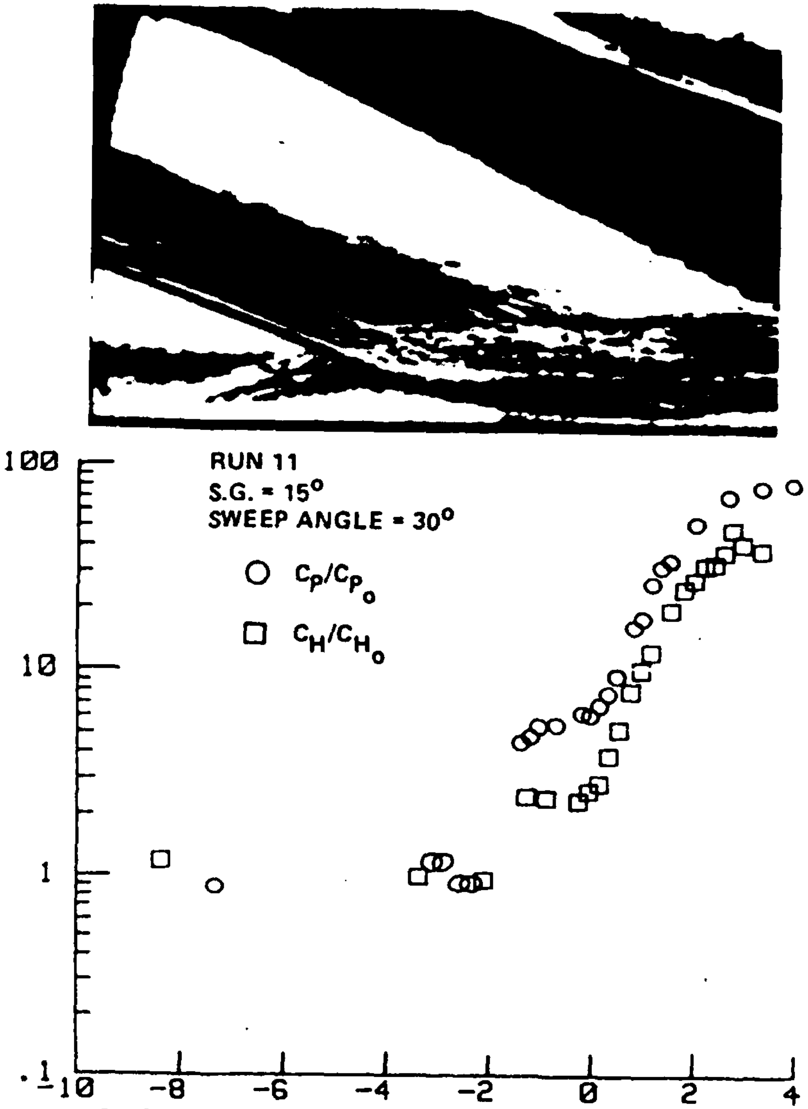

Fig. 15 Streamwise distribution of heat transfer and pressure through skewed-oblique-shock interaction (θ = 15° ψ = 30°)

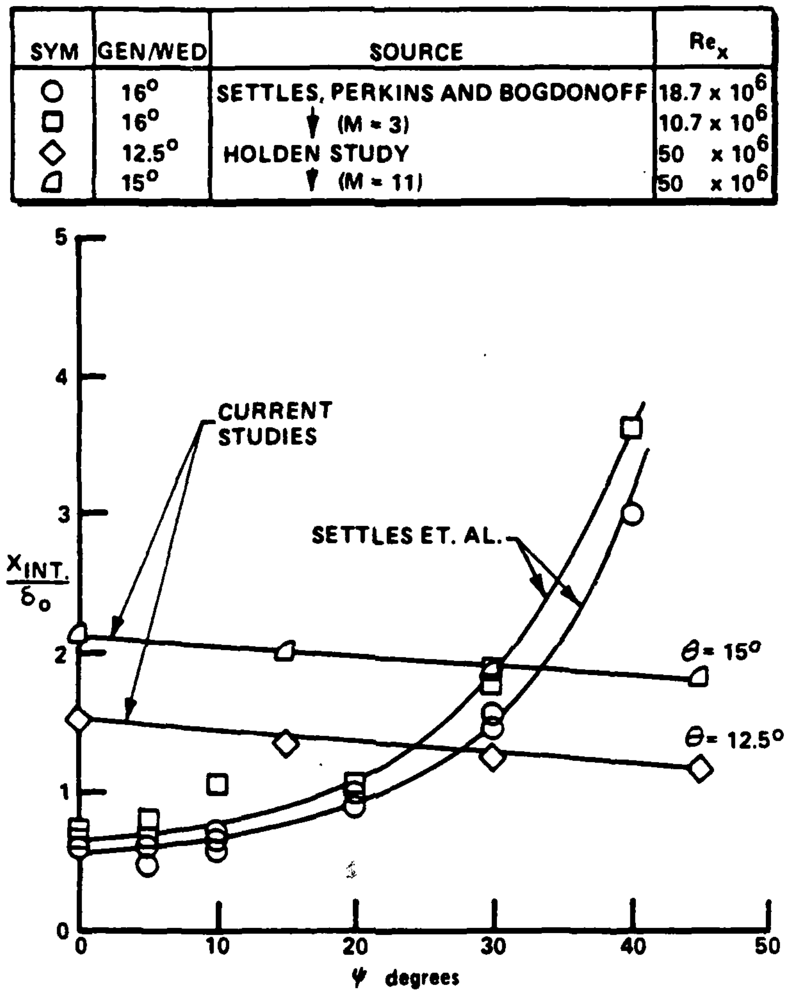

SYM	GEN/WED	SOURCE	Re_x
○	16°	SETTLES, PERKINS AND BOGDONOFF	18.7×10^6
□	16°	↓ (M = 3)	10.7×10^6
◇	12.5°	HOLDEN STUDY	50×10^6
◺	15°	↓ (M = 11)	50×10^6

Fig. 16 Variation of streamwise extent of interaction ahead of shock impingement (or corner) with sweep angle.

APPENDIX C

"Studies of Potential Fluid-Mechanical Mechanisms For Enhanced Stagnation-Region Heating"

Published in:

Thermophysical Aspects of Re-entry Flows
Log No. PS-3083
AIAA Progress Series, Astronautics and Aeronautics

PS 3083

STUDIES OF POTENTIAL FLUID-MECHANICAL MECHANISMS FOR ENHANCED STAGNATION-REGION HEATING

M.S. Holden*
Arvin/Calspan Corporation
Buffalo, NY 14225

---

*Member, AIAA
*Principal Research Scientist

This work was supported by AFOSR contract number F49620-79-C-0003.

M.S. HOLDEN

POTENTIAL FLUID MECHANICAL MECHANISMS

Presented as Paper 85-1002 at the AIAA 20th Thermophysics Conference, Williamsburg, VA, June 19-21, 1985. This work was supported by AFOSR contract F49620-79-C-0003.

AD-A174 662 VISCOUS INTERACTIONS AT HYPERSONIC SPEED(U) CALSPAN UB 2/2
RESEARCH CENTER BUFFALO NY* M S HOLDEN ET AL.
12 SEP 86 CUBRC-86611 AFOSR-TR-86-2072 F49620-84-K-0009
UNCLASSIFIED F/G 20/4 NL

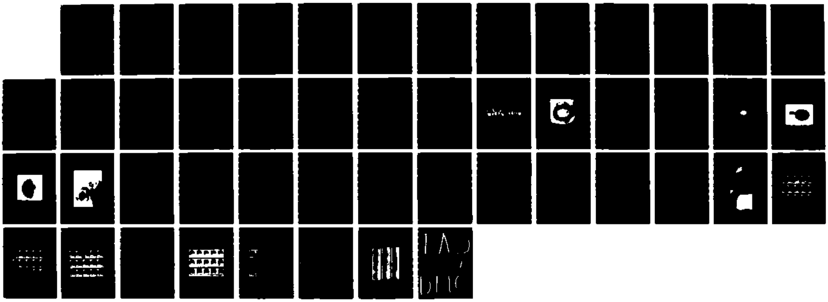

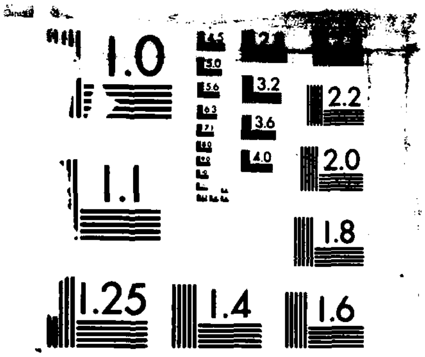
1.0
4.5
5.0
5.6
6.3
7.1
8.0
9.0
2.8
2.5
3.2
3.6
4.0
2.2
2.0
1.1
1.8
1.25
1.4
1.6

MICROCOPY RESOLUTION TEST CHART
[illegible] STANDARDS 1963 A

Abstract

A series of experimental studies have been conducted to examine the potential fluid mechanical mechanisms that may cause enhanced heating in the stagnation region of blunt bodies in hypersonic flow at high Reynolds numbers. The four mechanisms investigated were the boundary-layer transition close to the stagnation region, surface roughness and surface blowing in the stagnation region, and particle/shock layer interaction. These studies were conducted at Mach numbers of 6.5-13 and Reynolds numbers up to 50×10^6 based on the nosetip diameter. In the studies of transition on smooth spherical nosetips, it was found that moving the transition from the sonic line to the stagnation region with annular trips did not promote increased heating at the stagnation point. Similarly, while surface roughness was found to induce heating enhancements of up to 100% close to the sonic region, the stagnation point heating remained uninfluenced by roughness at the stagnation point. The studies of particle/shock layer interaction indicated that in high Reynolds number flow, where transition is close to or ahead of the sonic region, small particles ($< 1\ \mu m$) in the airflow can trip the boundary layer in the stagnation region causing tfansient increases in stagnation heating. Hypersonic facilities generating high Reynolds numbers may be intrinsically susceptible to stagnation point heating problems from minute, high-energy particles entrained into the flow. This aspect of their performance should be carefully monitored.

Introduction

Analysis based on conventional boundary-layer theory predicts that the boundary layer at or close to the stagnation point on a blunt body will be laminar under most flight conditions. However, flight measurements of stagnation point recession and heat transfer measurements in ballistic ranges and other ground test facilities have indicated that heating rates significantly larger than the laminar heating level can be generated in the stagnation region in high Reynolds number flows. The major questions therefore are: what is the basic mechanism(s) responsible for the heating enhancement and what is the best way to model this phenomenon?

To match flight measurements of nosetip recession, many of the nosetip shape change codes employ empirical relationships to enhance the heating levels in the stagnation region, with these expressions being employed once transition has moved within a certain fraction of the nose radius from the stagnation point. It is rationalized that, since the flow in the stagnation region is subsonic, pressure disturbances propagating forward from transition can promote increased heating in this region. However, it remains to be determined whether such relatively small disturbances can cause the significant heating enhancement factors that have been inferred from nosetip recession data. Another mechanism postulated for stagnation heating enhancement is roughness-induced heating augmentation. When nosetips constructed from composites such as carbon/carbon ablate, the carbon filler is convected from between the carbon weave, leaving a rough surface that could disturb the boundary layer in stagnation region and cause increased mixing or transition. However, because the roughness Reynolds number ($k U_\tau / \nu$) is zero at the stagnation point and the surface roughness does not induce increased heating in laminar boundary layers, an increased stagnation point heating rate can result only from upstream propagation through either the boundary layer or the nosetip material. Mass addition, which results from the ablation in the stagnation region, is generally associated with cooling; however, introducing a normal component of velocity at the wall under high Reynolds number conditions is destabilizing and may result in premature transition and, hence, increased heating levels.

When a hypersonic vehicle encounters clouds of dust or ice particles, the interaction between the particles and the shock layer, as the particles enter the shock layer and rebound, or cause secondary particles to be ejected from the vehicle surface, can give rise to important aerothermal effects. Nosetip erosion resulting from particle impact has been of primary concern to designers of ballistic re-entry vehicles. However, in flows with medium to light dust loading, the increased heating resulting from particle/shock layer interaction can exceed the dust-free levels by as much as a factor of 10. The experimental studies conducted at Calspan[1] of the increased heat resulting from particle/shock layer interaction constituted one of the first systematic studies of the basic phenomenon. These studies, together with dust tunnel tests, showed that the gross heating levels to a blunt nosetip in a dusty flow cannot be explained in terms of impact energy alone. The difference between the measured heating rate and the heating rate estimated on the basis of impact energy was termed the "particle-augmented convective heating rate." Systems studies of this phenomenon by others linked the augmented convective heating rate to "particle loading" through an assumption that the heating enhancement mechanism is related to the increased vorticity introduced into the shock layer from the wakes of the particles. The relationships based on this assumption are still used today, despite its lack of validity. More recently, flight measurements have indicated that the disturbances to the shock layer resulting from particle interaction can produce an asymmetric aerodynamic load that causes a loss in accuracy of the trajectory of a ballistic re-entry vehicle. Heat-transfer measurements on blunt bodies in hypersonic facilities run at high Reynolds numbers may be influenced by disturbances induced by minute particles trip the boundary layer in the stagnation region. This phenomenon, which we believe occurs only in hypersonic facilities capable of generating Re_θ large enough to make the laminar boundary layers unstable in the stagnation region on a blunt body, cannot be easily detected without high-frequency heat-transfer instrumentation. Stagnation heat-transfer measurements made with low-frequency instrumentation in such flows will most certainly be in error.

The basic problem from the viewpoint of analysis revolves about modeling the characteristics of the boundary layer (laminar, transitional, or turbulent) at the stagnation point when transition occurs in the stagnation region. Since the flow is subsonic in the stagnation region, it is clear that pressure disturbances can be fed upstream. However, it remains to be determined whether such relatively small disturbances can induce the relatively large heating augmentations observed. It has been suggested that the measurements of enhanced stagnation point heating made in wind tunnels are influenced by tunnel noise. However, since measurements at high Reynolds numbers made in ballistic range studies and flight tests also exhibit stagnation point heating rates larger than those predicted using the Fay-

Riddell[2] laminar theory, clearly, tunnel noise cannot be the sole cause of the enhanced heating.

To illustrate some of the parameters that control stagnation point heating, we have correlated some of the measurements made during the nosetip studies at Calspan using the ablated nose shape models shown in Fig. 1 and the laminar blunt configuration of the model used in our particle interaction studies shown in Fig. 2. The measurements of stagnation point heating to the medium and blunt configurations from our studies at Mach 8 and 13, together with earlier measurements from ground tests and flight, have been compared with the Fay-Riddell theory in Fig. 3. Here we have plotted the ratio of the experimental measurement to theoretical prediction against the Reynolds number based on nosetip diameter. For Reynolds numbers less than 5 x 10^6, it can be seen that, while the theory slightly underpredicts the observed heating, the agreement can be said to be good. However, as the Reynolds number increases above this value, we observe increased heating in the stagnation region. When transition approaches the stagnation region, it can be postulated that turbulent fluctuations produce pressure disturbances of sufficient magnitude to disturb the flow at the stagnation point and, hence, increase the heating in this region. To examine this concept, we plotted the ratio of measured heating to the theoretical laminar value against the nondimensional distance from the stagnation point as shown in Fig. 4. This correlation clearly indicates that once the transition has moved to within one-tenth of a body diameter from the stagnation point, there is a significant increase in the ratio of the measured to theoretical heating rate.

In the first study described in this paper, we obtained detailed distributions of heating in and downstream of the stagnation region on a spherical nosetip, with natural transition and with a series of annular trips to trip transition just downstream of the stagnation region, as discussed above. We sought to determine whether the upstream influence of transition was sufficient to significantly increase the stagnation point heating. This investigation was followed by measurements on a rough spherical nosetip of the same dimensions to examine the effects of roughness on the stagnation point and stagnation region heating. In this latter study, the roughness height was selected to match the roughness of the transpiration cooled nosetips the measurements of which where used in the third phase of this study to examine the effects of blowing on stagnation region heating. Finally, we investigated the effects of dust in the stagnation region on stagnation region heating. Here, we used measurements with normal and highly cleaned tunnel conditions as well as launching dust from the model. The results of these separate investigations are combined to suggest an explanation for some of the measurements of enhanced stagnation region heating.

Objective and Design of the Experimental Studies

The major objective of these studies was to examine the basic mechanisms that could induce enhanced heating in the stagnation region of a blunt body in high Reynolds number hypersonic flow. While the correlations presented above suggest that the heating at the stagnation point may be increased when transition approaches the stagnation region, further studies are required to determine the mechanisms governing this interaction. Such studies should be conducted using a hemispherical nose shape rather than, for example, a "laminar blunt" configuration because there is a wealth of experimental and theoretical evidence available on spherical nosetip. To overcome questions associated with the effects of wind tunnel noise on stagnation point heating enhancement, the position of the transition should be controlled mechanically by employing trips on the models rather than controlling the streamwise position of transition by varying the Reynolds number of the freestream. Measurements of the heat transfer should be obtained at the stagnation point and in the stagnation region at a single test condition, moving transition toward the stagnation point, with the symmetric trip rings. A 12 in. spherical nosetips and "laminar blunt" configurations on which the transition occurred without tripping 3 in. from the stagnation point was selected for these studies. In order to examine the potential mechanism of upstream influence, tightly spaced high frequency heat-transfer and pressure instrumentation was employed in the stagnation region. This high frequency instrumentation was employed to locate and determine the structure of the transition region and follow and diagnose the disturbances generated from the interaction of the particle with the shock layer and the movement of transient disturbances along the body.

Experimental Facilities

The experimental studies were conducted in the 48 and 96 in. shock tunnels at Calspan Corporation at Mach numbers of 6.5-13 for Reynolds numbers up to 50×10^6 based on nosetip diameter. The shock tunnel, which is in essence a blowdown tunnel with a shock compression heater, was operated in the tailored interface mode[3] to obtain run times of between 5-15 ms. In this study, we used a new throat valve which was developed to replace the throat Mylar in the 96 in. tunnel. Under convectional operation, a Mylar diaphragm is ruptured by the incident shock to start the flow of air into the test section. Fragments of Mylar are swept past the model during the starting process of the tunnel; and only for large blunt models where they can rebound upstream is there evidence that Mylar particles persist into the steady run time. To eliminate all Mylar particles, we developed a fast-acting valve that can be withdrawn from the 1.8 in. throat in less than 2 ms. and that is timed to operate upon the arrival of the incident shock. Employing this valve, coupled with the conventional centerbody valve[3] used to terminate the flow, and carefully cleaning the driven tube, throat section, nozzle and test section, it is possible to virtually eliminate the particles in the flow. This degree of cleanliness, which far exceeds that obtained in conventional or blowdown facilities, is necessary to eliminate the particle-enhanced heating effects in high Reynolds number hypersonic flows where transition occurs close to the stagnation of the blunt body.

Models and Instrumentation

Four models were used in this study. The 12 in. diam spherical nosetip shown in Fig. 5 was used in the studies of transition on smooth and tripped nosetips. This model was highly instrumented in the stagnation region with high-frequency, thin-film instrumentation and with pairs of heat-transfer and pressure gages positioned adjacent to one another along a streamwise ray. Annular trips constructed from 10 and 20 mil grit were attached to the model at a number of streamwise stations as shown in Fig. 6. The model for the studies of stagnation point heating of a 12.5 mil rough spherical nosetip is shown in Fig. 7. The size, shape, and spacing of the roughness were selected to be equivalent to the effective roughness of the transpiration-cooled model, to be described later. Silver calorimeter gages constructed[4] with conical roughness elements were installed at the stagnation point along a streamwise ray in the spherical model as shown in Fig. 7. The transpiration model, shown in Fig. 8, was developed earlier for studies of blockage heating effects of transpiration-cooled nosetips[4], and subsequently used to study massive blowing during Jovian entry. This model contained a large number of thin-film heat-transfer and pressure gages and, for the current studies, was run with a nitrogen coolant. We studied the effects of particle shock layer interaction on the stagnation point using the "laminar blunt" configuration shown in Fig. 2. The model was instrumented with 80 thin-film gages and 28 high-frequency pressure gages positioned so that a high density of instrumentation was concentrated in one quadrant of the model, while the balance of the instrumentation is distributed symmetrically about the model axis. Single and multiple particles were launched from the surface of the model using three particle launchers contained within the model. Each launcher assembly was mounted in seismic mass, which was in turn mounted in the model with a soft-rubber suspension system. Particles 1-800 µm were launched either individually, sequentially, or in batches. The size and density of the particles launched and the launch speed were chosen with the aid of a simple numerical code so that the particles penetrated to specified distances in the shock layer.

Results and Discussions

Roughness Tripped Transition Effects on Stagnation Region Heating

The initial studies were conducted with the completely smooth hemisphere. Annular trips with different roughness characteristics were then attached to two different radii close to the nosetip (see Fig. 6) to move the tripped transition region relative to the stagnation region without changing the unit Reynolds number of the freestream and the tunnel noise.

The distributions of heat transfer to the smooth configurations at Mach 11 for Reynolds numbers of 11×10^6 and 4×10^6, based on body diameter, are shown in Figs. 9 and 10, respectively. It can be seen that, for a Reynolds number of 11×10^6, transition is complete by 38 deg from the stagnation point, while at an Re_d of 4×10^6, the boundary layer remains laminar around the entire hemisphere. Both the stagnation point heating rates and the heating distributions are in relatively good agreement with the laminar theory until the transition begins. In the following runs, we introduced the trips at 11.50 deg and 7.16 deg from the stagnation point using roughnesses of 10 and 20 mil grit sizes. Fig. 11 shows that, with the 10 mil grit trip at 11.50 deg, transition is induced behind the trip causing the heat-transfer to increase around the model, reaching a maximum value close to the sonic point. Both the form of the heat transfer distribution and the position of the point of maximum heating are consistent with predictions from turbulent theory. As can be seen from Fig. 11, the introduction of the trip induces large heating rates immediately downstream of the trip. However, observations of the mean and fluctuating levels of the heat-transfer and pressure upstream of the trip in the stagnation region did not provide any indication of the upstream influence. We moved the trip closer to the stagnation point (7.16 deg), initially employing the same degree of roughness in the trip ring. The measurements made on this configuration are shown in Fig. 12. It can be seen that the trip caused a small reduction in heating just ahead of the trip and a large increase in heating immediately behind the trip; the trip is no more (or possibly less) effective in tripping the boundary layer. More important, we did not observe an influence of the trip on the stagnation point heating or on the fluctuating pressure levels in the stagnation region.

We then left the trip location fixed and increased the roughness on the trip ring from 10 to 20 mils. This modification caused a considerable increase in the disturbance generated by the trip (as can be seen in Fig. 13), which induced significant reductions in the heating ahead of the trip and significant increases behind the trip. The local perturbations upstream and downstream of the trip and, of more importance, the upstream influence of the trip were not significantly different from the studies with the 10 mil roughness trip at the same location. Since our earlier measurements indicated that the trip at 11.50 deg appeared more effective in inducing transition for $Re_d = 11 \times 10^6$, we chose to use this location for the studies at an $Re_d = 4 \times 10^6$. Fig. 14 shows the distribution of heating around the hemisphere with a 20 mil trip at 11.50 deg. We see that immediately behind the trip there is a large increase in the heat transfer; however, the heating rates decay with increasing downstream distance until, at 35 deg, they return to the laminar values. This results principally from the very rapid expansion to which the boundary layer is being subjected.

Surface Roughness Effects on Stagnation Region Heating

In a number of earlier studies[4] we investigated the effects of surface roughness on the heat transfer to slender and wide-angle cones, it was found that in the laminar flow ahead of transition the heat transfer to the constant-pressure, rough surface remained at the laminar level. We found, as did earlier researchers, that for low values of Re_k ($U_\tau K/\nu_w$) there is little roughness-induced heating enhancement. Thus, in the stagnation region where the skin friction is small, it is difficult to rationalize the mechanism of roughness-enhanced heating except through the mechanism of tripping. Again, since the Reynolds number at the stagnation point is small, tripping the boundary-layer close to the stagnation point is also difficult. Only when the roughness elements become a large fraction of the boundary layer thickness can protruberance heating be considered as a viable mechanism for enhanced heating in the stagnation region.

In the current study, we selected (on the basis of our earlier work) a 12.5 mil tightly spaced conical roughness, a dimension comparable with the boundary-layer thickness, as well as being equivalent to the roughness of the transpiration-cooled nosetip used in the subsequent study. This roughness height, shape and spacing were shown earlier to give heating enhancements equal to those generated by 12.5 mil sand grain roughness. The model, coated with this roughness and containing 12 rough calorimeter gages, is shown in Fig. 7. The distributions of heat transfer to the rough hemisphere for the two Reynolds number conditions studied are shown in Fig. 15. In both cases, the distributions exhibit the form of turbulent heating with transition just downstream of the stagnation region; and in both cases the stagnation point heating remains at a laminar level. A further comparison between these measurements and those obtained on the smooth hemisphere and the smooth wall theories are shown in Fig. 16. While we observe the roughness-induced heating factors approaching two in the sonic region, the heating at the stagnation point is in good agreement with laminar theory. Since the roughness, height, and boundary-layer thickness were of comparable dimensions at the stagnation point for the highest Reynolds number condition selected for this study and we did not find any stagnation point heating enhancement, we felt it was unrealistic to perform experiments at conditions where we would obtain thinner boundary layers or have to select larger roughnesses. Our measurements suggest that, in the absence of lateral heat conduction along the body, and for roughnesses less than the stagnation boundary-layer thickness, surface roughness does not contribute to stagnation point heating enhancement.

Studies with Transpiration-Cooled Models

The measurements made in the studies of transpiration cooling conducted at Calspan were designed principally to examine how the separate and combined effect of the surface roughness and of small blowing influenced the heating in the stagnation region. The measurements on the model with zero blowing presented in Fig. 17 clearly show that the intrinsic roughness of the surface causes heating enhancement factors close to two in the region of maximum local Reynolds number. In fact, it can be seen by comparing Figs. 16 and 17 that the heat-transfer measurements on the conically rough hemisphere are in good agreement with those obtained on the non blowing transpiration-cooled nosetip (TCNT), with the exception of the region close to the stagnation point. In this region, the gages were mounted on the lip, downstream of the cavities in the transpiration-cooled model such that they would be biased toward the larger heating levels. When a small amount of blowing ($m/\rho u c_H = 0.032$) was introduced, the heating rates over a major part of the transpiration-cooled model dropped to levels close to those recorded on the smooth model, as shown in Figs. 17 and 18. On the basis of these measurements, it could be postulated that the initial effect of mass addition from a rough ablating nosetip is to modify the flow around the roughness elements by eliminating the cavity flows in such a way that the momentum defect introduced by the roughness is small. Again, the heating on the stagnation region is equal to or less than the laminar stagnation level.

It is important to observe that the effect of mass addition is to remove surface roughness as an important characteristic parameter. This poses serious questions for the correlation of flight measurements in terms of an effective surface roughness and the computational procedures in which the ablation rate is determined from heating levels enhanced by surface roughness effects. Although experimental studies of the combined effects of mass addition and surface roughness are not easily constructed, the total lack of cold-wall measurements to validate the prediction methods in this area should be redressed.

Particle Tripped Transition

While we were unable to explain stagnation point heating augmentation directly in terms of the upstream influence of the transition, two sets of observations provide a basis for explaining heating enhancement. The first was made in the study on the smooth hemispherical model and a second in a companion study with a transpiration-cooled hemispherical nosetip. During the present studies with blunt nonblowing nosetips, we observed that, in hypersonic flow at the highest Reynolds number conditions, when a small particle enters the shock layer, the transient disturbance induced by its presence was sufficient to trip the boundary layer, and induce increased surface heating. As the "particle-induced" disturbance was swept downstream over high-frequency thin-film and pressure gages, these gages indicated a rapid decay of the disturbance in the streamwise direction. While transient heating augmentations on the order of 20% were induced in the stagnation region by particle interactions, when the disturbance had been swept 15 deg from the stagnation point, the perturbation in surface heating dropped to below 5%.

The measurements also illustrate how surface curvature has a highly stabilizing effect on boundary layer transition. Only with high-speed photography and high-frequency, heat-transfer instrumentation can such phenomena be detected and analyzed. Hypersonic facilities generating high Reynolds numbers may be intrinsically susceptible to stagnation point heating problems from minute, high-energy particles entrained into the flow. This aspect of their performance should be carefully monitored.

Mechanisms of Particle-Enhanced Heating: Minute-Particle/Boundary Layer Interaction

In our studies with the hemispherical nosetips and the particle-launch model at the lower Reynolds numbers ($Re_d < 10^6$), we were unable to detect heating disturbances with the thin-film gages that could be associated with the wake of the large particles within the shock layer launched with the particle launcher or disturbance introduced by minute Mylar or dust particles from the driver section of the tunnel. However, for conditions where Reynolds numbers of over 10^7 were generated, examination of the high-frequency outputs from the thin-film gages on the hemispherical model indicated disturbances induced by minute dust particles. From our previous studies, we recognized that such particles are associated with the transition.

The high-frequency response of the heat-transfer gages and recording equipment (thin-film gages and Biomation recorders) enabled us to follow the disturbances as they were swept downstream over the closely spaced instrumentation. We observed that, while there was an initial growth of the disturbance in the stagnation region, downstream of the stagnation region the strong favorable pressure gradient caused the disturbance to decay rapidly and finally disappear well before the sonic line. Thus time-averaging the measurements of the heat-transfer gages in the stagnation region or using slow-response heat-transfer instrumentation could lead to heat-transfer distributions with larger than laminar values at the stagnation point, with the heating rates returning to laminar values away from the stagnation region as the instabilities were dissipated. We believe that this mechanism is the one principally responsible for the enhanced stagnation point in high Reynolds number hypersonic flow. Again, it must be emphasized that this phenomenon will occur only when the boundary layer in the stagnation region has a large enough Re_θ for it to be intrinsically unstable. Our experience suggests that tunnel noise causes enhanced heating through the mechanism of tripping the boundary layer, rather than increasing the vorticity in a laminar boundary layer.

Toroidal-Vortex/Boundary Layer Interaction

When dust particles rebound with sufficient energy to interact with the bow shock, measurements on blunt ellipsoids and on the laminar blunt configuration employed in the particle-launch studies indicate that a definitive mechanism causing particle enhanced heating is associated with the formation of toroidal vortices by particle/body shock interaction. Two examples of the incipient formation of these vortices at the shock front are shown in Fig. 19. When the particle arrives at the shock front with momentum sufficient only to cause a small dimple, a disturbance is generated which is propagated back through the shock layer as a toroidal vortex.

A sequence of photographs showing the small dimple which occurs as the particle reaches the bow shock and the subsequent formation of a toroidal vortex is provided in Fig. 20. The abrupt change in shock curvature at the junction between the particle and the body shock creates a shear layer that subsequently rolls up into the vortex ring as the particle is driven back into the shock layer. The vortex ring is then convected toward the model, expanding in diameter as it approaches the surface. Correlating the heat transfer time histories with the movie sequence reveals that increased heating rates are observed at the model surface over a period of just over 1 ms, the time taken for the vortex to traverse the shear layer and expand across the model. As the ring passes over the heat-transfer gages, their outputs increase to 1.5-3 times their undisturbed values. If the flow is initially laminar over the nosetip, the vortex acts to trip the boundary layer. Then, the basic enhancement mechanism is transitional to turbulent heating. For fully turbulent flows, the enhancement (which is significantly less) is associated with the enhanced local freestream vorticity.

Particle/Body-Shock Interaction

When particles are ejected from the shock layer such that they remain within one body diameter of the surface, a stable particle/body-shock interaction occurs, inducing enhanced heating by the free shear layer/boundary-layer interaction (free shear layer impingement).

A sequence of photographs showing the development of a region of shock/shock interaction leading to heating augmentation resulting from small-particle penetration is shown in Fig. 21. Here, the momentum on the particle was just sufficient for the particle to reach 0.7 of the body diameter ahead of the model. As the particle moved ahead of the bow shock, the shock wave associated with the particle and the flow behind it interacted with the original bow shock, inducing a shear layer at their point of intersection. This shear layer swept radially outward across the face of the model, increasing the local heat transfer at its base by as much as a factor of 10. In this sequence, the shear layer reached the model periphery just as the particle was being driven back to the model surface and the shear layer then collapsed inward in a quasi-steady fashion, disappearing as the particle re-entered the shock layer. The period of increased heating was just over 1 ms, the time taken for the particle to exit and re-enter the shock layer. Pressure levels just above the pitot level were observed at the base of the shear layer, while those within the annulus corresponded roughly with those achieved by compression through the conical shock associated with the particle. The heating rates associated with such interactions have been explored by Holden in spiked body flows[6], by Edney[7], and by Keyes and Hains[8] in regions of shock interference.

Effects of Separated Pulsating Flow

When the particle is launched with sufficient momentum for it to reach one body diameter ahead of the body, a dramatic change occurs in both the character of the inviscid flow and the pressure and heat transfer on the model surface. Here the entire flowfield begins pulsating, as demonstrated by the high-speed movie sequences of Fig. 22. These sequences, which were taken at Mach 6.5, demonstrate considerable similarity in mechanics of oscillation. This oscillation (termed the 'E' oscillation in this study) is very similar to pulsating flows observed over spiked bodies[6] or highly indented nose shapes[9]. The occurrence of these massive pulsations appears independent of particle size and, once the particle has reached one body diameter ahead of the surface, the axial motion of the particle is strongly influenced by the flow oscillations. The nondimensional frequency (fD/U) was found to lie between 0.17 and 0.19 and appeared to be relatively independent of Mach number; particle velocity, size, or penetration; and model size. The oscillation is initiated when the shear layer or jet formed by particle/spike shock/bow shock interaction reattaches to the body surface, trapping a conical region of gas. The mass which is being continuously added to this region through the conical shock drives the local stagnation point at the base of the shear layer toward the periphery of the model. This region collapses as the entrapped gas escapes when the shear layer moves off the body, and the sequence begins again with bow shock re-establishing and the particle shock/bow shock interaction reforming the shear layer. Perhaps the most intriguing question is why two distinct shock structures, one around the minute particle and a second around the model, are not formed at this juncture. Both the pressure and heat-transfer records exhibit large excursions from ambient conditions. After the tunnel starting process, the gage is exposed to a period of constant heating equal to that observed for the unperturbed flow. The heating rate increases sharply as the particle interacts with the shock and the shear layer sweeps across the face of the model. A decrease in heating occurs as a bulbous shock layer is formed and the flow "collapses" toward the body. This pattern is repeated in a flow oscillation of surprising regularity and persistence. While the heating rates across the model vary with time, the magnitudes of the maximum values do not appear sensitive to the exact particle trajectory, as can be seen from the measurements made in two runs (shown in Fig. 23) at identical freestream conditions but with different particle trajectories. If the particle travels off-axis, permitting an asymmetric interaction region and asymmetric spillage, an oscillatory interaction region can still be observed, as shown in Fig. 24. While the period of augmented heating is less for these cases, augmentation factors of over 5 are observed. Again, the major mechanism is interference heating resulting from shock/shock interaction.

Multiple-Particle Shock/Shock Layer Interaction

When three particles are launched simultaneously, a combination of extremely complex interactions occurs, as illustrated in Fig. 25. The ambient heating, as well as the heating resulting from the particle shock/bow shock interaction, is shown in Fig. 26. Here, we observe an increase in heating across the entire face of the model that exceeds the ambient heating by a factor of over 400%. Pulsations occur alternately about the particles in the shock layer in a manner dissimilar from the gross pulsations shown for a single particle launched along the axis. We have also observed that, in the latter case, a far greater penetration occurs for the same initial momentum. Here, we believe the flow reversal that occurs in the large pulsation decreases the drag of the particle or creates drag in the reverse direction. Clearly, increasing the number of particles in the shock layer increases the heating augmentation.

Launching a spray of 5 mil particles into the shock layer, as shown in Fig. 27, produces interactions that are similar to those observed in ballistic ranges as well as the multiple-particle interactions described earlier. While studies in a ballistic range can duplicate the particle/nose-tip impact, a very limited amount of data can be taken in these studies. Large heating augmentation occurs in the presence of both turbulent boundary layers and roughness.

Conclusions

Experimental studies have been conducted to examine the potential fluid mechanical mechanisms that cause enhanced heating in the stagnation region of blunt bodies in high Reynolds number hypersonic flow. These studies were conducted at Mach numbers of 6.5-13 and Reynolds numbers of up to 50×10^6 based on nosetip diameter. In the studies of tripped transition on smooth spherical nosetips, it was found that moving transition from the sonic line to stagnation region with annular trips, while increasing the heat transfer downstream of the trips, did not promote increased heating at the stagnation point. Similarly, while surface roughness was found to induce heating enhancements of up to 100% close to the sonic region, the stagnation point heating remained uninfluenced by roughness at the stagnation point. The results of the investigation of the effect of small blowing over spherical nosetips suggested that the initial decrease in the heating levels downstream of the stagnation point resulted principally from a decrease in roughness-induced heating effects, as the roughness elements are immersed in the layer of injectant. The studies of particle/shock layer interaction indicated that in high Reynolds number flow, where transition is close to or ahead of the sonic region, small particles ($<1 \mu m$) in the airflow can trip the boundary layer in the stagnation region, causing transient increases in stagnation heating. In many cases, the particle-induced disturbances generated in the stagnation region decay as they are convected downstream around the spherical nosetip, so that the transient heating enhancement is observed principally in the stagnation region. Larger particles, ejected from the surface, can cause heating augmentation factors of over 10 by inducing particle shock/bow shock interactions with the resultant shear or jet impingement on the surface of the nosetip.

Acknowledgement

This work was supported by the U.S. Air Force Office of Scientific Research under Contract F49620-79-C-0003.

References

[1] "Maneuvering Vehicle Aerothermodynamics Experiments Program," Calspan Corp., Buffalo, NY, Final Report for 2 July 1979 - 15 Dec. 1981, BMO Rept. TR-82-16, Nov. 1981.

[2] Fay, J. and Riddell, F.R., "Theory of Stagnation Point Heat Transfer in Dissociated Air," Journal of the Aeronautical Sciences, Vol. 25, Feb. 1958, pp. 73-85, 121.

[3] "Calspan Hypersonic Shock Tunnel, Description and Capabilities," Calspan Corp., Buffalo, NY, March 1973.

[4] Holden, M.S., "Studies of Boundary Layer Transition and Surface Roughness Effects in Hypersonic Flow," Calspan Corp., Buffalo, NY, Rept No. 6430-A-5, Final Report, Oct. 1983.

[5] Wong, J.L., private communication, May 1983.

[6] Holden, M.S., "Experimental Studies of Separated Flows at Hypersonic Speeds Part I: Separated Flows over Axisymmetric Spiked Bodies," AIAA Journal, Vol. 4, (April 1966).

[7] Edney, B.E., "Anomalous Heat Transfer and Pressure Distributions on Blunt Bodies in the Presence of an Impinging Shock," The Aeronautical Research Institute of Sweden, Rept FAA-115, Feb. 1968.

[8] Keyes, J.W. and Hains, F.D., "Analytical and Experimental Studies of Shock Interference Heating in Hypersonic Flows," NASA TN-D-7139, May 1973.

[9] Holden, M.S., "Studies of Transitional Heating and Flow Instabilities Over Ablated Nose Shapes," Calspan Corp., Buffalo, NY, Rept. AB-5646-A1-1, Sept. 1975.

Fig. 1 Models of the mildly ablated nose shapes used in the experimental studies.

Fig. 2 Particle launch model.

Fig. 3 Variation of stagnation point heating with Reynolds Number based on nosetip diameter.

Fig. 4 Variation of stagnation point heating with distance of the transition point from the stagnation point.

Fig. 5 Smooth hemispherical model for blunt-body transition studies.

Fig. 6 Smooth hemispherical model showing position of trip ring.

Fig. 7 Hemispherical nosetip coated with 12.5 mil conical rough surface.

Fig. 8 Hemispherical transpiration-cooled nosetip installed in tunnel.

Fig. 9 Distribution of heat transfer to the smooth hemispherical nosetip.

Fig. 10 Distribution of heat transfer to the smooth hemispherical nosetip.

Fig. 11 Heat-transfer distribution to the hemispherical nosetip with trip ring (K = 10 mil).

Fig. 12 Distribution of heat transfer around hemispherical nosetip with annular trip (K = 10 mil).

Fig. 13 Heat-transfer distribution to hemispherical nosetip with annular trip (K = 20 mil).

Fig. 14 Heat-transfer distribution to hemispherical nosetip with annual trip (K = 20 mil).

Fig. 15 Rough-wall heating to hemisphere.

Fig. 16 Comparison between the smooth wall turbulent theories and smooth- and rough-wall measurements ($M = 11.2$, $Re_D = 11 \times 10^6$, $K = 12.5$).

Fig. 17 Heat-transfer measurements on TCNT and smooth hemispherical nosetip.

Fig. 18 Heat-transfer measurements indicating that small blowing on rough nosetip initially acts to bring down heating levels to smooth-wall values.

Fig. 19 Shock/particle interaction generating ring vortexs over a blunt ellipsoid.

Fig. 20 Particle induced ring vortex interaction over flat-ended cylinder.

Fig. 21 "Stable" flow resulting from small particle penetration of bow shock.

Fig. 22 Particle-induced large-scale ("E") oscillation (Mach 6.5).

Fig. 23 Heat transfer distribution to the face of the model for a fully oscillating flow.

Fig. 24 Photographic sequence of particle/shock interaction from single particle launch.

Fig. 25 Multiple-particle interactions over the blunt nosetip.

Fig. 26 Heating rates resulting from multiple-particle interactions.

Fig. 27 Dust interactions in the shock layer.

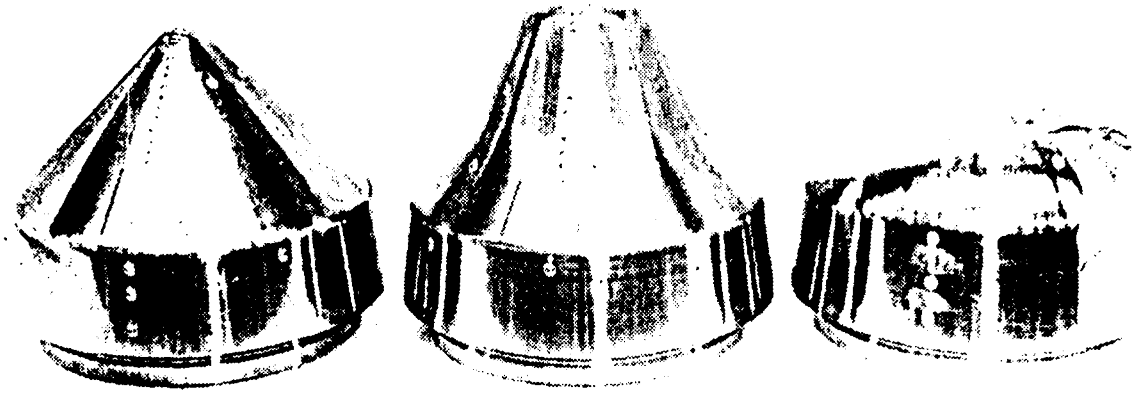

BICONIC TRI-CONIC BLUNT

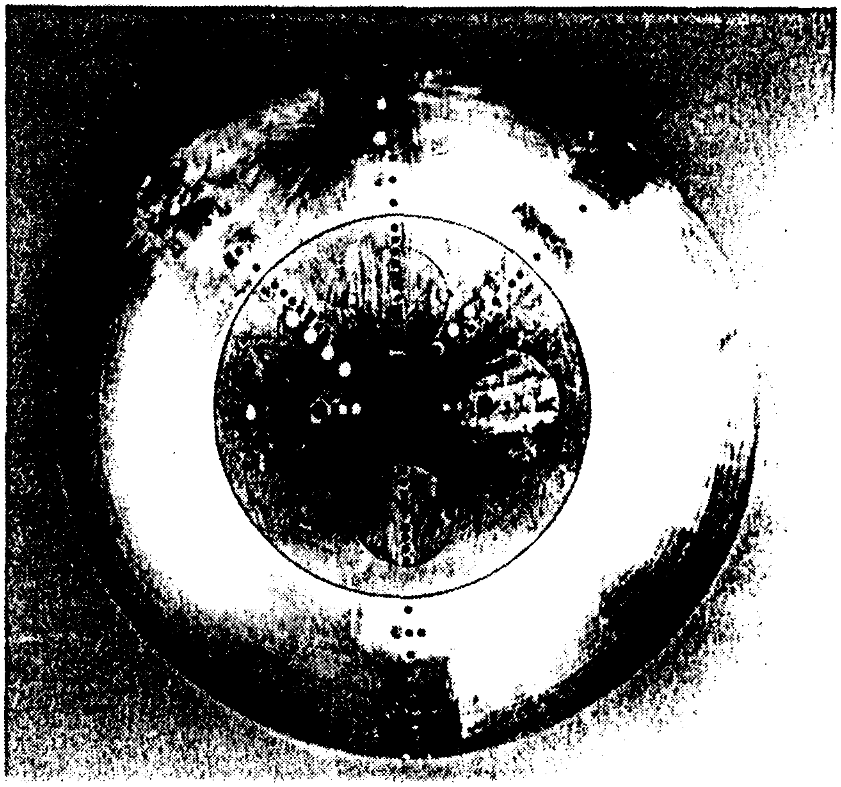

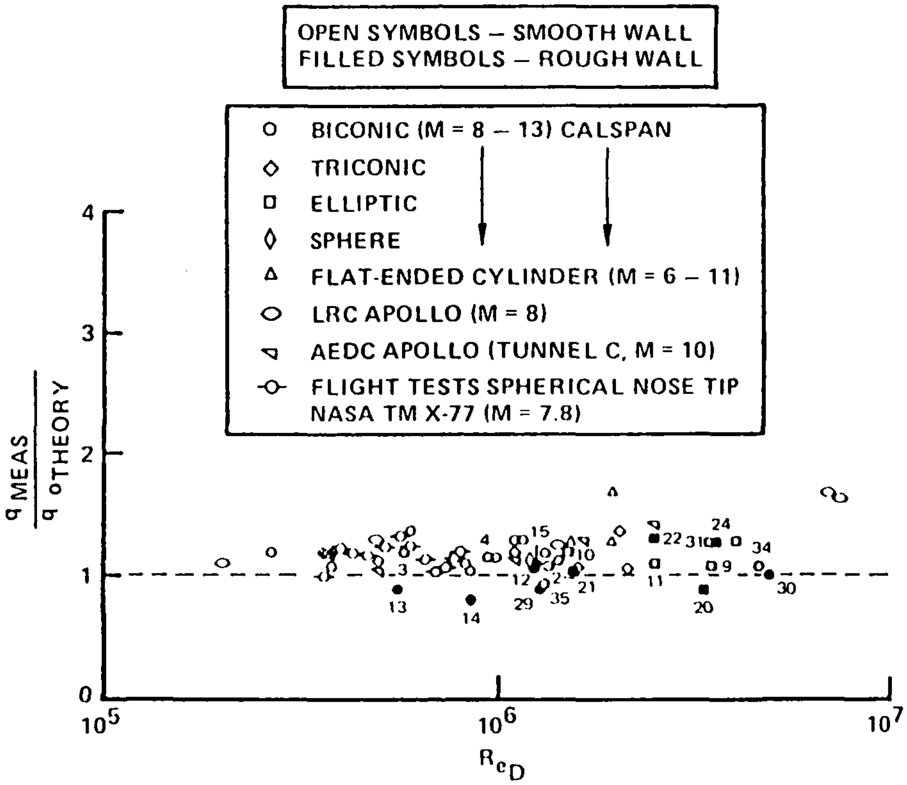
OPEN SYMBOLS – SMOOTH WALL
FILLED SYMBOLS – ROUGH WALL
○ BICONIC (M = 8 – 13) CALSPAN
◇ TRICONIC
□ ELLIPTIC
◊ SPHERE
△ FLAT-ENDED CYLINDER (M = 6 – 11)
○ LRC APOLLO (M = 8)
◁ AEDC APOLLO (TUNNEL C, M = 10)
-○- FLIGHT TESTS SPHERICAL NOSE TIP
NASA TM X-77 (M = 7.8)
4
3
2
1
0
q MEAS / q THEORY
10^5
10^6
10^7
Re_D
4
15
10
24
22
31
34
3
12
2
21
11
9
30
13
14
29
35
20

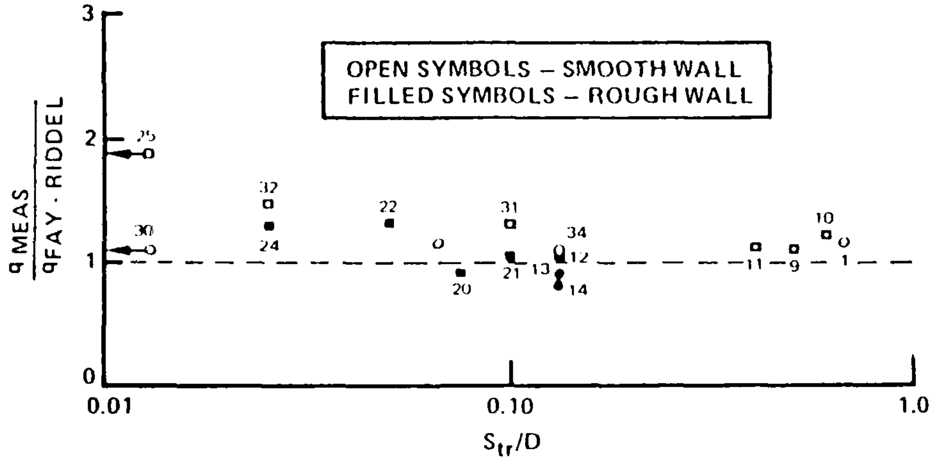
OPEN SYMBOLS – SMOOTH WALL
FILLED SYMBOLS – ROUGH WALL
$q_{MEAS} / q_{FAY \cdot RIDDEL}$
3
2
1
0
0.01
0.10
1.0
S_{tr}/D
25
30
32
24
22
20
31
21
13
34
12
14
11
9
10
1

TOP

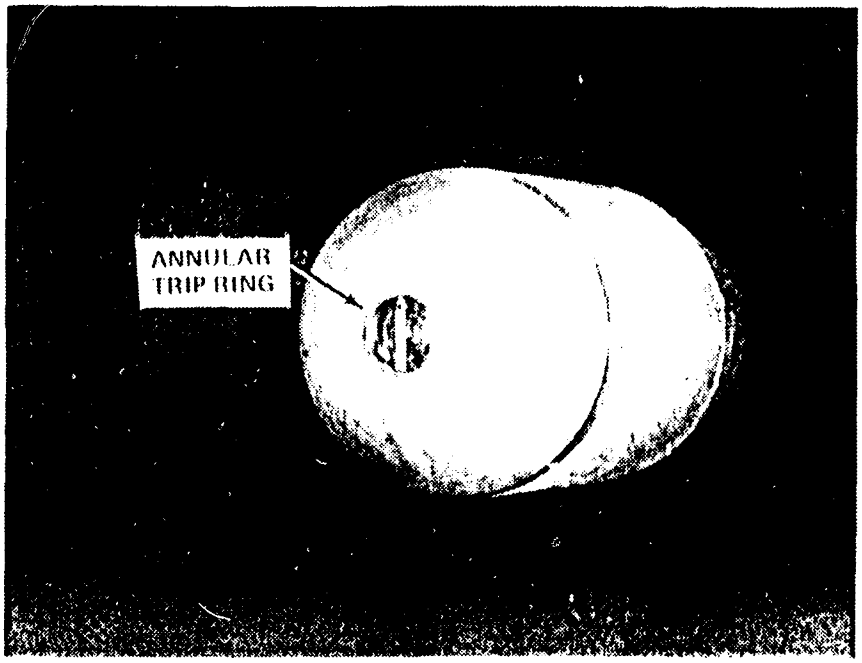
ANNULAR TRIP RING

Top

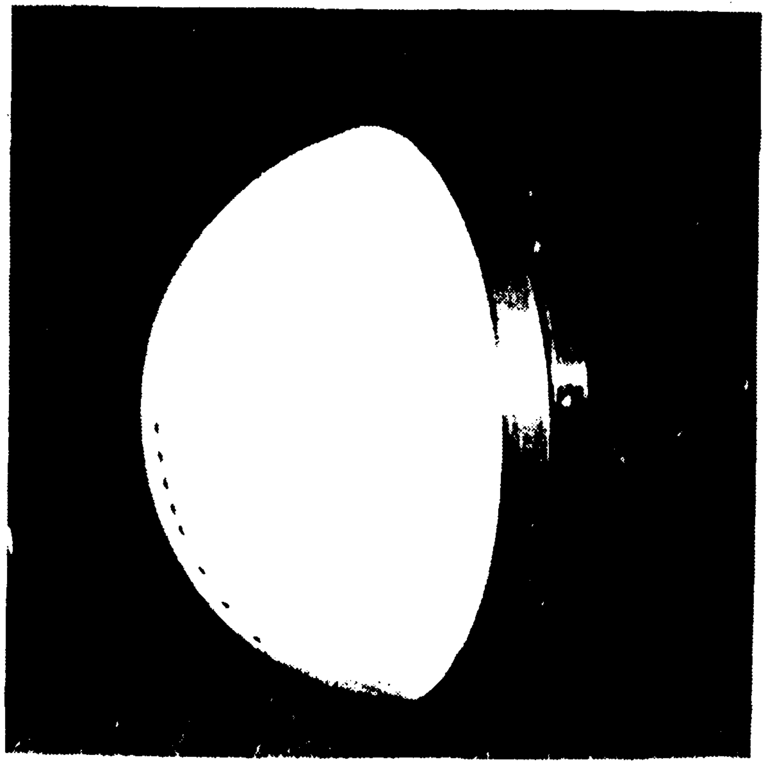

Top

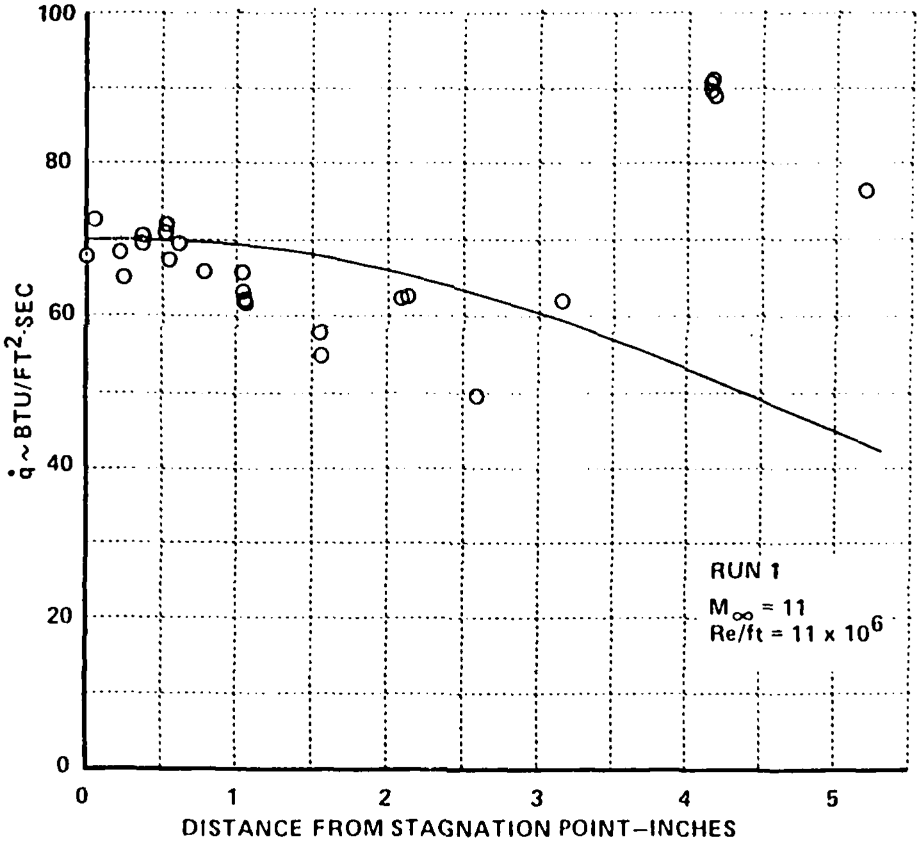
100
80
60
40
20
0
$\dot{q}$ ~ BTU/FT^2-SEC
0
1
2
3
4
5
DISTANCE FROM STAGNATION POINT–INCHES
RUN 1
M_∞ = 11
Re/ft = 11 x 10^6

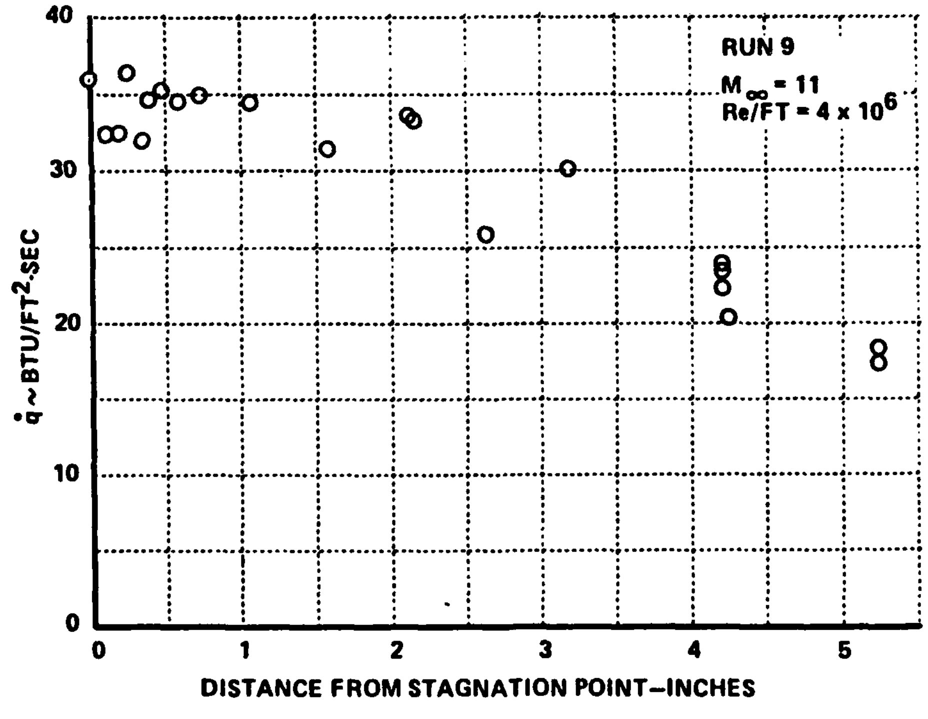
RUN 9
$M_\infty = 11$
$Re/FT = 4 \times 10^6$
$\dot{q}$ ~ BTU/FT^2·SEC
40
30
20
10
0
0
1
2
3
4
5
DISTANCE FROM STAGNATION POINT–INCHES

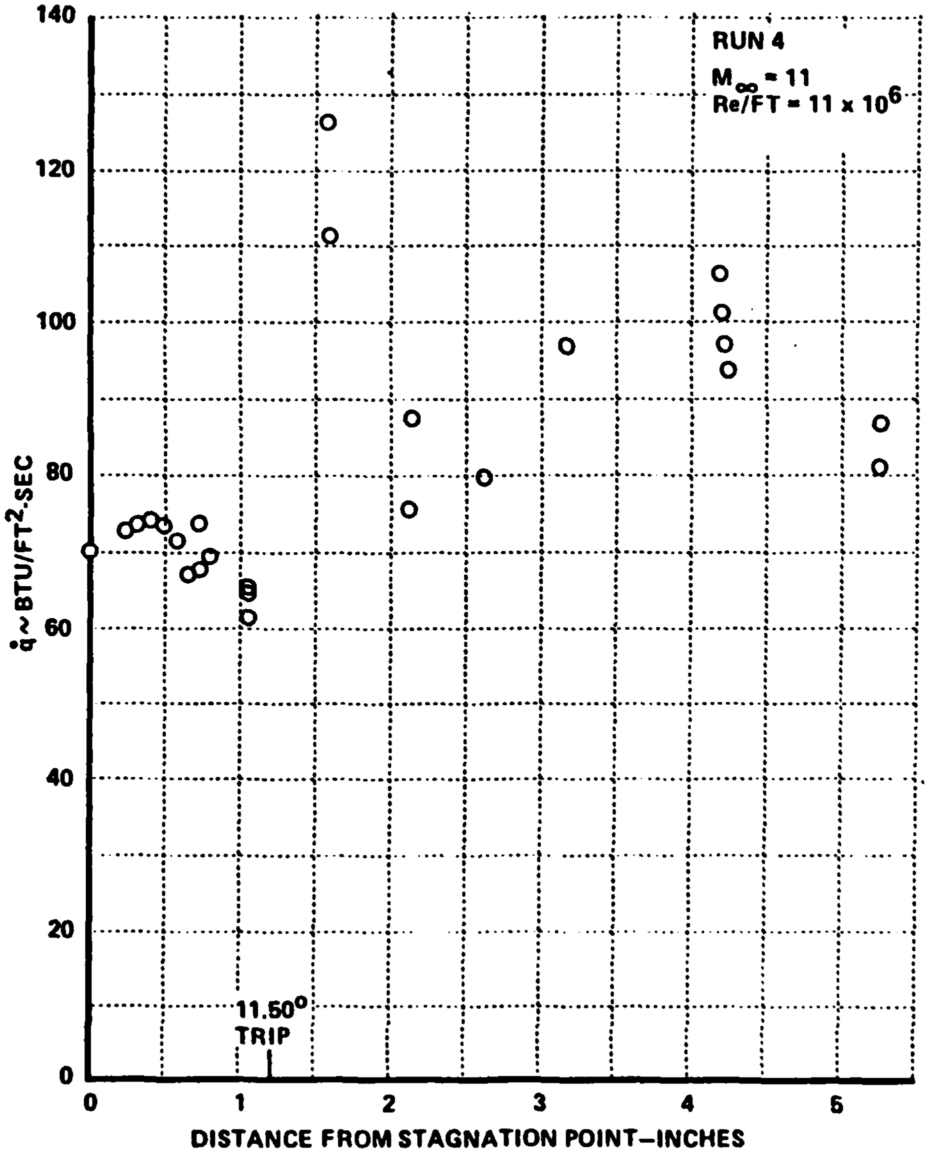
RUN 4
$M_\infty = 11$
$Re/FT = 11 \times 10^6$
$\dot{q} \sim BTU/FT^2 \cdot SEC$
140
120
100
80
60
40
20
0
11.50°
TRIP
0
1
2
3
4
5
DISTANCE FROM STAGNATION POINT–INCHES

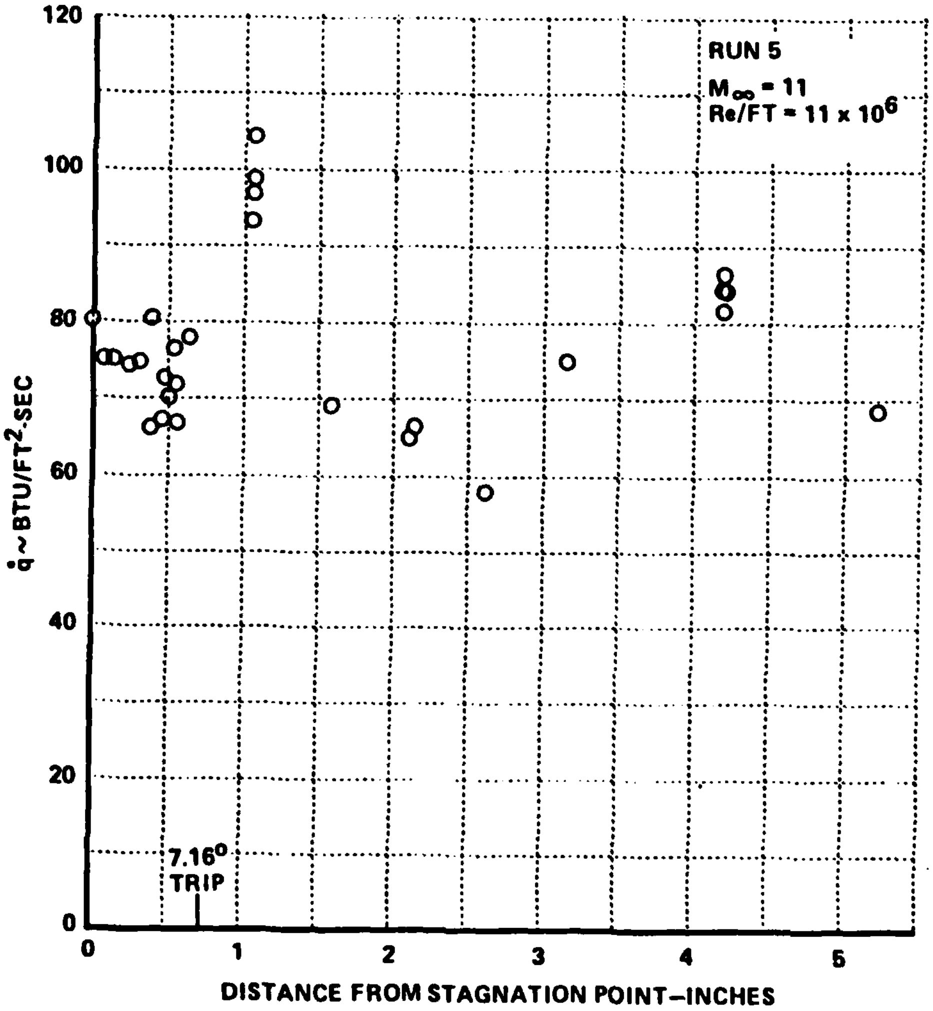
RUN 5
$M_\infty = 11$
$Re/FT = 11 \times 10^6$
120
100
80
60
40
20
0
$\dot{q}$ ~ BTU/FT^2-SEC
7.16°
TRIP
0
1
2
3
4
5
DISTANCE FROM STAGNATION POINT—INCHES

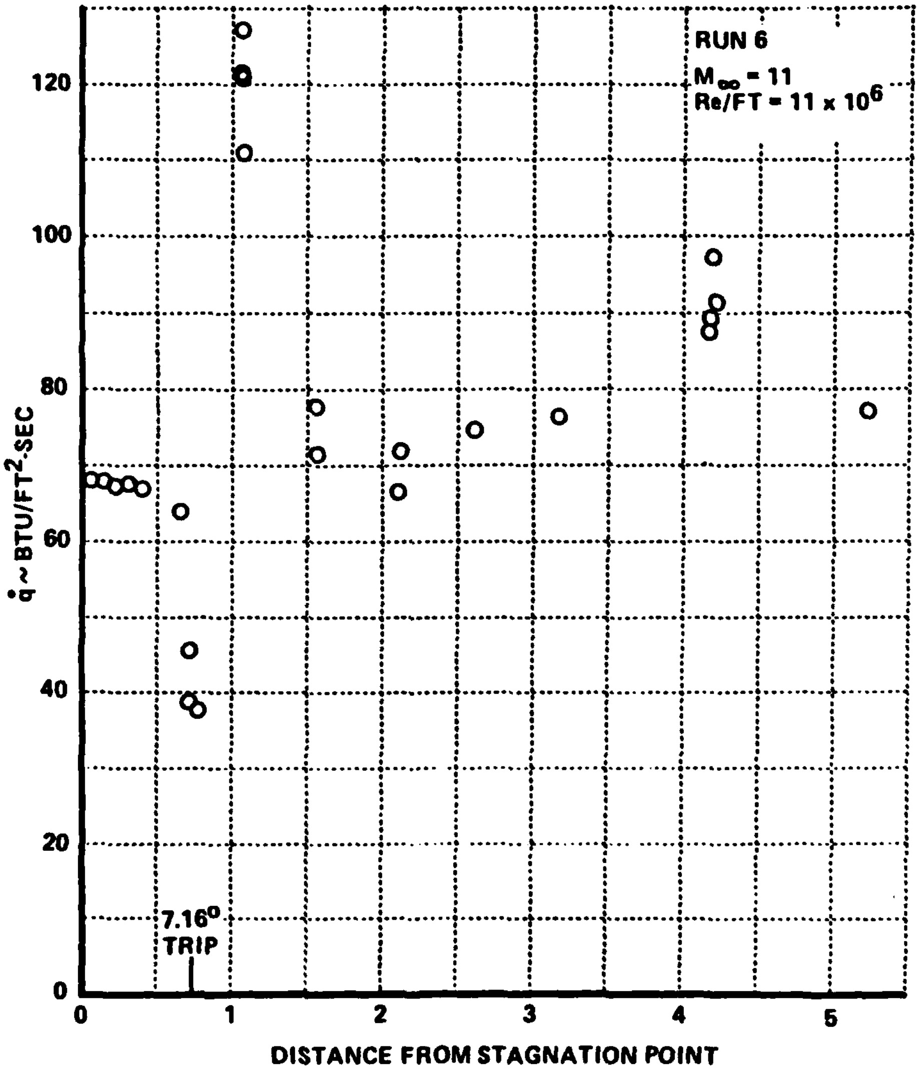
RUN 6
M_∞ = 11
Re/FT = 11 x 10^6
$\dot{q}$ ~ BTU/FT^2-SEC
0
20
40
60
80
100
120
0
1
2
3
4
5
DISTANCE FROM STAGNATION POINT
7.16°
TRIP

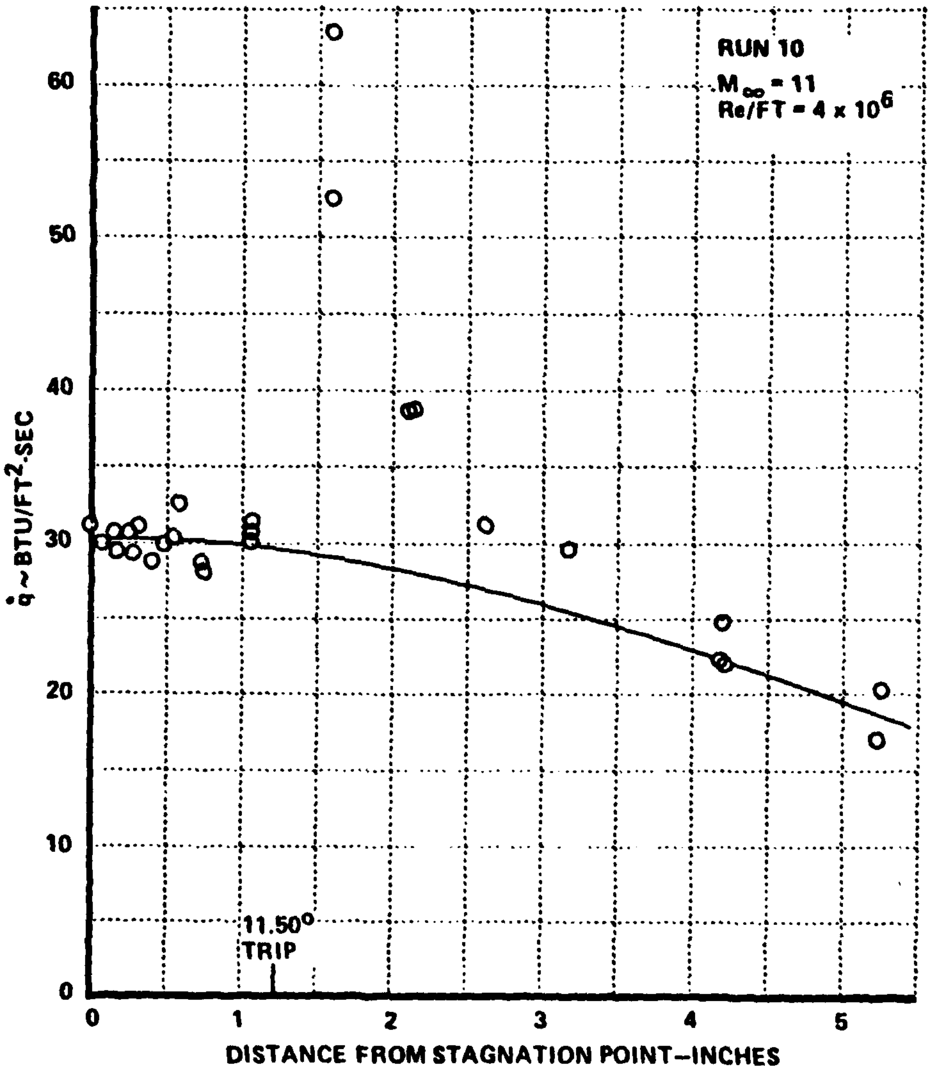
RUN 10
$M_\infty = 11$
$Re/FT = 4 \times 10^6$
$\dot{q}$ ~ BTU/FT^2-SEC
0
10
20
30
40
50
60
0
1
2
3
4
5
DISTANCE FROM STAGNATION POINT—INCHES
11.50°
TRIP

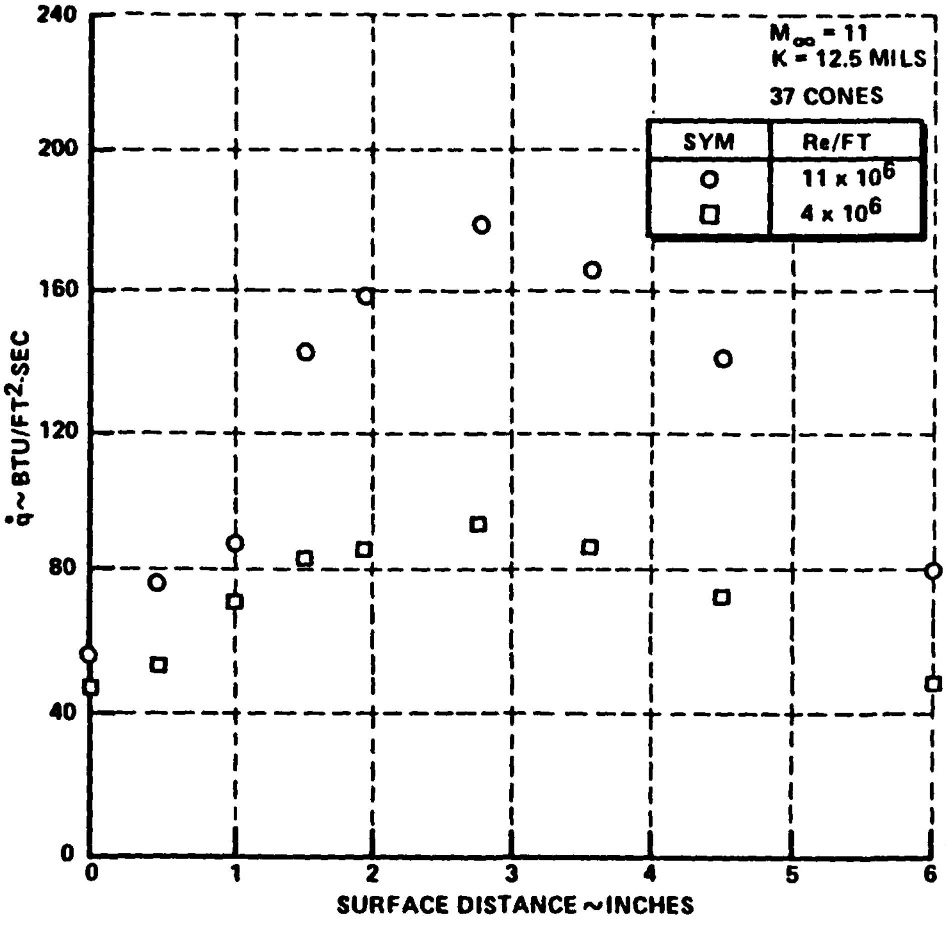

240
200
160
120
80
40
0
$\dot{q}$ ~ BTU/FT^2-SEC
0
1
2
3
4
5
6
SURFACE DISTANCE ~ INCHES
$M_\infty = 11$
K = 12.5 MILS
37 CONES
SYM
Re/FT
○ 11 x 10^6
□ 4 x 10^6

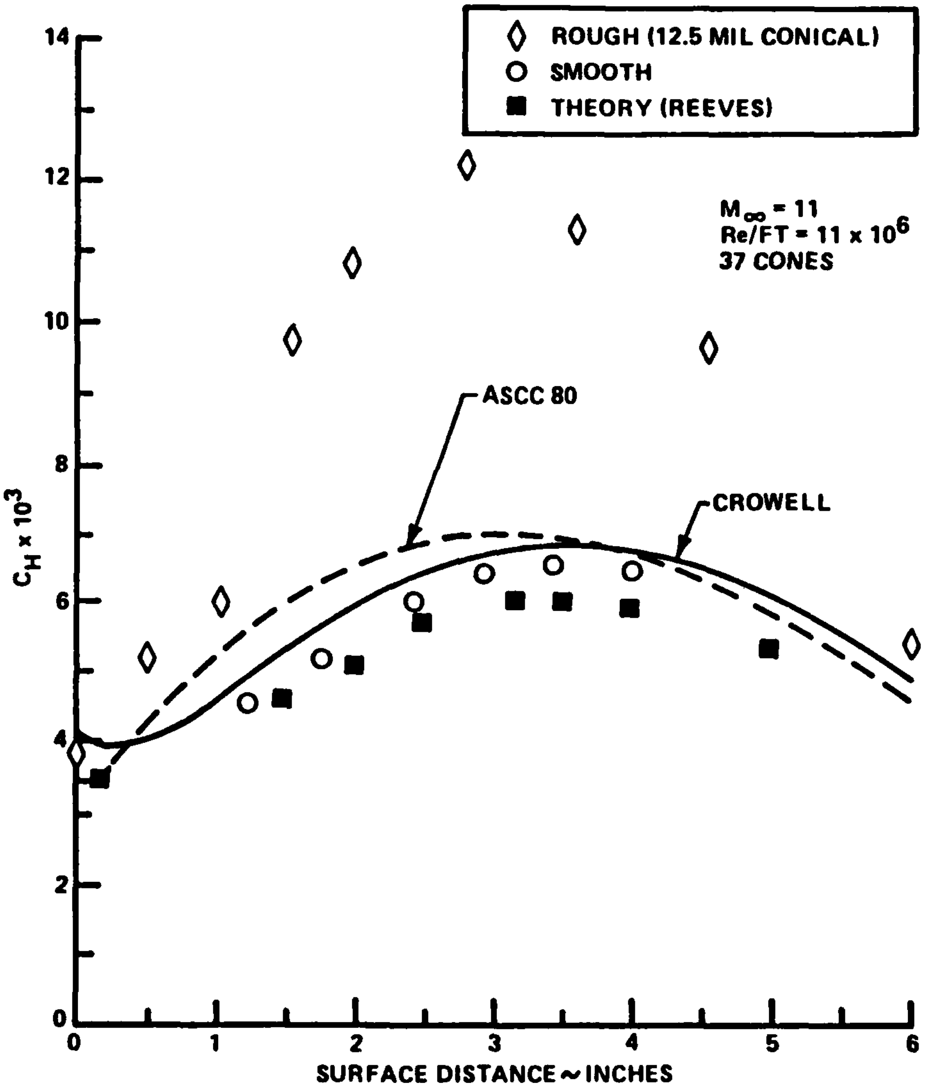
◊ ROUGH (12.5 MIL CONICAL)
○ SMOOTH
■ THEORY (REEVES)
$M_\infty = 11$
$Re/FT = 11 \times 10^6$
37 CONES
ASCC 80
CROWELL
$C_H \times 10^3$
14
12
10
8
6
4
2
0
0
1
2
3
4
5
6
SURFACE DISTANCE ~ INCHES

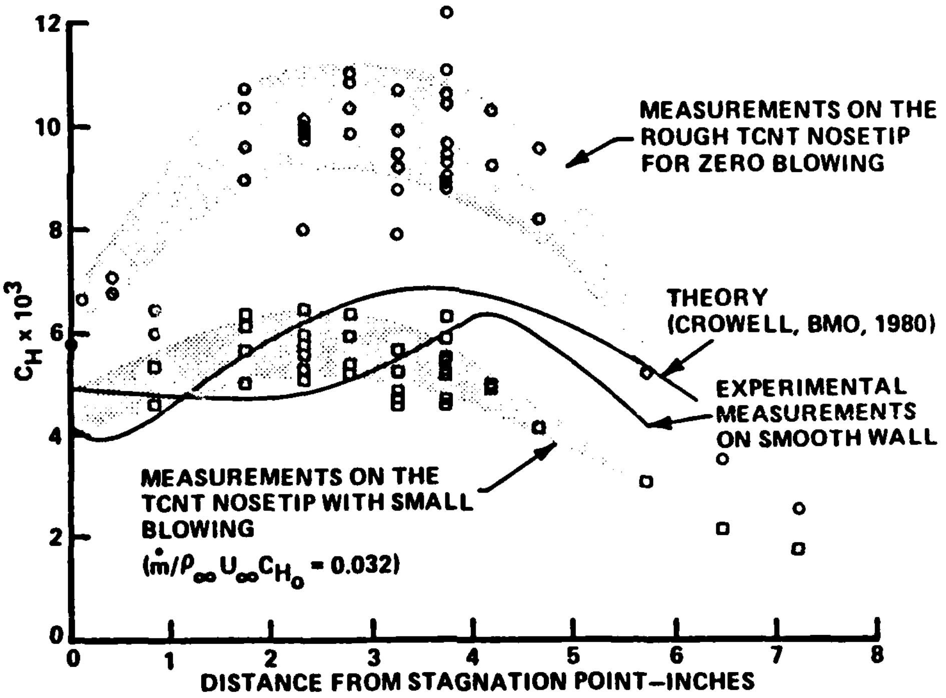

12
10
8
6
4
2
0
$C_H \times 10^3$
0
1
2
3
4
5
6
7
8
DISTANCE FROM STAGNATION POINT–INCHES
MEASUREMENTS ON THE ROUGH TCNT NOSETIP FOR ZERO BLOWING
THEORY (CROWELL, BMO, 1980)
EXPERIMENTAL MEASUREMENTS ON SMOOTH WALL
MEASUREMENTS ON THE TCNT NOSETIP WITH SMALL BLOWING
$(\dot{m}/\rho_\infty U_\infty C_{H_0} = 0.032)$

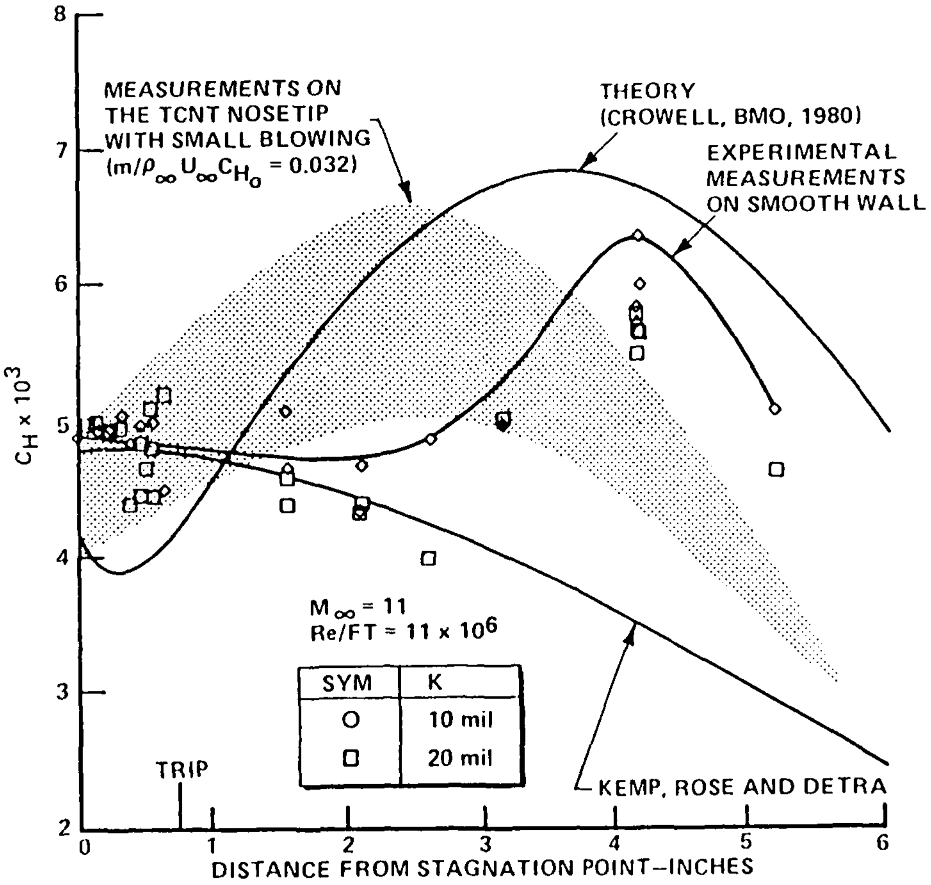
MEASUREMENTS ON
THE TCNT NOSETIP
WITH SMALL BLOWING
$(\dot{m}/\rho_\infty U_\infty C_{H_0} = 0.032)$
THEORY
(CROWELL, BMO, 1980)
EXPERIMENTAL
MEASUREMENTS
ON SMOOTH WALL
$M_\infty = 11$
$Re/FT = 11 \times 10^6$
SYM
K
O
10 mil
□
20 mil
TRIP
KEMP, ROSE AND DETRA
$C_H \times 10^3$
DISTANCE FROM STAGNATION POINT–INCHES
2
3
4
5
6
7
8
0
1
2
3
4
5
6

TOP

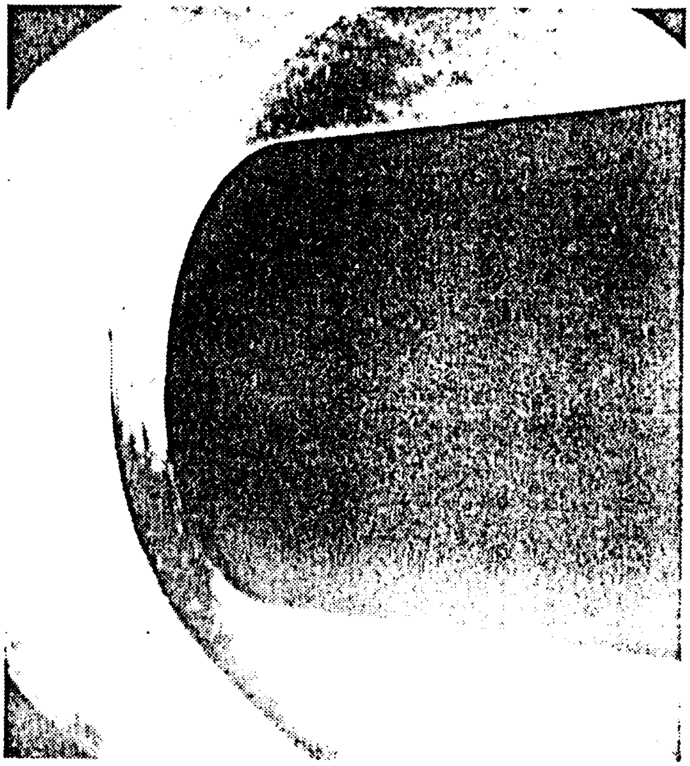

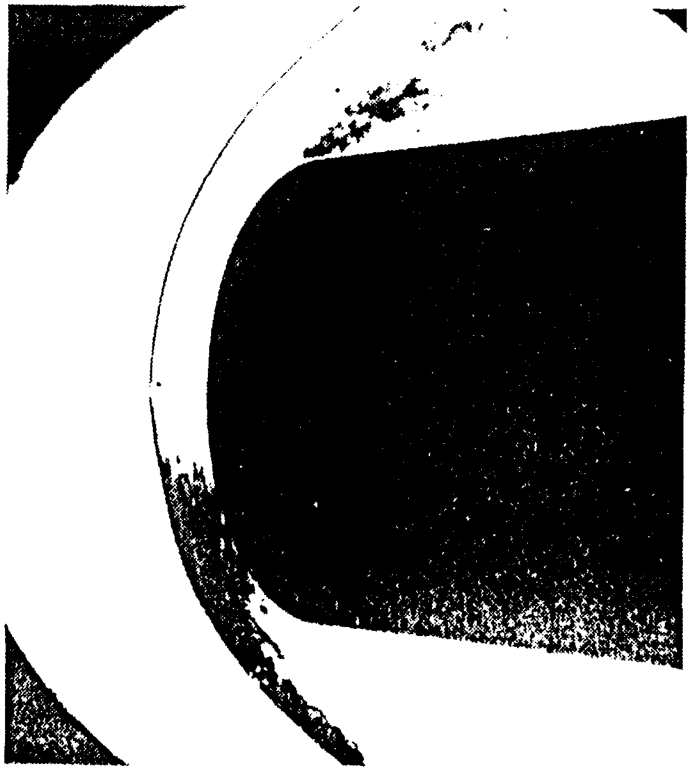

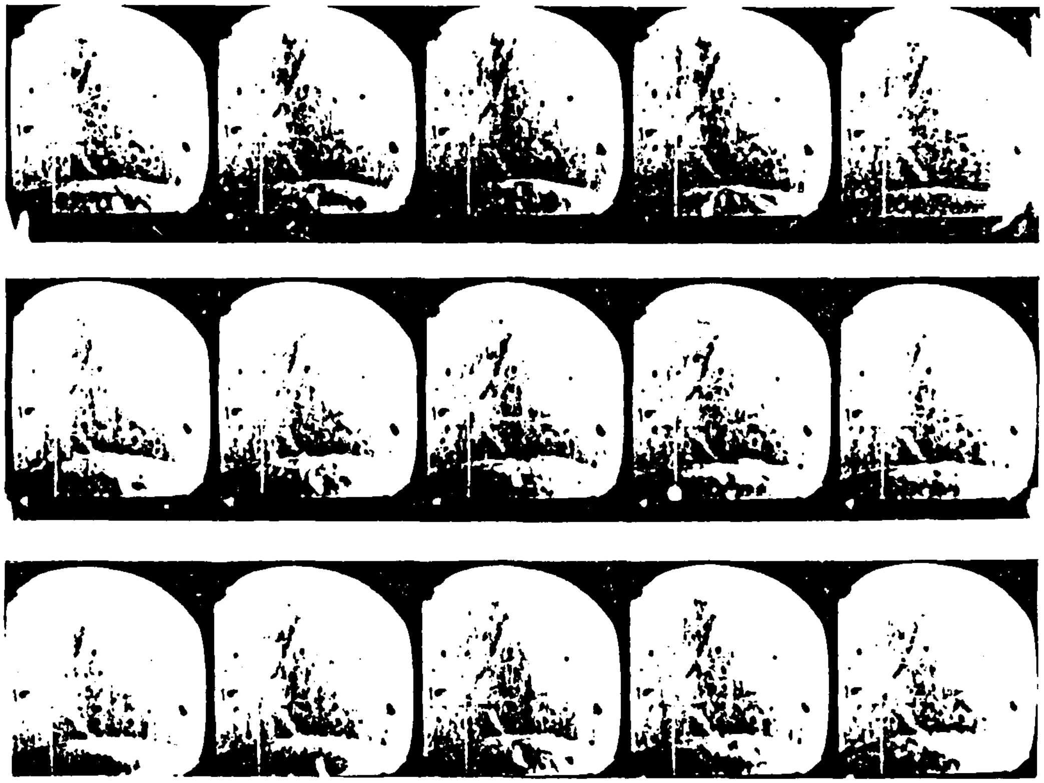

Top

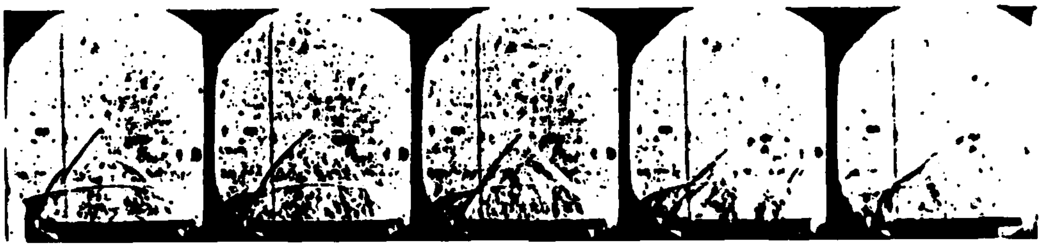

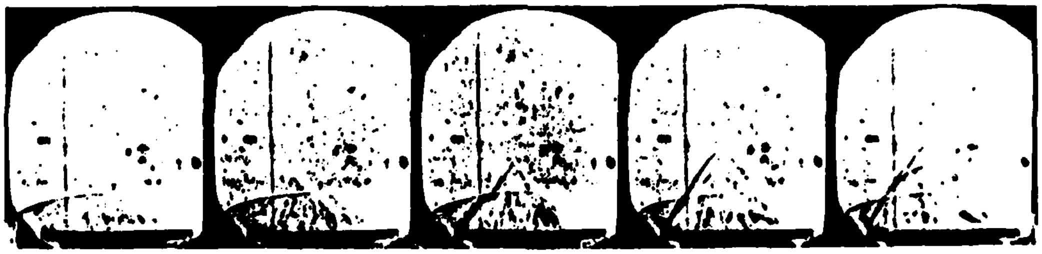

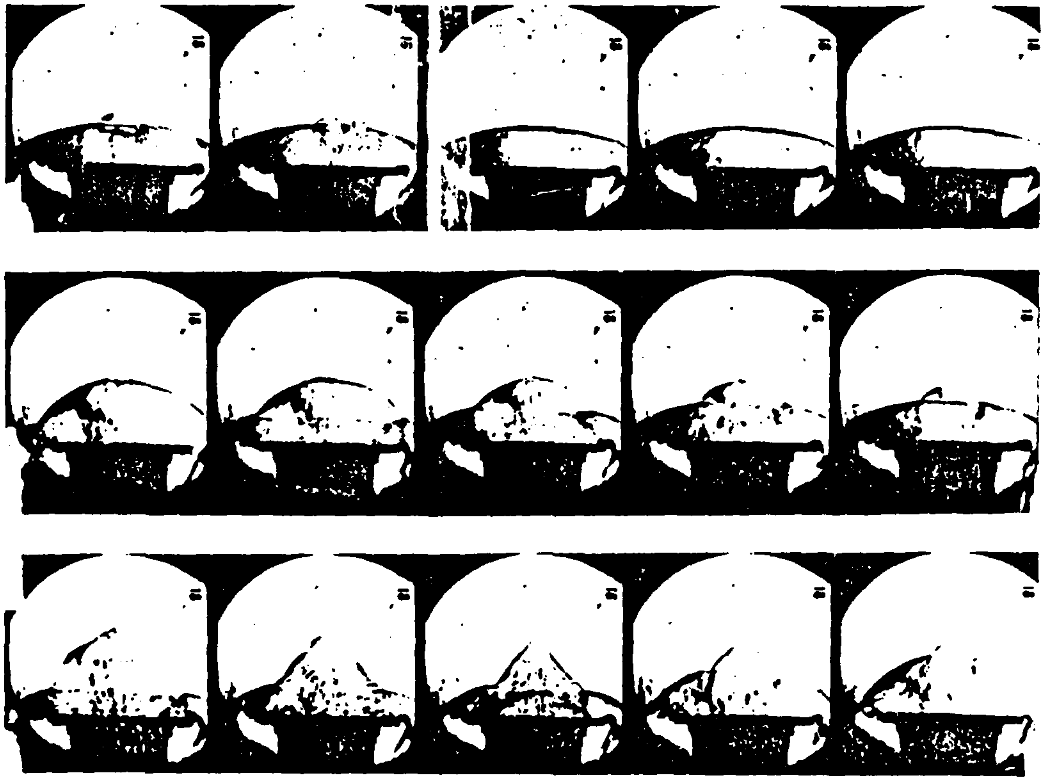

TOP

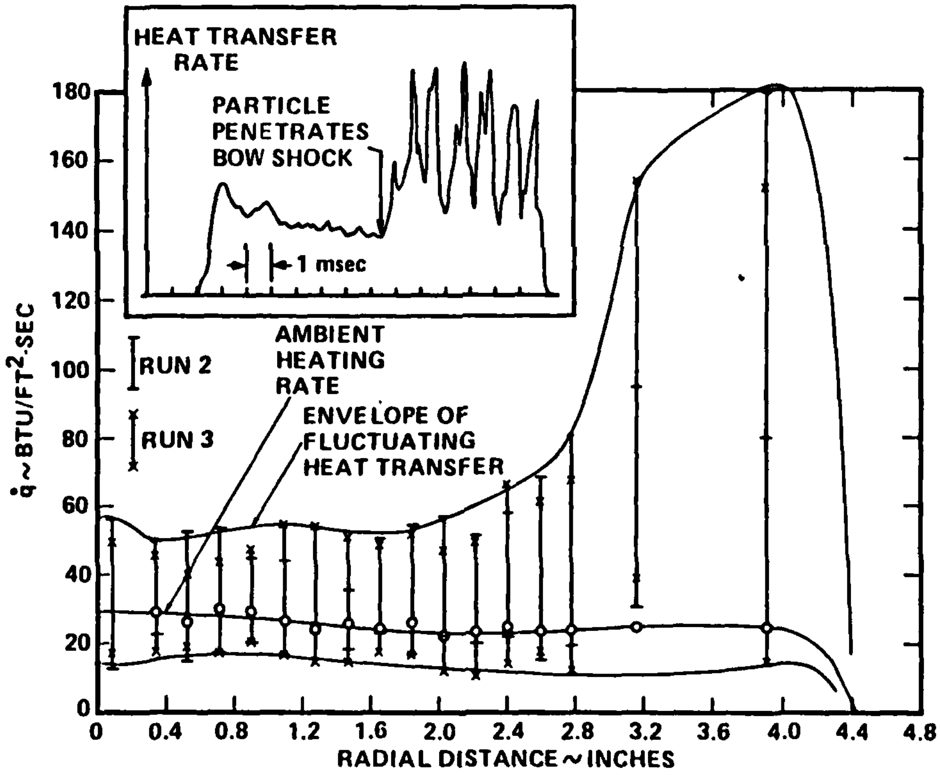

HEAT TRANSFER RATE
PARTICLE PENETRATES BOW SHOCK
1 msec
180
160
140
120
100
80
60
40
20
0
$\dot{q}$~BTU/FT^2·SEC
RUN 2
RUN 3
AMBIENT HEATING RATE
ENVELOPE OF FLUCTUATING HEAT TRANSFER
0
0.4
0.8
1.2
1.6
2.0
2.4
2.8
3.2
3.6
4.0
4.4
4.8
RADIAL DISTANCE~INCHES

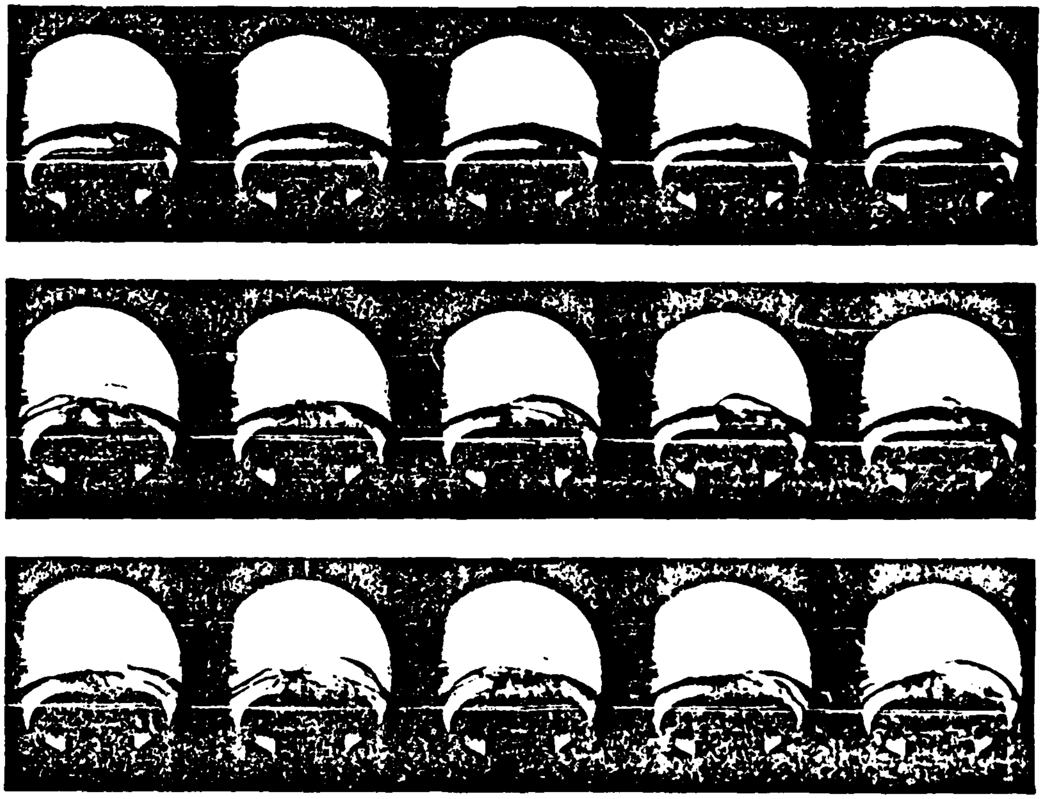

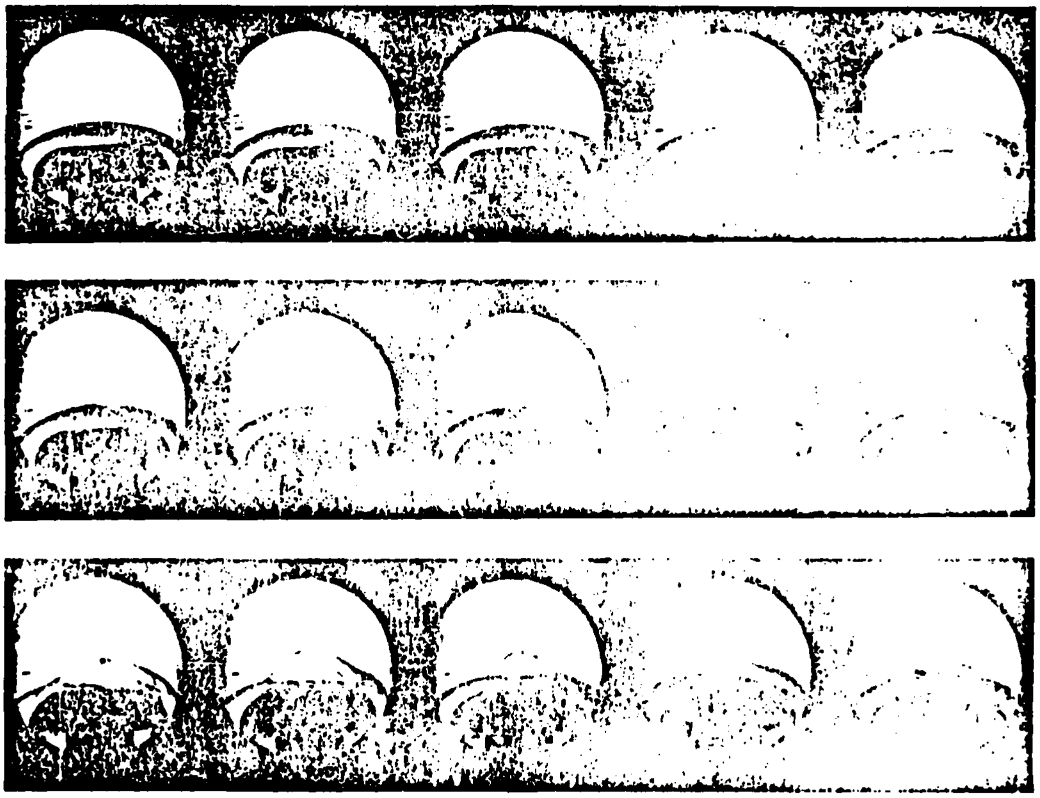

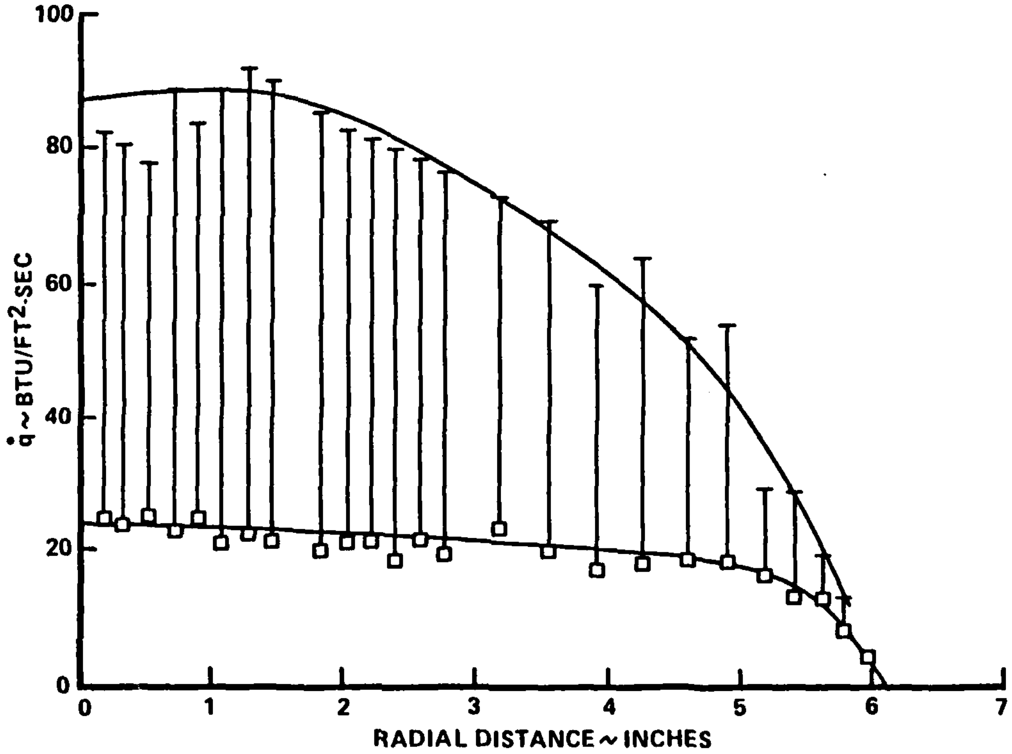
100
80
60
40
20
0
$\dot{q}$~BTU/FT^2·SEC
0
1
2
3
4
5
6
7
RADIAL DISTANCE ~ INCHES

TOP

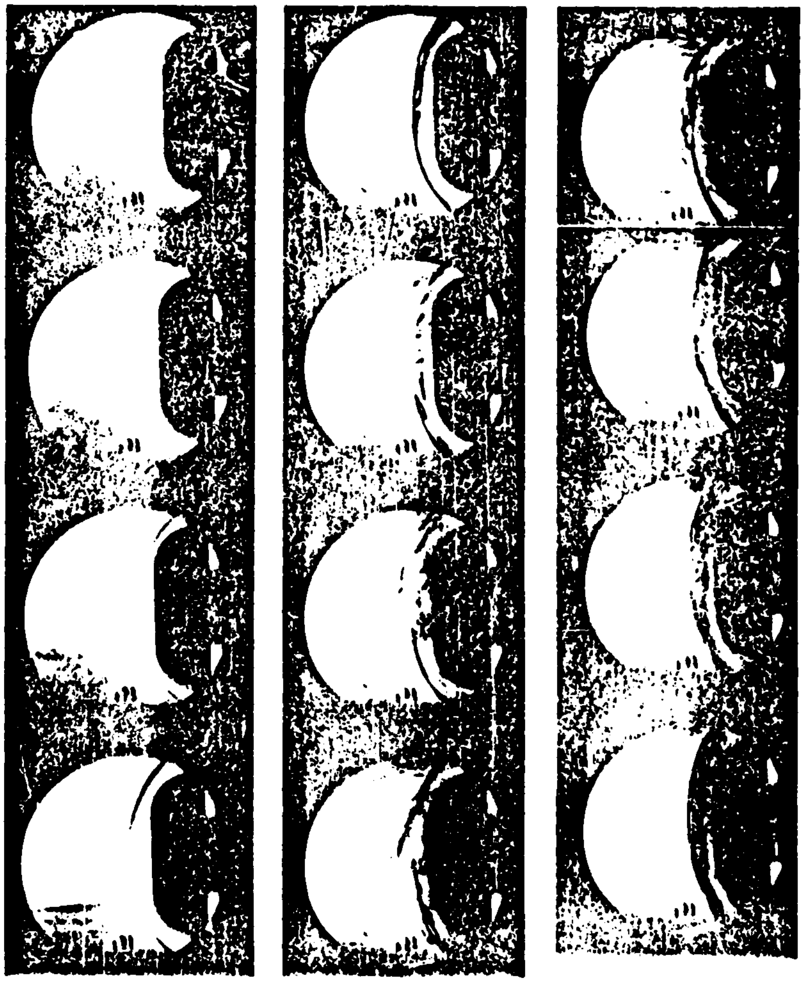

END

/ — 87

DTIC